Nagoya Institute of Technology

Synthesis of Graphene and Molybdenum Disulfide and Fabrication of Their Hybrid Structures

by

Sachin Maruti Shinde

A thesis submitted to Department of Frontier Materials of
Nagoya Institute of Technology
in partial fulfilment of the
requirements for the degree of
Doctor of Philosophy (PhD)

March 2016

Declaration of Authorship

I, Sachin Maruti Shinde, declare that this thesis titled, 'Synthesis of Graphene and Molybdenum Disulfide and Fabrication of Their Hybrid Structures' and the work presented in it are my own. I confirm that:

- This work was done wholly or mainly while in candidature for a research degree at this University.
- Where any part of this thesis has previously been submitted for a degree or any other qualification at this University or any other institution, this has been clearly stated.
- Where I have consulted the published work of others, this is always clearly attributed.
- Where I have quoted from the work of others, the source is always given. With the exception of such quotations, this thesis is entirely my own work.
- I have acknowledged all main sources of help.
- Where the thesis is based on work done by myself jointly with others, I have made clear exactly what was done by others and what I have contributed myself.

Signed: _____

Date: _____

अनेकसंशयोच्छेदि, परोक्षार्थस्य दर्शकम् ।
सर्वस्य लोचनं शास्त्रं, यस्य नास्ति अन्धैव सः ॥

(aneka-samshayo chchhedi, paroksh arthasya darshakam sarvasya lochanam shastram, yasya nasti andhaiva sah)

It blasts many doubts, foresees what is not obvious science is the eye of everyone, one who hasn't got it, is like blind.

Hitopadesh

Acknowledgements

Pursuing a Ph.D. project is both a painful and an enjoyable experience. It is just like climbing a high peak, step by step, accompanied by bitterness, hardships, frustration, encouragement and trust and with the help of so many kind people. Though it will not be enough to express my gratitude in words to all those people who helped me, I would still like to give my many thanks to all these people.

First of all, I would like to give my sincere thanks to my honorable supervisor, **Prof. Masaki Tanemura**, who accepted me as his Ph.D. student in his lab. Thereafter, he offered me so much advice, patiently supervising me, and always guiding me in the right direction. I have learnt a lot from him, without his help I could not have finished my dissertation successfully.

Special thanks are also given to **Assoc. Prof. Golap Kalita**. He is the one responsible for bringing me here. He has played the most vital part in helping me to design experiments and in writing manuscripts. His encouragement and help made me feel confident to fulfill my desire and to overcome every difficulty I encountered. It is not sufficient to express my gratitude to him with only few a words.

I would like to give special thanks to **Prof. Maheshwar Sharon** and **Dr. Madhuri Sharon** for their guidance. They have set the pavement of research for me and because of them only I am here today. I have been fortunate that I got their guidance at a very crucial stage of my life.

I also appreciate the advice of the committee members, and **Prof. Yo Ichikawa**, for his critical comments, which enabled me to notice the weaknesses of my dissertation and thereby make the necessary improvements according to their comments.

I am also thankful to my senior **Dr. Subash Sharma** from whom I learnt many things and because he was there at every stage to guide me. I express my sincere thanks to **Miss. Amutha Thangaraja, Mr. Ritesh Vishwakarma, Mr. Remi Papon, Mr. Mohamad Saufi Rosmi, Dr. Yazid Yaakob, Dr. Zurita Zulkifli** and **Mr. Kamal Sharma** for their valuable co-operation. I am especially thankful to all my lab-mates for their help specially **Mr. Hirano, Mr. Tsuchiya, Mr. Matsui and Mr. Sugiura**. I appreciate assistance of **Mr. Nakamura, Mr. Hiraoka, Mr. Wakamatsu, Mr. Taniyama**, **Mr. Watanabe** and **Mr. Nikhil Bharadwaj** as well. They were always present to solve my problems.

I acknowledge my indebtedness to **NGK** for providing me with scholarship during my Ph.D. program. Without this support it would not have possible for me to complete this research.

I am very grateful to my **Aai** and **Pappa (Parents), Bhau (Brother), Tai and Akka (Sister)** and **Sanjay Dada (Brother in Law)**. Their understanding and love encouraged me to work hard and

to continue pursuing a Ph.D. project abroad. Aai and Pappas firm and kind-hearted personality has affected me to be steadfast and never bow down to difficulty.

Last but not least, I am greatly indebted to my lovely Chikidi **Lalitha (fiance)**. She is the backbone and the origin of my happiness. Her constant love and support without any complaint or regret has enabled me to successfully complete this Ph.D. project.

Nagoya Institute of Technology

Abstract

In this dissertation I discussed the synthesis of graphene, N-doped graphene, Molybdenum Disulfide (MoS_2) and Vertically Alighned Carbon Nanotubes (VACNTs) using Chemical Vapour Deposition (CVD) method and their various applications. Further; amalgamation of graphene with these 2 dimensional and 0D material to form heterostructures were performed and memory device application was investigated. These studies will be supported by several kinds of characterizations like Optical Microscopy, Raman Spectroscopy, Scanning Electron Microscopy (SEM), Transmission Electron Microscopy (TEM), X-Ray Photoelectron Spectroscopy (XPS), Current (I)-Voltage (V) and four probe for sheet resistance.

Chapter 1 gives a brief introduction about graphene, N-doped graphene, MoS_2 and CNTs with their properties, synthesis, method of transfer and characterizations. Then I will explain about motivation of my thesis and finally will conclude with references.

Chapter 2 comprises of all instrumental methods including synthesis of Graphene, MoS_2, VACNTs and N-doped graphene. Device fabrication also included in this chapter in detail. All experimental details have been discussed in detail with the help of schematic diagrams for better understanding.

Chapter 3 discusses chemical vapour deposited large-area graphene transfer process to different flexible substrates which is one of the most critical aspect to explore wide range of reliable applications. Here, we have developed a simple and effective approach of polymer-free graphene transfer process onto a moldable flexible substrate. The as-synthesized graphene on Cu foil was hot pressed and attached to the substrate depending on the moldable temperature without any structural deformation. By etching the base Cu foil, a clean coating of graphene was obtained on the Cellulose Acetate (CA) based substrate. The developed process can be significant for graphene transfer on various moldable substrate materials.

In **Chapter 4**, the synthesis of a 3D structure of VACNTs and graphene from a single solid carbon source has been discussed. Graphene growth on Cu foil is achieved using solid camphor as the carbon source, whereas the VACNTs are obtained by adding a small amount of ferrocene in the camphor feedstock with minimum contamination from the Fe catalyst. Highly dense VACNTs were grown on a transferred graphene film to fabricate the hybrid structure. Achieving a seamless contact of VACNTs-graphene film is significant for low contact resistance and thereby practical device application.

In **Chapter 5**, we demonstrate the fabrication of a hybridized structure of CVD graphene and MoS_2 to configure a memory device application. Elongated hexagonal and rhombus shaped MoS_2 crystals are synthesized by sulfurization of thermally evaporated MoO_3 thin film. STEM studies reveal atomic level structure of the synthesized high quality MoS_2 crystals. In the prospect of a memory device fabrication, Poly(methyl methacrylate)(PMMA) is used as an insulating dielectric material as well as a supporting layer to transfer the MoS_2 crystals. In the fabricated device, PMMA-MoS_2 and graphene layers act as the functional and electrode materials, respectively. Distinctive bi-stable electrical switching and non-volatile rewritable memory effect is observed in the fabricated PMMA-MoS_2/graphene heterostructure.The developed material system and demonstrated memory device fabrication can be significant for next generation data storage applications.

Chapter 6 discusses about the synthesis of N-doped graphene by using Camphor (carbon source) and Melamine, Triazine and Polyacrylonitrile (PAN) (nitrogen source) solid precursors in a CVD technique. Different ratios of camphor and this materials were used to tune the at % of N during graphene synthesis. Rate of evaporation and amount are the key factors to get good quality of N-doped graphene. Melamine with the 5.2 at % of N was found to be the best precursor for N-doped graphene synthesis confirmed by XPS analysis. Triazine and PAN were having at % of N as 2.6 and 0.7 respectively.

Brief conclusions and future directions are discussed in **Chapter 7**.

Abbreviations

1, 2 and 3D	1, 2 and 3 **D**imensional
DI H_2O	**De**ionized Water
AP	**A**tmospheric **P**ressure
CVD	**C**hemical **V**apour **D**eposition
sccm	**S**tandard **C**ubic **C**entimeter per **M**inute
PMMA	**P**oly (**m**ethyl)**m**eth**a**crylate
CA	**C**ellulose **A**cetate
PVC	**P**olyvinyl **C**hloride
PTFE	**P**oly**t**etra**f**luoro**e**thylene
AFM	**A**tomic **F**orce **M**iscroscopy
SEM	**S**canning **E**lectron **M**icroscopy
TEM	**T**ransmission **E**lectron **M**icroscopy
XPS	**X**-ray **P**hotoelectron **S**pectroscopy
CNT	**C**arbon **N**anotubes
VA	**V**ertically **A**ligned
SW	**S**ingle **W**alled
MW	**M**ulti **W**alled
TMDC	**T**ransition **M**etal **Dic**halcogenides
MoS_2	**M**olybdenum **D**isulfide
MoO_3	**M**olybdenum **O**xide
FET	**F**ield **E**ffect **T**ransistor
SAED	**S**elected **A**rea **E**letron **D**iffraction
HAADF	**H**igh **A**ngle **A**nnular **D**ark **F**ield
STEM	**S**canning **T**unneling **E**lectron **M**icroscope
HRS	**H**igh **R**esistance **S**tate
LRS	**L**ow **R**esistance **S**tate
HOMO	**H**ighest **O**ccupied **M**olecular **O**rbital
LUMO	**L**owest **U**noccupied **M**olecular **O**rbital
N-Doped	**N**itrogen **D**oped
PAN	**P**oly**a**cryl**n**itride
1, 3, 5-Triazine	**T**riazine

Contents

List of Figures

Dedicated To

my beloved parents

and

lovely fiancèce

Chapter 1

Introduction

1.1 Graphene

In the last few years graphene has become one of the most discussed topics in physics and material science [1, 2]. The huge increase of publications per year is outrunning previous physics-hypes on other carbon allotropes like fullerenes and nano-tubes [3]. The word graphene is derived from the word graphite and the suffix -ene that is used for polycyclic aromatic hydrocarbons like naphthalene, anthracene, coronene and, in the simplest case, benzene [4]. Thus, the term graphene refers to one strictly 2D mono-layer of graphite as shown in FIGURE 1.1. Not only graphite, but carbon nano-tubes and fullerenes also possess the hexagonal structure [5].

Since in graphite the distance between the graphite planes is huge ($3.37A^{\circ}$) compared to the distance of carbon atoms within the same plane ($1.42A^{\circ}$), graphene serves as a model particularly for the description of this 3D material [6,7]. This was first done by P.R. Wallace, who used graphene as a simple theoretical model to calculate the band structure of graphite in 1947 [6]. Wallace correctly identified graphene as a zero-gap semiconductor and understood that the mean free path within a graphene sheet must be extraordinarily high [10]. Only nearly 40 years later DiVincenzo and Mele pointed out that the linear dispersion of the electronic band structure near the K-point in graphene, has a zero effective mass of the charge carriers as a consequence in graphene [11]. The reason this rather simple phenomenon was not understood earlier, was the lack of interest by the scientific community. In 1937 Landau had theoretically demonstrated that strictly 2D crystals were thermodynamically unstable [12], and thus scientific interest in a clearly 2D crystal system such as graphene was mostly limited to theoretical modeling.

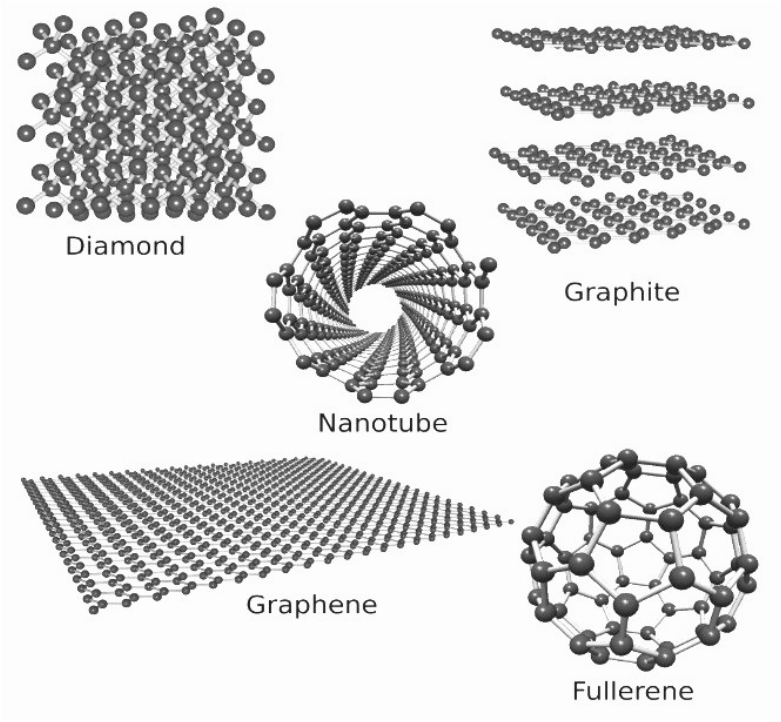

FIGURE 1.1: Diamond and graphite have been known since prehistoric times. Nanotubes were discovered in 1991 [8]; fullerenes in 1985 [9]. The year graphene was discovered depends strongly on the point of view.

1.1.1 Properties

The majority of the outstanding properties of graphene are a consequences of the extraordinary band structure at the fermi surface. It is important to become aware of the fact that only the p_z

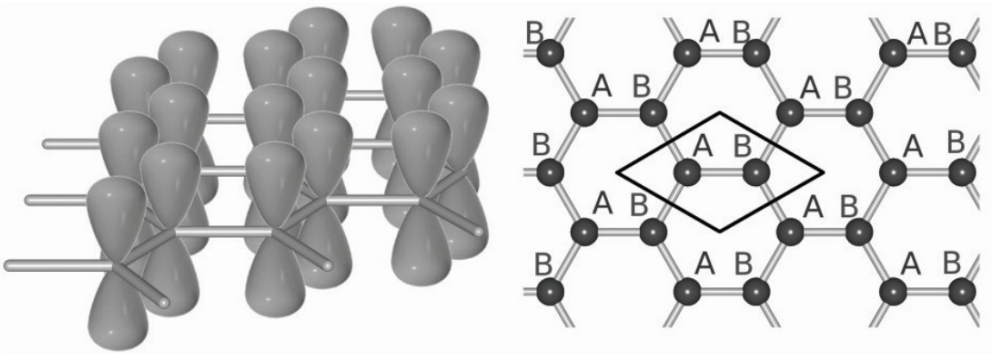

FIGURE 1.2: Models of graphene.(left): The graphene p_z states are perpendicularly orientated to the graphene layer. (right): The graphene lattice with the two graphene sublattices denoted and the unit cell drawn in

electrons contribute to transport phenomena in graphene, since carbon has two electrons in the s-shell and four electrons in the p-shell; the low-lying s-electrons do not contribute to the transport in graphene, while three of the four p-shell electrons are necessary to keep the sp^2-bonds from each carbon atom to its three neighbours. Thus, the p_z orbitals that are mirror symmetric to the

graphene plane, as one can see in FIGURE 1.2 are the only electrons that contribute to electronic transport phenomena.

1.1.1.1 Mechanical Properties

Single layer of graphene is one of the most rigid materials. Youngs modulus of graphene is a remarkably high $\sim 1TPa$ with an ultimate tensile strength of $130GPa$ [13]. Graphene is harder than diamond and stronger (~ 300 times) than steel. Although graphene is robust, this nano-sheet can be stretched up to 20% of its initial length. Having these mechanical properties, mechanically strong composite material can be produced with graphene.

1.1.1.2 Thermal Properties

Graphene has very high thermal conductivity. The thermal conductivity of graphene is $5000Wm^1K^1$ whereas, the thermal conductivity of SWNT is $3500Wm^1K^1$ [14]. Ho et al. reported the experimental thermal conductivity of bulk graphite as $2000Wm^1K^1$ [15]. Nika et al. compared thermal conductivity of bulk graphite and graphene and they mentioned (theoretically) that thermal conductivity of single layer graphene depends on the flake size and ranges from $3000 - 5000Wm^1K^1$ [17].

1.1.1.3 Electrical Properties

In graphene each C atom is connected to three other C atoms and leaves one free π electron. The electrical conductivity of graphene is $6000Scm^1$ [20]. Moreover, the resistance of graphene is $10 - 6\Omega cm$ at low temperature. Graphene is a zero-band gap semiconductor with an electronic mobility of $150,000cm^2V^{-1}s^{-1}$ at room temperature [18].

1.1.2 Graphene Synthesis

There are many techniques to synthesize graphene for different purposes. Based on the availability of facilities and quality of required graphene one can choose appropriate synthesis technique.

1.1.2.1 Exfoliation Technique

Graphite is made of large number graphene layers attached with weak Van-der Waals force. Exfoliation technique was the first method to obtain few layer of graphene from graphite by breaking interaction between neighbouring graphene layers mechanically or chemically and peeling

off graphene layers from graphite. First successful attempt to obtain few layer graphene by exfoliation was done by Novoselov et al [19]. On HOPG they formed few micron deep many mesas by dry etching in oxygen plasma. Obtained sample was put on photoresist and baked so that obtained mesas can stick to photoresist. Afterwards, layers were peeled off from graphite sheet using scotch tape and thin flakes, attached to photoresist were released in acetone and transferred to a Si substrate, which were found to be single to few layer graphene sheets.

1.1.2.2 Desorption of Si from Silicon Carbide (SiC)

Epitaxial growth of graphene by thermal desorption of Si from SiC is one of the most popular techniques. Graphene is grown by thermal decomposition of Si on (0001) surface plane of 4H-SiC or 6H-SiC substrate [20]. Number of graphene layers grown on substrate depends on the temperature and typical result is 1-3 graphene layers. Rollings et al [21] was successful to produce one atom thick graphene film. Further modifications were done using Ni thin film coated SiC substrate at lower temperature which helped to obtain continuous large area graphene layers [22].

1.1.2.3 Growth from solid carbon Precursor

Graphene with large area and controllable thickness can be synthesized from solid carbon sources such as polymer films or small molecules deposited on a metal catalyst substrate at as low temperature as $800°C$ [23]. In studies the solid carbon source used was a spin-coated PMMA thin film ($100nm$) and the metal catalyst substrate was a Cu film. A single uniform layer of graphene was formed on the substrate at a temperature as low as $800°C$ and as high as $1000°C$ for $10min$, with a reductive gas flow (H_2/Ar) at low temperature conditions [23].

1.1.2.4 Reduction of Graphene Oxide (GO)

Basis idea of synthesis of graphene like sheets from graphite oxide is the exfoliation of graphene oxide into individual graphene oxide sheets and further chemical reduction of obtained individual graphene oxide sheets [24]. Graphite oxide can be achieved by oxidative treatment of graphite using any of three principal methods developed by Brodie [25], Hummer [26], and Staudenmeire [27]. Graphite oxide is electrically insulating and because of that one cannot use it for electronic applications but it can be restored close to the level of graphite by chemical reduction of graphite oxide [28]. Due to hydrophilic nature of GO, after a suitable ultrasonic treatment it is easy to get graphene oxide thin sheets by exfoliation in water [29].

1.1.2.5 Chemical Vapour Deposition (CVD)

Few layer of graphene can be synthesized either by using thermal CVD or plasma-enhanced(PE) CVD. In case of thermal CVD most of the graphene synthesis has been done using Ni or Cu substrate and precursor gas mixture of H_2 and CH_4 or other hydrocarbons and Ar gas as carrier gas. Quality and thickness of grown graphene depend on the cooling and heating rate, process temperature, ratio of gases, thickness and crystallinity of substrate. Yu et al. reported three to four graphene layers grown on polycrystalline Ni foils of $500nm$ thickness, using thermal CVD method [30]. Similarly, X. Li et al. [31] has shown the successful growth of high quality, continuous graphene on Cu foil by thermal CVD. PECVD technique is also useful for graphene synthesis as this process reduces the consumption of energy and avoids the amorphous carbon formation [32]. Graphene was synthesized on various substrates like Si, W, Mo, Zr, Ti, Hf, Nb, Ta, Cr, 304 stainless steel, SiO_2 and Al_2O_3 [33] using radio frequency PECVD.

1.1.2.6 Direct CVD of graphene on a dielectric substrate

Due to the disadvantages of previously known graphene synthesis techniques in terms of cost, quality of graphene, control on thickness and number of layers of graphene, large scale fabrication and transferring step, there was a necessity of better, economic and effective method for large scale growth of high quality graphene with single or few layer. Hence, a method for direct CVD growth of single to few graphene layer on dielectric substrate is needed. Ismach et al. illustrated a method for direct CVD of single to few layer graphene film on dielectric substrate using a sacrificial copper film [33]. Significant results of direct deposition of graphene were obtained on quartz substrate and M-plane sapphire.

1.1.3 Graphene Transfer

There are different ways to transfer graphene on arbitrary substrates. Following are few techniques;

1.1.3.1 Wet Chemical Etching

In this method Graphene was first coated by a thin layer of PMMA and then baked at $120°C$ to evaporate the solvent. The metal layer was then removed by Ni or Cu etchant, leaving only the PMMA/ graphene film. The film is cleaned by DI H_2O and then transferred onto a targeting substrate. After evaporating water vapor away, PMMA was removed by acetone, leaving a graphene film on top of the targeting substrate [34].

1.1.3.2 Stamp Method

In the stamp method, the graphene and growth substrate are picked up by an elastomeric stamp and stamped onto the desired substrate. The stamp is removed mechanically. In the self-release transfer method, a specific polymer film (self-release layer) is first spun-cast over the graphene. An elastomeric stamp is then placed in conformal contact with the self-release layer. The growth substrate is etched away to leave the graphene/self-release layer on the elastomeric stamp. The graphene is then brought into contact with the desired substrate by stamping and the stamp is removed mechanically. Finally, the self-release polymer is dissolved under mild conditions in a suitable solvent [35].

1.1.3.3 Bubbling Transfer

(a) Electrochemical:
For bubbling transfer of graphene, Cu substrates with the grown graphene were spin-coated with PMMA at $2,000rpm.$ for $1min$, and cured at $180°C$ for $30min.$ The bubbling time depends on the size of the graphene and the constant current used. The current density was usually $0.11Acm^{-2}$, and the corresponding electrolytic voltage was usually $5 - 15V$ [36].

(b) Electroless:
In this method, initially, a PMMA support/carrier layer is deposited on the graphene. The substrate is then transferred into NH_4OH + H_2O_2 + H_2O ($1 : 1 : 3$ vol %) bath in which bubbling due to the release of O_2 gas occurs. The O_2 gas bubbles intercalate at the graphene substrate interface leading to gradual detachment of the PMMAgraphene film. The separated film is transferred onto the target substrate and PMMA is removed using hot acetone vapor. This marks the end of successful transfer of graphene onto an arbitrary target substrate [37].

1.1.3.4 Roll to roll process Transfer

After growth, the graphene film grown on copper foil is attached to a thermal release tape (Jinsung Chemical Co. and Nitto Denko Co.) by applying soft pressure($0.2MPa$) between two rollers. After etching the copper foil in a plastic bath filled with copper etchant, the transferred graphene film on the tape is rinsed with DI H_2O to remove residual etchant, and is then ready to be transferred to any kind of flat or curved surface on demand. The graphene film on the thermal release tape is inserted between the rollers together with a target substrate and exposed to mild heat ($90 - 120°C$), achieving a transfer rate of $150 - 200mm\,\mathrm{min}$ and resulting in the transfer of the graphene films from the tape to the target substrate [38].

1.1.4 Graphene Characterization

In support of graphene synthesis research, a standard characterization techniques have been developed to determine the structure of the films. Each technique gives a different perspective of the structure and performance of the film. Raman spectroscopy gives cursory information about the bond structure of the sample, and can be used to get an estimate of graphene film thickness. SEM can pick out characteristic film defects on the micron scale. More involved techniques like TEM and AFM resolve atomic structure, though only over small ranges.

1.1.4.1 Optical Microscopy

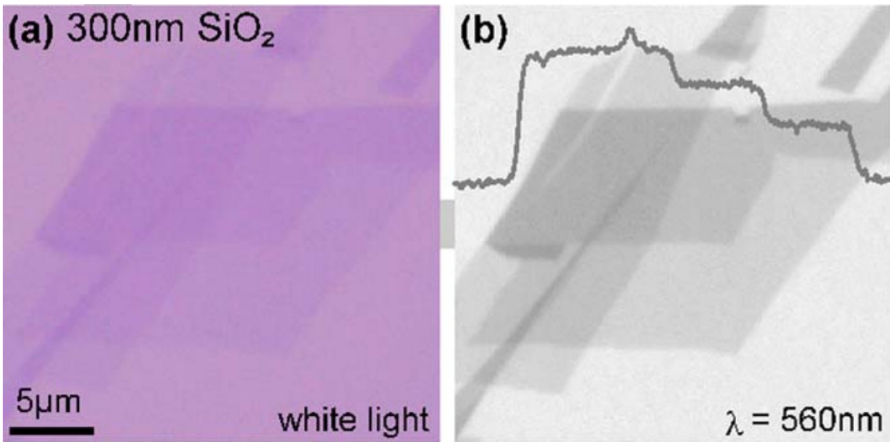

FIGURE 1.3: Optical microscopy of exfoliated graphene on silcon with 300nm SiO_2 using (a) white light and (b) green light [39]. In (b) a line plot overlay of image contrast shows discrete steps. Relative thicknesses of few layer graphene can be determined optically

On silicon substrates with certain thicknesses of oxide coating ($90nm$ or $300nm$), single layer graphene is visible due to thin film interference phenomena. This method was developed by Geim et al. and used to characterize exfoliated graphene samples. The exact number of layers is difficult to determine precisely by this method, but single layer differences in thickness between adjacent flakes can be resolved easily [39].

1.1.4.2 AFM

An atomic force microscope scans a sample with an atomically sharp cantilever to create a contour plot of the sample surface. AFM excels at distinguishing changes in thickness, and in some cases can provide atomic resolution images. However, AFM measurements are time-intensive and require finding lucky edges between the bare substrate and an area of interest to get true height information. Scans on the order of $10\mu m$ across are large for this technique, so searching large samples for single layer material is not practical with AFM. However, if the

edge between a silicon substrate and a graphene flake is located, AFM can give precise height information about the edge.

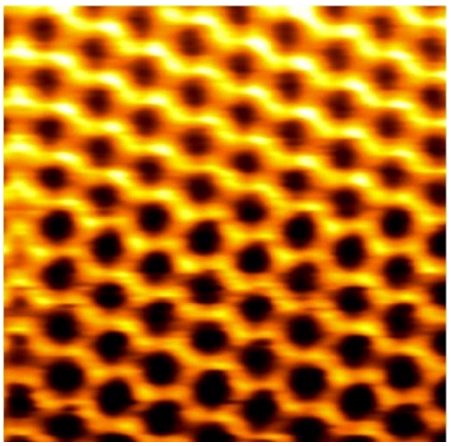

FIGURE 1.4: An atomic resolution AFM image of a graphite flake [40]

1.1.4.3 Electron Microscopy

SEM scans a high energy beam of electrons across the surface of a sample and collects scattering information to reconstruct an image. SEM can resolve features down to a few nanometers, so atomic resolution is not possible. However, SEM gives useful qualitative information about CVD graphene films. SEM is the primary technique used for film characterization on the native copper substrate. In FIGURE 1.5 graphene crystals and film can be seen on Cu substrate.

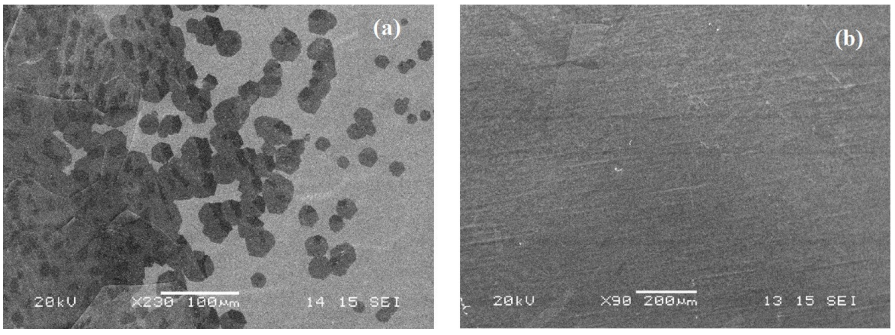

FIGURE 1.5: An SEM image of (a) graphene crystals and (b) film on copper

TEM, is an electron microscopy technique which can resolve atomic features. TEM is the electron analog of optical microscopy: electrons pass through and interact with a transparent sample and are collected at a detector to form an image. Because of the much smaller de Broglie wavelength of electrons as compared to optical light, much smaller features can be resolved. TEM provides the best images of the structure of single and bi-layer graphene films. FIGURE 1.6 is an excellent example of TEM characterization.

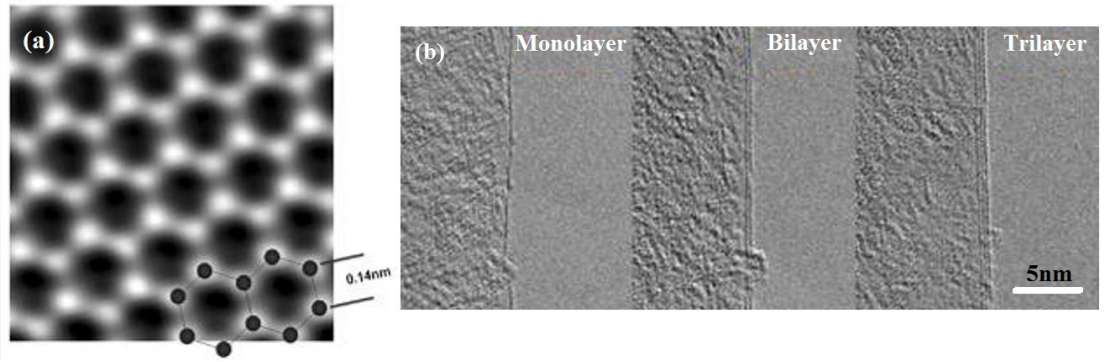

FIGURE 1.6: A high-resolution transmission electron micrograph showing (a) individual carbon atoms arranged hexagonally in a perfect graphene sheet [41] and (b) Number of layers [38].

1.1.4.4 Raman Spectroscopy

Raman spectroscopy is an important characterization tool used to probe the phonon spectrum of graphene. Raman spectroscopy of graphene can be used to determine the number of graphene layers and stacking order as well as density of defects and impurities. The three most prominent peaks in the Raman spectrum of graphene and other graphitic materials are the G band at $1580cm^{-1}$, the 2D band at $2680cm^{-1}$, and the disorder-induced D band at $1350cm^{-1}$ (FIGURE 1.7). The intensity ratio of the G and D band can be used to characterize the number of defects in a graphene sample [42].

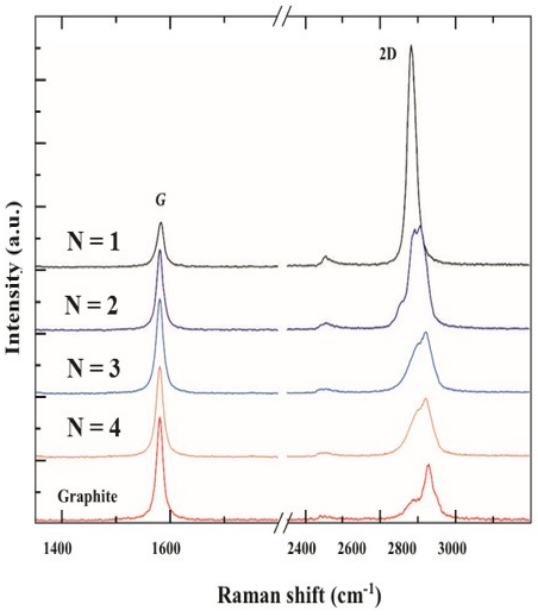

FIGURE 1.7: Layer dependence of graphene Raman spectrum. Raman spectra of N = 1-4 layers of graphene on Si/SiO_2 and of bulk graphite. Figure adapted from [44].

The line shape of the 2D peak, as well as its intensity relative to the G peak, can be used

to characterize the number of layers of graphene present as illustrated in FIGURE 1.7. Single-layer graphene is characterized by a very sharp, symmetric, Lorentzian 2D peak with an intensity greater than twice the G peak. As the number of layers increases, the 2D peak becomes broader, less symmetric, and decreases in intensity [43].

1.1.5 Graphene Doping

Among all properties, the unique electronic properties are assumed to be the most intriguing aspect of graphene, for example, outstanding ballistic transport properties and longest mean free path at room temperature[45], distinctive integral and half-integral quantum hall effect [46] , the highest mobility [47] to increase the speed of devices, and so on. The mobility of graphene is significantly higher than that of the widely-used semiconductor Si, of approximately $1400 cm^2 V^{-1} s^{-1}$. Consequently, graphene has been considered as a candidate material for applications in post-silicon electronics. However, most electronic applications are handicapped by the absence of a semiconducting gap in pristine graphene. For example, the devices made from the zero-bandgap graphene are difficult to switch off, losing the advantage of the low static power consumption of the complementary metal oxide semiconductor (CMOS) technology. Therefore, opening a sizeable and well-tuned bandgap in graphene is a significant challenge for graphene-based electron-devices. Liu group synthesized N-doped graphene by CVD, using a $25nm$ thick Cu film on a Si substrate as the catalyst under H_2 (20% in Ar) atmosphere and CH_4 + NH_3 as the C and N source, respectively [48]. Lately, Zhang et al. [49] synthesized the N-doped graphene using the embedded C and N by CVD method. After further improvement, CVD method will have great prospect for producing large-scale high-quality single-layer substitutional doped graphene. The intact pristine graphene has a perfect structure, and it is difficult to introduce foreign atoms in the whole plane. Gong group reported the N-doping of graphene through NH_3 annealing after N^+ ion irradiation [50], and the stable and homogenous N-doped graphene can be reproducibly obtained.

1.2 Molybdenum Disulfide (MoS_2)

The basic unit of MoS_2 is composed of a molybdenum atom coordinated with six sulphur atoms. It is organized in two layers of sulphur atoms forming a sandwich structure, with a layer of molybdenum atoms in the middle. Each sulphur atom is coordinated with three molybdenum atoms within a single 2D layer of MoS_2. The bulk material is formed of these 2D layers held together by van der Waals forces.

MoS_2 is a layered material, of which neighbouring layers are coupled by van der Waals interactions with an interlayer spacing of $0.65nm$. Each layer consists of a partially ionically-bonded

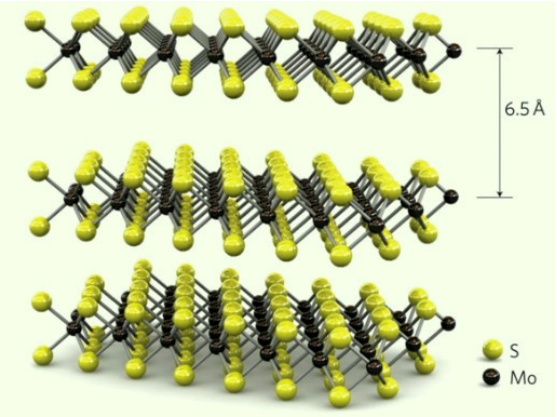

FIGURE 1.8: Atomic structure of layered hexagonal MoS_2

$S - Mo - S$ sandwich structure with Sulphur atoms arranged in two hexagonal planes and a plane of Mo atoms in between, as shown in FIGURE 1.8 [51].

1.2.1 Properties of MoS_2

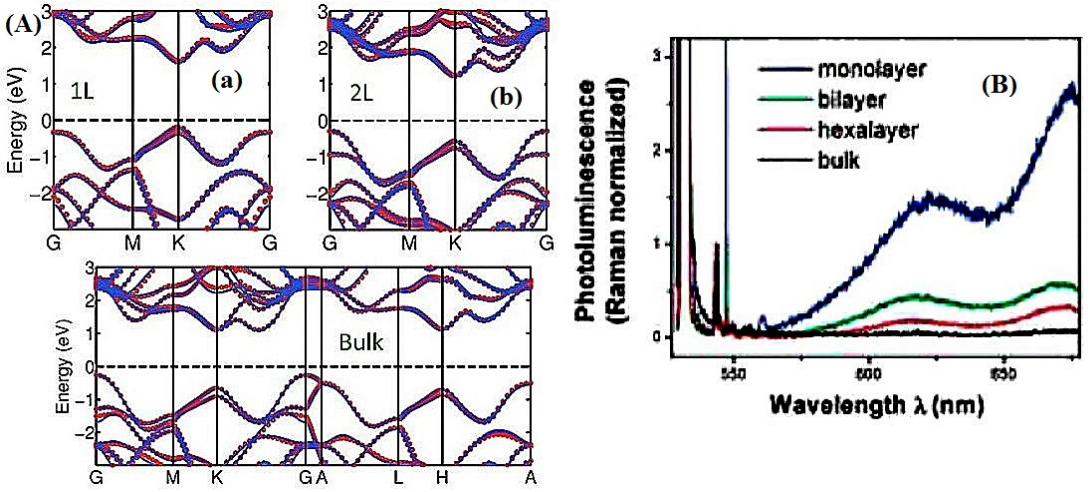

FIGURE 1.9: (A) Calculated band structures of (a) 1L (b) 2L (c) Bulk MoS_2. The arrows indicate the lowest energy transitions. (B) Photoluminescence spectra normalized by Raman intensity for MoS_2 layers with different thickness.

MoS_2 belongs to the family of TMDs, a semiconductor with strong spin-orbit interactions, and coupled spin-valley degrees of freedom. Electron-electron interaction effects are important in TMD semiconductors because of their in-plane effective masses are comparatively large $(m* \sim 0.4)$. In practice, TMDs have been mostly used as channel material in FET, in both top and back 6 gated configurations, showing intrinsic mobility at room temperature up to $50cm^2/V \cdot s$ and more than 10^5 on/off ratio.

1.2.2 MoS_2 Synthesis

1.2.2.1 Exfoliation

Graphene's successful exfoliation from bulk graphite paves way for the fabrication of other graphene-like 2D materials [80] through the simple "Scotch-tape Method" [52]. Due to high quality monolayers occurring from mechanical exfoliation, this method is popularly used for intrinsic sheet production and fundamental research [53]. Nevertheless, this method is not suitable for practical applications on a large scale due to its low yield and disadvantages in controlling sheet size and layer number. In 2012, Karim Gacem's group proposed a general technique for fabricating high quality 2D layered materials, which was called anodic bonding. Sizes of few-layer MoS_2 obtained were relatively controllable and larger, ranging from $10mm$ to several hundred microns [55].

1.2.2.2 CVD Synthesis

CVD approach has attracted widely attention because it could synthesis $2D$ TMDCs on a wafer-scale, which shows great potential toward practical applications like large-scale integrated electronics. This method not only could prepare continuous single film with certain thickness, but highlight in directly growth layered heterostructures, which would largely avoid interfacial contamination introduced during layer by layer transfer process. Typically, the following precursors are used to prepare MoS_2 film, including Mo based compound powder [56], deposited Mo based film [57], ammonium thiomolybdates [$(NH_4)_2MoS_4$)] film [58] and MoS_2 powder [59].

1.2.2.3 Sulfurization of Mo based compounds

In 2012, for the first time, Lain-Jong Li's group reported a CVD method to synthesis large-area, monolayer MoS_2 films on SiO_2 substrate in ambient environment. MoO_3 and S powders acted as solid reactants and SiO_2 substrate should be pretreated by graphene-like molecules to increase nucleation points [56]. AFM cross-sectional profile characterization illustrates the thickness of MoS_2 layer is about $0.72nm$, very close to that of mechanically exfoliated single layer. Later in 2013, Yifei Yu's group proposed a self-limiting CVD method under a pressure around $2Torr$ to prepare uniform MoS_2 films of centimeters by changing MoO_2 to molybdenum chloride ($MoCl_5$) as precursors [60].

1.2.2.4 Sulfurization of Mo and Mo based oxides

To further improve the uniformity in large areas, Yongjie Zhan's group pre-deposited a thin layer of Mo ($\sim 1-5nm$) on SiO_2 by e-beam evaporation, and then this substrate was placed in a tube furnace to react with sulfur vapor at $750°C$ [61]. The resulted samples were bi- or tri-layered in thickness [61]. Lain-Jong Li's group further adopted the similar way to thermally deposit MoO_3 thin films on the sapphire substrate. After two-step thermal reaction, MoO_3 was successfully sulfurized to be MoS_2 with few layer [62].

1.2.2.5 Thermal decomposition of $(NH_4)_2MoS_4$

Another effective approach to synthesis MoS_2 films in wafer scale with high controllability was through simple thermolysis of $[(NH_4)_2MoS_4]$. Keng-Ku Liu's group reported to have prepared bi- or tri-layer continuous films on insulating substrates through this method [58]. It was also confirmed that the second-step high temperature sulfurization process could improve the crystallization to a large extent.

1.2.2.6 Vapor-solid growth from MoS_2 powder

One particular and straightforward synthesis method needs to be mentioned was proposed by Sanfeng Wu and his coworkers in 2013, based on a vapor-solid growth mechanism, demonstrating the preparation of monolayer MoS_2 films on various insulating substrates [63]. As-grown flakes were about $25mm$ in dimension, with a maximum of $\sim 35\%$ at $\sim 1.92eV$ exhibiting substantial PL polarization at room temperature, which was comparable to that of samples prepared by mechanical exfoliation ($\sim 40\%$ at $300K$) [63].

1.2.3 Transfer of MoS_2

1.2.3.1 Transfer Using NaOH

To transfer as-grown MoS_2 onto fresh SiO_2 ($300nm$)/Si substrates, the MoS_2 film was coated with a layer of PMMA by spin-coating followed by baking at $100°C$ for $10min$. After that, the PMMA-capped MoS_2 was then put into a NaOH(2 M) solution at $100°C$ for $30min$. The PMMA-supported MoS_2 film was then transferred to DI H_2O to remove the etchant and residues. A fresh SiO_2/Si substrate was then used to fish out the PMMA-capped MoS_2 film, followed by drying on a hot-plate ($100°C$ for $10min$). The PMMA was removed by acetone,IPA, followed by DI water and chloroform rinsing [64].

1.2.3.2 Transfer Using Ultrasonic

As-grown MoS_2 on the growth substrate (SiO_2/Si, mica, STO, or sapphire) is first spin-coated with PMMA, which is then cured. The PMMA/MoS_2/substrate stack is then immersed into a beaker of water kept in an ultrasonic cleaner. Within one minute, the edge of the PMMA/MoS_2 film can be seen detaching from the substrate, eventually causing the PMMA/MoS_2 stack to float to the surface of the water. The delaminated PMMA/MoS_2 films can then be transferred onto any target substrate. Once the film is deposited on the target substrate, the PMMA can then be removed with acetone; this is the same process as the one used in graphene transfer. Notably, the entire delamination process uses only water, and involves no chemical etchants or hazardous pollutants [65].

1.2.4 Characterization of MoS_2

1.2.4.1 Optical Microscopy

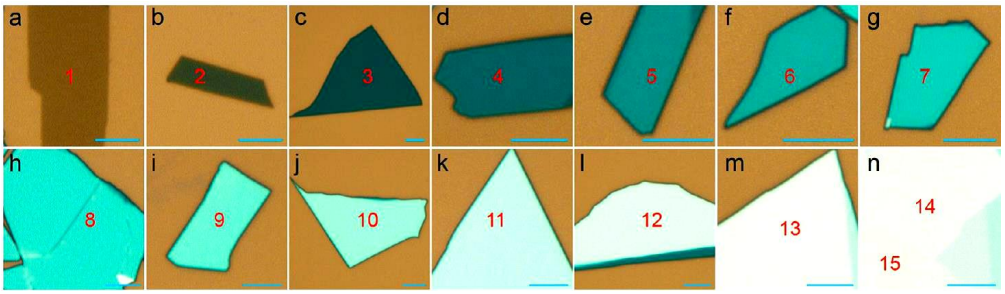

FIGURE 1.10: (a-n) Color optical images of 1L-15L MoS_2 nanosheets on $90nm$ SiO_2/Si. The scale bar is $5\mu m$ for each image. The digitals shown in (a_n) indicate the layer numbers of corresponding MoS_2 nanosheets [66]

1.2.4.2 Raman Spectroscopy

MoS_2 shows two prominent Raman features; the in-plane E^1_{2g} mode at $\sim 385cm^{-1}$ and the out-of-plane A^1_g mode at $\sim 405cm^{-1}$ [FIGURE 1.11(a)-(b)]. These two modes are sensitive to the number of MoS_2 layers as shown in FIGURE 1.11(c). The A^1_g mode upshifts, while the E^1_{2g} mode downshifts with increasing thickness, as shown in FIGURE 1.11(d). The frequencies of the modes reach those of bulk MoS_2 at approx six layers [93].

The stiffening of the A^1_g mode with thickness can be explained qualitatively by the effect of the interlayer van der Waals attractions. FIGURE 1.11(e) shows the line widths of the E^1_{2g} and A^1_g modes as functions of the number of layers. The linewidth of the A^1_g mode decreases with increasing thickness, while that of E^1_{2g} is nearly independent of thickness. Thus, the frequencies

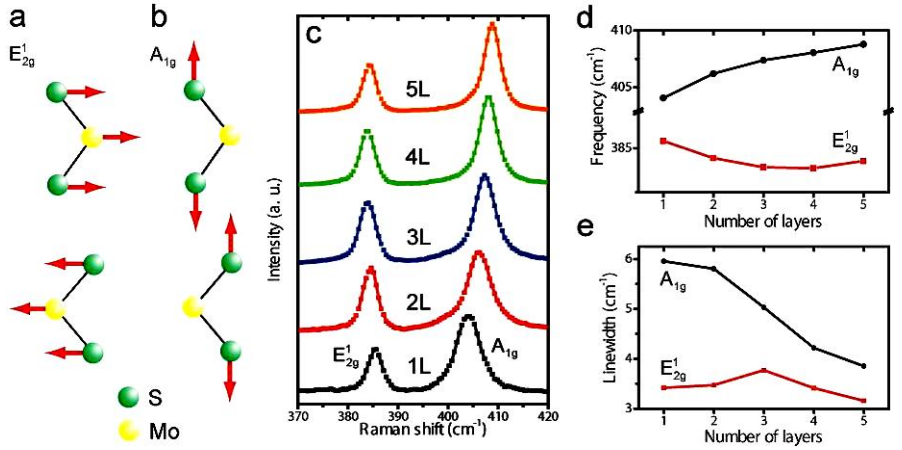

FIGURE 1.11: The Raman spectra of atomically thin MoS_2 (a) and (b) Vibrations of S and Mo atoms for the E^1_{2g} and A^1_g modes(c) Raman spectra showing layers of MoS_2 (d) The frequencies of the E^1_{2g} and A^1_g modes as functions of the number of layers (e) The linewidths of the E^1_{2g} and A^1_g modes as functions of the number of layers [67].

of the Raman E^1_{2g} gand A^1_g modes, along with the linewidth of the A^1_g mode, can be used to determine the thickness of atomically thin MoS_2.

1.2.4.3 Photoluminescence Study of MoS_2

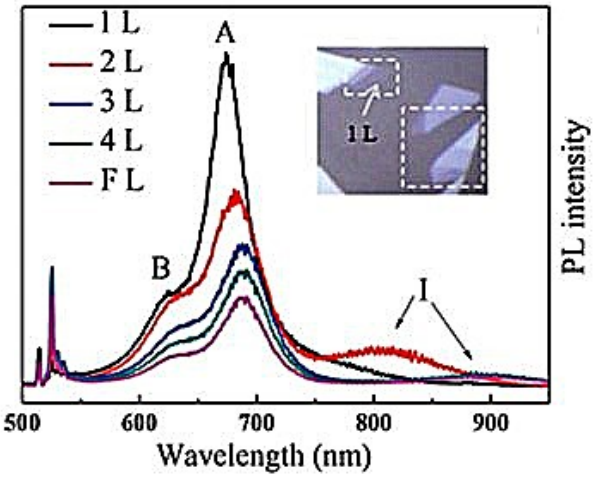

FIGURE 1.12: PL spectra of the MoS_2 films obtained at $514nm$ laser excitation [69]

The PL intensity decreased with increasing atomic thickness due to the direct to-indirect bandgap transition. The average PL spectra obtained from each film thickness region displayed this trend, as shown in FIGURE 1.12. Two exciton PL peaks at $1.83eV$ and $1.98eV$ originated from the transition in the K-point of the Brillouin zone [68].

1.2.4.4 TEM characterizations of MoS_2

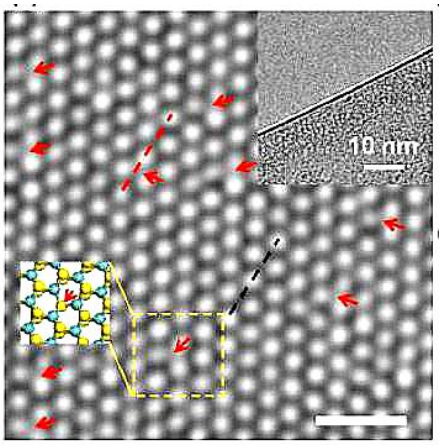

FIGURE 1.13: Atomic structures of a single-layer MoS_2 by aberration-corrected TEM. The SV vacancies are highlighted by red arrows. Upper inset shows the MoS_2 sample edge to confirm the single-layer nature. Lower inset shows the schematics of the highlighted region. Scale bar, $1nm$ [70].

1.3 Carbon Nanotubes (CNT)

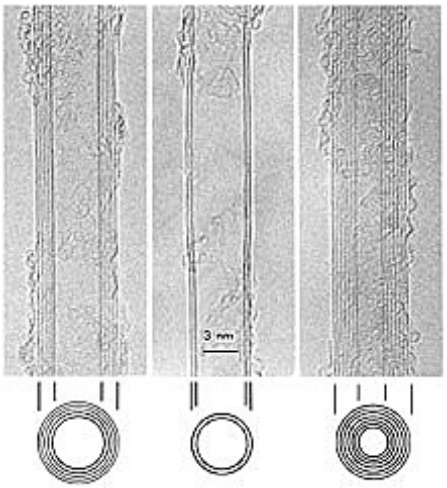

FIGURE 1.14: TEM images of MWNTs observed by Sumio Iijima (Source: Iijima 1991) [72]

By rolling a graphene sheet into a cylinder and capping both end of the cylinder with a half of fullerene molecule a carbon nanotube is formed. Harry Kroto discovered C60 molecule in 1985 [71] while experimenting a laser ablation system for the vaporization of graphite by laser beams and depositing them on a copper collector and it was the beginning of a new area in carbon material science. At 1990s arc discharge method was reported in order to make large quantities of the C60 molecule. In 1991, Iijima experimented this technique in order to observe fullerene and by passing large current between two graphite rods, he vaporised them and condensed them

on Cu tip. When he looked at the result through an electron microscope, he noticed something unexpected, he discovered CNTs [72] at the negative electrode of an arc discharge. They were tiny tubes of pure carbon with a large amount of other forms of carbon. These first CNTs were like Russian dolls, several concentric layers with caps at the end, so they were called MWCNTs. TEM images of these tubes are shown in figure 1.14. Only two years later, in 1993, SWCNTs could be grown using Co metal catalysts by arc discharge method [73].

1.3.1 Properties of CNTs

The atomic arrangements of carbon atoms are responsible for the unique electrical, thermal, and mechanical properties of CNTs. These properties are discussed below:

1.3.1.1 Electrical Conductivity

A metallic CNT can be considered as highly conductive material. Chirality, the degree of twist of graphene sheet, determines the conductivity of CNT interconnects. Depending on the chiral indices, CNTs exhibit both metallic and semiconducting properties. The electrical conductivity of MWNTs is quite complex as their inter-wall interactions non-uniformly distribute the current over individual tubes. Electrodes are placed to measure the conductivity and resistivity of different parts of SWNT rope. The measured resistivity of the SWNT ropes is in the order of $104\Omega cm$ at $27°C$, indicating SWNT ropes to be the most conductive carbon fibers [74].

1.3.1.2 Strength and Elasticity

Each carbon atom in a single sheet of graphite is connected via strong chemical bond to three neighbouring atoms. Thus, CNTs can exhibit the strongest basal plane elastic modulus and hence are expected to be an ultimate high strength fiber. The elastic modulus of SWNTs is much higher than steel that makes them highly resistant. Although pressing on the tip of nanotube will cause it to bend, the nanotube returns to its original state as soon as the force is removed. This property makes CNTs extremely useful as probe tips for high resolution scanning probe microscopy. Although, the current Youngs modulus of SWNT is about $1TPa$, but a much higher value of $1.8TPa$ has also been reported [75]. It has been observed that the elastic modulus of MWNTs is not strongly dependent on the diameter. Primarily, the moduli of MWNTs are correlated to the amount of disorder in the nanotube walls [76].

1.3.1.3 Thermal Conductivity and Expansion

CNTs can exhibit superconductivity below $20K$ (approximately $-253°C$) due to the strong in-plane C-C bonds of graphene. The strong C-C bond provides the exceptional strength and stiffness against axial strains. Moreover, the larger interplane and zero in-plane thermal expansion of SWNTs results in high flexibility against non-axial strains. Due to their high thermal conductivity and large in-plane expansion, CNTs exhibit exciting prospects in nanoscale molecular electronics, sensing and actuating devices, reinforcing additive fibers in functional composite materials, etc. Recent experimental measurements suggest that the CNT embedded matrices are stronger in comparison to bare polymer matrices [77].

1.3.1.4 Field Emission

Under the application of strong electric field, tunnelling of electrons from metal tip to vacuum results in field emission phenomenon. Field emission results from the high aspect ratio and small diameter of CNTs. The field emitters are suitable for the application in flat-panel displays. For MWNTs, the field emission properties occur due to the emission of electrons and light. Without applied potential, the luminescence and light emission occurs through the electron field emission and visible part of the spectrum, respectively [78].

1.3.2 Synthesis of CNTs

There are several methods used for fabrication of CNTs. The focus is to find a technique that is easy, can produce cheap CNTs of high quality, with high production rate (which yields a lot of CNTs per unit of time) and that produces CNTs with minimal defects. Additionally, it is very important to be able to control the diameter, chirality, the number of shells (for a MWCNT) and the purity, since all these parameters will influence the properties [79]. There are several methods for synthesis of CNTs, but three of them are considered as the general and widely known synthesis methods [80].

1.3.2.1 Arc Discharge

This method is known to be the first synthesis method for the production of CNTs, since the discovered tubes were synthesized by this technique. It was originally used in the production of the C60 (buckyballs), but because of its simplicity it is still one of the most common fabrication methods. The most frequently used arc discharge technique is the electric charge method, commonly known as the electric arc discharge. An electric arc discharge is generated between two graphite electrodes in this method, which causes the graphite to vaporize and condense at

the cathode. The process is done under an inert atmosphere that consists of He or Ar. A very high temperature is obtained that allows transition of carbon from solid- to gas-phase without passing through an intermediate liquid phase (sublimation).

1.3.2.2 Laser Ablation

This method vaporizes a piece of graphite by irradiation with a Nd YAG laser in a chamber with temperature of $12000°C$ in a flow of inert gas, such as He or Ar. The vapour is carried with the gas flow to a cooled wall of quartz tube where it condenses into a mixture of fullerenes and CNTs. As in the arc discharge method, a purification step is needed to obtain the CNTs. The laser ablation method is capable of yield up to 70% and is able to produce SWCNTs and MWCNTs. It is especially known to give SWCNTs of high quality and purity.

1.3.2.3 CVD

CVD is a parent to a family of processes where deposition of a solid material on a surface is caused by reactions with the precursor gases in the chamber and the heated surface of the substrate. The growth process of the CNTs involves decomposition of carbon containing gases where carbon is diffused towards a heated substrate which is coated with catalyst particles. The carbon binds to these particles and acts as a nucleation site for the initiation of CNT growth.

Since it is impossible to remove the catalyst particle during growth, post treatments are necessary. Since the target is CNTs of high purity, a purification step is required, which can be done by acid treatment, oxidative treatments in the gaseous phase/liquid phase and ultrasound methods [79].

The two most important parameters in the synthesis of CNTs by CVD is the size of the catalyst particle and the carbon source. The major advantage with CVD is that it allows more control over the morphology and structure of the produced CNTs and can give controlled alignment, such as producing small free standing SWCNTs if the process parameters are controlled, instead of the mixtures which is obtained by the arc discharge and laser ablation method. The CVD is known to produce CNTs of high purity and offers a yield between $20 - 100\%$. Even though it possesses promising characteristics, the main problem with this method is the scalability and reproducibility in the production of CNTs [81].

1.3.3 Characterization of CNTs

This study is a parametric study whose aim is to find optimal growth and pretreatment conditions for high quality and high yield, therefore, through characterization of obtained CNTs is essential.

In this study, the catalyst was characterized by XRD, N_2 adsorption (BET surface area) and SEM, and purified and unpurified CNT samples were analyzed with SEM, thermo-gravimetric analysis (TGA), Raman spectroscopy, and TEM.

1.3.3.1 SEM Study

SEM is nothing but study of sample morphology by scanning the surface with a high energy beam of electrons. SEM is the first step to characterize the CNTs. Using SEM, morphology of CNTs, their dimensions and their orientations can readily be seen [82]. Diameters of CNTs also can be measured roughly with SEM.

1.3.3.2 TEM Study

The internal microstructure and crystal structure of samples which are thin enough to transmit electrons can be analyzed with TEM. TEM is used to measure outer and inner radius and linear absorption coefficient for CNT studies. It is the most useful instrument in order to determine the diameter of SWNTs and MWNTs and the number of walls. The inter shell spacing of MWNTs [83] also is studied with high resolution TEM and found between the ranges of $0.34 - 0.39nm$. Another subject studied with TEM is SWNTs helicity [84].

1.3.3.3 Raman Spectroscopy Study

The characteristic spectrum of SWNTs includes three main zone. At low ($100 - 250cm^{-1}$), intermediate ($300 - 1300cm^{-1}$) and high ($1500 - 1600cm^{-1}$) frequencies [85].

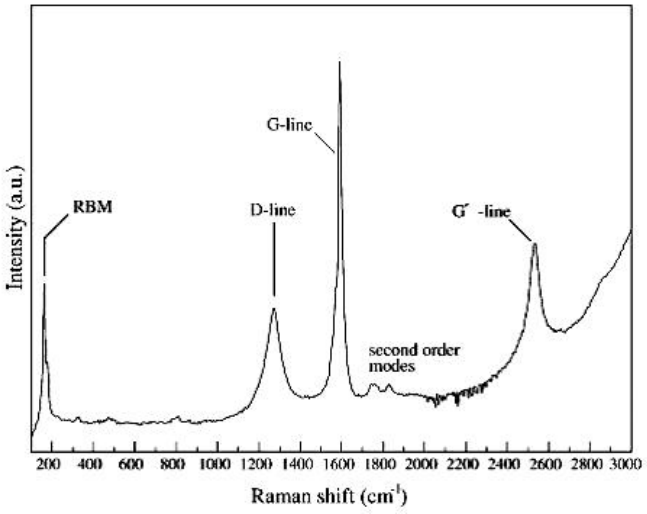

FIGURE 1.15: Raman spectrum of CNTs [90]

There are two main first order peaks for carbon-based materials. The first one is the D peak, it is observed around $1300cm^{-1}$ for excitation He-Ne laser, or at $1350cm^{-1}$ for an Ar ion laser. The D peak shows the presence of defects [86]. The other one is the G peak and observed at about $1580cm^{-1}$, which is related to the in-plane vibrations of the graphene sheet [87]. Ratios of the D peak to the G peak is significant for CNT characterization because it gives the amount of disorder within nanotubes [88]. A small I_D/I_G ratio, in the range of 0.1-0.2, indicates that the defect level in the atomic carbon structure is low, and it means that reasonable crystalline quality observed [89].

1.4 Graphene-MoS_2 Hybrids

As graphene and single layer MoS_2($SLMoS_2$) have complementary physical properties, it is natural to combine graphene and $SLMoS_2$ in specific ways to create heterostructures that mitigate any negative properties [91, 92]. A few experiments have investigated the advanced properties of graphene/MoS_2 heterostructures. Britnell et al. found that graphene/MoS_2 heterostructures have high quality photon absorption and electron-hole creation properties because of the enhanced light-matter interactions in the $SLMoS_2$ [91]. As discussed earlier, graphene has outstanding mechanical properties. These mechanical properties have been used to protect MoS_2 films from radiation damage [93]. Recently, Larentis et al. measured the electron transport in graphene/MoS_2 heterostructures and observed a negative compressibility in the MoS_2 component [94].

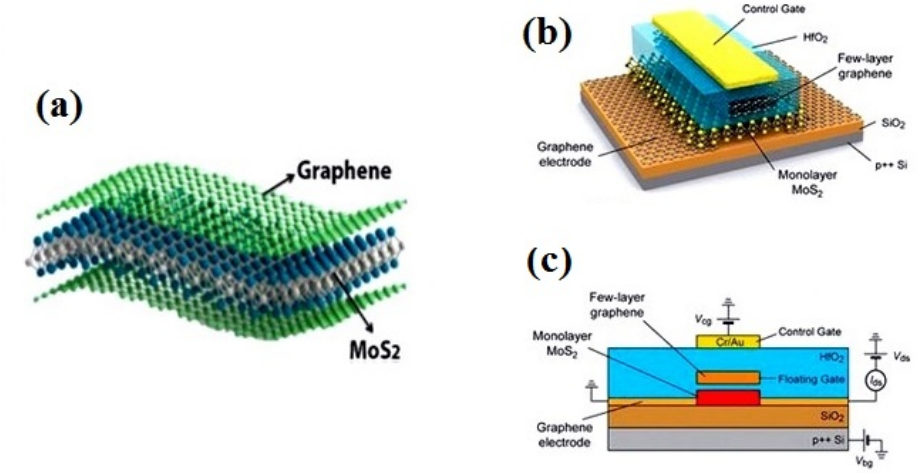

FIGURE 1.16: (a)MoS_2/graphene heterostructure memory layout (b) 3D schematic view of the memory device based on single-layer MoS_2 (c) Schematics of a heterostructure memory cell with a single-layer MoS_2 semiconducting channel, graphene contacts and multilayer graphene MLG floating gate. The MLG floating gate is separated from the channel by a thin tunnelling oxide [94].

This surprising phenomenon could be explained based on the interplay between the Dirac and parabolic bands for graphene and MoS_2, respectively. Yu et al. fabricated high-performance electronic circuits based on a graphene/MoS_2 heterostructure with MoS_2 as the transistor channel and graphene as the contact electrodes and the circuit interconnects [95].

1.5 Graphene-CNT Hybrids

Two most exotic classes of functional carbon materials representing 1D and 2D nanostructures. With an intention of combining them together in to a single structure, in this communication, we report on vertically aligned, interconnected graphene arrays grown on arrays of CNTs.

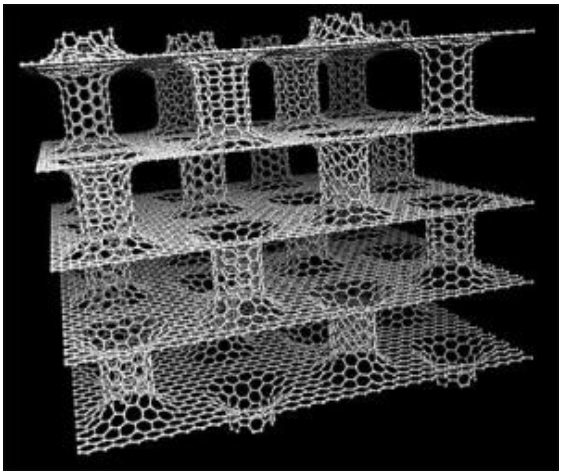

FIGURE 1.17: Pillared graphene:A novel 3-D network nanostructure proposed for enhanced hydrogen storage [100]

A heterostructure comprised of the integration of a 1D material having a basis in its 2D complement may deliver fascinating properties both for fundamental understanding as well as practical implications [95]. Theoretical investigations of such structures reveal well defined deviations from the honeycomb carbon lattice near the junction. Recently, studies have also suggested the possibility of intriguing new transport properties, such as coupling and resonance of electronic states [97, 98]. It has been shown that stacked graphene CNTs can act as moderate photoconductors [99]. In addition, efficient and economically viable hydrogen storage possibility has also been envisioned [100]. Also, physical mixtures of CNTs and graphene exhibit high transparent conductance [101].

1.6 Motivation

Since Moores law approaches its physical limit in Si-based electronics, the world has been actively searching for new material options that can push performance beyond its traditional

boundaries. Quasi 2D (Q2D) materials have countless novel properties and have attracted intense research interest over the past decades. The Q2D family currently contains the following materials: graphene, hexagonal boron nitride, 2D honeycomb silicon, layered TMD (including MoS_2 and WS_2), black phosphorus, and 2D ZnO. Among the Q2D family of materials, graphene and MoS_2 are well known for their excellent mechanical flexibility and transport properties and applications thereof.

To harvest their full advantage in bendable electronic devices, it is highly desirable to transfer graphene on to several flexible substrates, making it eligible for flexible electronics. In this route, transferring graphene on to cellulose paper, cloth, and 2D materials can be an interesting approach. This will widen the graphene application window for the future. The fabrication process solely based on 2D materials and their heterostructures is very important to extract some of their unique properties. So far, the circuits that have been constructed based on 2D materials typically rely on a metal to form contacts and interconnects, which is one of the key limitations to the circuit flexibility. A high-quality junction between a semiconductor and a metallic contact with no energy barrier is crucial for high-performance devices, but is hard to achieve for 2D TMD because of their large bandgap.

On the other hand, the recent emergence of graphene, a one atom thick sp^2-hybridized 2D honeycomb lattice of a carbon allotrope, has opened up innumerable opportunities in the field of materials science and nanotechnology research. The weakness of graphene can be overcome by doping it with heteroatoms like B and N, by which a band gap can be introduced in the graphene making it practically available for all semiconducting applications. The other way is, developing structures wherein graphene acts as a platform for support, scaffold, or a 2D planar substrate for anchoring other nanomaterials. For example, CNTs, whose properties emerge in the axial direction, can be functionalized onto the surface of graphene, combining the properties of these two carbon allotropes in all directions while allowing for an increased active surface area and faster electron transfer kinetics. This transformation of 2D graphene into 3D architectures expands the functionality of nanomaterials and serves as novel hybrid electrode material for applications in electronic energy storage.

1.7 Outline of Thesis

The following thesis is mainly about synthesis of Graphene, MoS_2 and CNT with their heterostructure fabrication. It also includes study of transfer of the graphene on different kind of moldable substrates (in this case CA) by hot press technique. Synthesis of N-doped graphene is also discussed.

Chapter 1 gives a general introduction about all possible synthesis and transfer techniques for given materials as well as their application in the heterostructure formation.

Chapter 2 explained all instrumental processes in detail. Schematic diagrams are provided for the better understanding.

Chapter 3 discuss about polymer free transfer of graphene on cellulose acetate moldable and flexible substrate like CA. This transfer was done with the help of hot press technique and without the use of PMMA.

Chapter 4 describes Graphene-CNT hybrid structure for the interconnect application. Both graphene and CNTs were synthesized by CVD method. A 3D structure was fabricated by growing VACNTs on transferred graphene.

In **Chapter 5**, a non-volatile memory device was fabricated using graphene as a metal electrode and MoS_2 as a charge trapping semiconductor with on/off ratio of as high as 2.5E3.

In **Chapter 6**, incorporation of nitrogen in the graphene during CVD synthesis have investigated using Melamine, PAN and Triazine as a N-source whereas Camphor as a carbon source

Finally, **Chapter 7** will present overall summary of dissertation about above mentioned approaches and futuristic work.

References

[1] K. Geim, Science 324 (2009) 1530–1534

[2] H. C. Neto, F. Guinea, N. M. R. Peres, K. S. Novoselov, and A. K. Geim, Reviews of Modern Physics 81 (2009) 109–161

[3] Barth and W. Marx, Tech. Rep. 118 (2008)

[4] H. P. Boehm, R. Setton, and E. Stumpp, Pure Appl.Chem., (1994) 1893–1901

[5] R. Saito, G. Dresselhaus, and M. S. Dresselhaus, Physical Properties of Carbon Nanotubes. Imperial College Press (1998)

[6] P. R. Wallace, Phys. Rev., 71 (1947) 622–634

[7] G. S. Painter and D. E. Ellis, Phys. Rev. B, 1 (1970) 4747–4752

[8] S. Wang and P. R. Buseck, Chemical Physics Letters, 182 (1991)

[9] H. Kroto, J. Heath, S. O'Brien, R. Curl, and R. Smalley, Nature 318(1985) 162–163

[10] J.W. McClure, Phys.Rev., 108 (1957) 612–618

[11] D. P. DiVincenzo and E. J. Mele, Phys. Rev. B 29 (1984) 1685–1694

[12] L. D. Landau, Phys. Z. Sowjetunion, 11 (1937) 26-35

[13] Lee, C.; Wei, X.; Kysar, J. W.; Hone, J. Science 321 (2008) 385-388

[14] Balandin, A. A.; Ghosh, S.; Bao, W.; Calizo et al, Nano Letters 8 (2008) 902-907

[15] Ho, C. Y.; Powell, R. W.; Liley, P. E. Journal of Physical and Chemical Reference Data 1 (2009**)** 279-421

[16] Nika, D. L.; Ghosh, S.; Pokatilov, E. P.; Balandin, A. A.Applied Physics Letters 94 (2009) 203103

[17] Du, X.; Skachko, I.; Barker, A.; Andrei, E. Y. Nature nanotechnology 3 (2008**)** 491-495

[18] Meyer, J. C.; Geim, A. K.; Katsnelson, M. I.; Novoselov, K. S.; Booth, T. J.; Roth, S. Nature 446 (2007**)** 60-63

[19] Novoselov K.S., Geim A.K., Morozov S.V., Jiang D., Zhang Y., Dubonos S.V., Grigorieva I.V., and Firsov A.A. Science 306 (2004) 666-669

[20] Wu Z., Ren W., Gao L., Liu B., Jiang C., and Cheng H.. Carbon 47(2009) 493

[21] Rollings E., Gweon G.H., Zhou S. Y., et al. Journal of Physics and Chemistry of Solids 67 (2006) 2172-2177

[22] Amini S., Garay J., Liu G., Balandin A.A., Abbaschian R. J. Appl. Phys., 108 (2010) 094321

[23] Sun Z., Yan Z., Yao J., Beitler E., Zhu Y., and Tour J. M. Nature letter 468 (2010) 549-552

[24] Stankovich S., Piner R.D., Nguyen S.T., Ruoff R.S.Carbon 2006; 44 (2006) 3342–3347

[25] Brodie B.C. Ann. Chim. Phys. 59 (1860) 466–472

[26] Hummers W., Offeman R. J. Am. Chem. Soc.80 (1958) 1339

[27] Staudenmaier L. Dtsch. Chem. Ges 31 (1898) 1481–1499

[28] Bourlinos A.B., Gournis D., Petridis D., Szabo T., Szeri A., Dekany I. 19 (2003) 6050–6055

[29] Titelman G.I., Gelman V., Bron S., Khalfin R.L., Cohen Y., Bianco-Peled H. Carbon 43 (2005) 641-649

[30] Yu Q., Lian J., SiriponglertS., Li H., Chen Y. P., and Pei S. S. Appl. Phys. Lett., 93 (2008) 113103

[31] Li X., Cai W., An J., Kim S., Nah J., Yang D., Piner R., et al. Science, 324 (2009) 1312

[32] Wang J. J., Zhu M. Y., Outlaw R. A., Zhao X., Manos D. M., Holloway B. C., Mammana V. P. Applied Physics Letters 85 (2004) 1265

[33] Ismach A., Druzgalski C., Penwell S., Schwartberg A., Zheng M., Javey A., Bokor J., and Zhang Y. Nano Lett., 10 (2010) 1542-1548

[34] Zhang Y, Zhang L, Zhou C, Accounts .Chem. Res 46 (2013) 2329-2339.

[35] Jae-Young Choi, Nature Nanotechnology 8 (2013) 311–312

[36] L. Gao, et al, Nature Communications 3 (2012) 699

[37] Sandeep Gorantla a, Alicja Bachmatiuk bc, Jeonghyun Hwang et al, Nanoscale 6 (2014) 889-896

[38] Bae S et al, Nat. Nanotechnology 5 (2010) 574–578

[39] P. Blake, E.W. Hill, A.H. Castro Neto, K.S. Novoselov, D. Jiang, R. Yang, T.J. Booth,and A.K. Geim. App. Phys. Lett., 91 (2007)1063124

[40] H.P. Boehm, A. Clauss, U. Hofmann, and G.O. Fischer. Proceedings of the Fifth Conference on Carbon, 1962

[41] Albert Dato, Zonghoon Lee, Ki-Joon Jeon, et al, Chem Comm.(2009) 6095-6097

[42] M. A. Pimenta, G. Dresselhaus, M. S. Dresselhaus, et al, Physical Chemistry Chemical Physics 11 (2007) 1276–1291

[43] Y. Y. Wang, Z. H. Ni, T. Yu et al., Journal of Physical Chemistry C 112 (2008) 10637–10640

[44] V. Yu, Optics and chemical vapour deposition of graphene monolayers on various substrates, Ph.D. thesis, Mcgill University (2010)

[45] Gunlycke, D.; Lawler, H. M.; White, C. T. Phys. Rev. B 75 (2007) 085418

[46] Novoselov, K. S.; Jiang, Z.; Zhang, Y.; Morozov, S. V.; Stormer, H. L.; Zeitler, U.; Maan, J.C.; Boebinger, G. S.; Kim, P.; Geim, A. K. Science 315 (2007) 1379.

[47] Du, X.; Skachko, I.; Barker, A.; Andrei, E. Y. Nat. Nanotech. 3 (2008) 491-495.

[48] Wei, D. C.; Liu, Y. Q.; Wang, Y.; Zhang, H. L.; Huang, L. P.; Yu, G. Nano Lett. 9 (2009), 1752-1758

[49] Zhang, C.; Fu, L.; Liu, N.; Liu, M.; Wang, Y.; Liu, Z. Adv. Mater. 23 (2011)

1020-1024
[50] Guo, B.; Liu, Q.; Chen, E.; Zhu, H.; Fang, L.; Gong, J. R. Nano Lett. 10 (2010) 4975-4980
[51] Q.H. Wang, K. Kalantar-Zadeh, A. Kis, J.N. Coleman, and M.S. Strano, Nature Nanotechnol. 7 (2012), 699–712
[52] Li H, Wu J, Yin Z, Zhang H. Acc Chem Res 47 (2014) 1067-1075
[53] Novoselov KS, Geim AK, Morozov SV, Jiang D, Zhang Y, Dubonos SV, et al. Electric field effect in atomically thin carbon films. Science (2004) 1067-1075
[54] Radisavljevic B, Radenovic A, Brivio J, Giacometti V, Kis A. Nat Nanotechnol 6 (2011) 147-150
[55] Gacem K, Boukhicha M, Chen Z, Shukla A. Nanotechnology 23 (2012) 1-5
[56] Lee YH, Zhang XQ, Zhang W, Chang MT, Lin CT, Chang KD, et al. Adv Mater 24 (2012) 2320-2325
[57] Zhan Y, Liu Z, Najmaei S, Ajayan PM, Lou J. Small 8 (2012) 966-971
[58] Liu KK, Zhang W, Lee YH, Lin YC, Chang MT, Su CY, et al. Nano Lett 12 (2012) 1538-1544
[59] Wu S, Huang C, Aivazian G, Ross JS, Cobden DH, Xu X. ACS Nano 7 (2013) 2768-2772
[60] Yu Y, Li C, Liu Y, Su L, Zhang Y, Cao L. Sci Rep 3 (2013) 1-6
[61] Zhan Y, Liu Z, Najmaei S, Ajayan PM, Lou J. Small 8 (2012) 966-971
[62] Lin YC, Zhang W, Huang JK, Liu KK, Lee YH, Liang CT, et al. Nanoscale 4 (2012) 6637-6641.
[63] Wu S, Huang C, Aivazian G, Ross JS, Cobden DH, Xu X. ACS Nano 7 (2013)2768-2772
[64] Lin YC, Zhang W, Huang JK, Liu KK, Lee YH, Liang CT, Chu CW, Li LJ Nanoscale. 8 (2012) 6637–6641
[65] Donglin Ma , Jianping Shi, Qingqing Ji1 , Yu Zhang et al, Nano Research 8 (2015) 3662–3672
[66] H. Li, J. Wu, X. Huang, G. Lu, J. Yang, X. Lu, Q. H. Xiong, H. Zhang: ACS Nano 7 (2013) 10344-10353.
[67] C. Lee, H. Yan, L.E. Brus, T.F. Heinz,J. Hone, and S. Ryu, ACS Nano 4 (2010) 2695–2700
[68] A. Splendiani, L. Sun, Y. Zhang, T. Li, J. Kim, C. Y. Chim, G. Galli and F. Wang, Nano Lett., 10 (2010) 1271–1275
[69] Krishna P. Dhakal et al, Nanoscale, 6 (2014) 6 13028–13035
[70] Hao Qiu, Tao Xu, Zilu Wang, Wei Ren, Haiyan Nan, Zhenhua et al,, Nat. Commun. 4 (2013) 2642
[71] Kroto HW, Heath JR, O'Brien SC et al ,Nature 318 (1985)162–163
[72] Sumio Iijima, Nature, 354 (1991) 56–58
[73] Toshinari Ichihashi, Sumio Iijima et al., Nature 363 (1993), 603–605

[74] M. S. Dresselhaus, A. Jorio, M. Hunter, R. Saito, J. H. Hafner, C. M. Lieber, T. McClure, G. Dresselhaus Physical Review Letters 86 (2001) 1118–1121
[75] Jin Yuan Heish, Jian Ming Lu, Min Yi Huang, Nanotechnology 17 (2006) 3920–3924
[76] L. Forro, S. Garaj, L. thein Nga, R. Gaal, J.M. Bonard, Journal Of Applied Physics 91 (2002) 10107
[77] Jinquan Wei, Bingqing Wei, Xiangfeng Zhang, Chemical Physical Letters 362 (2002) 285–290
[78] Xiaohan Wang, Harry chou, Cheng Tan, M.S. Bharathi Science 342 (2013) 720–723
[79] H. M. Morinobu Endo,.Japanese Journal of Applied Physics 45 (2006) 4883-4892
[80] C.T. Wirth, S. Hofmann, J. Robertson, Diamond & Related Materials 18 (2009) 940-945
[81] Naiqin Zhao et al, Material Letters 60 (2006) 159-163
[82] Andreas Thess, Roland Lee, Pavel Nikolaev et al, 273 (1996) 483-487
[83] Kiang, M. Endo, P. Ajayan, G. Dresselhaus, M. Dresselhaus Phys. Rev. Lett., 81 (1998) 1869
[84] J.M. Cowley, Richard E. Smalley, Andreas Thess, Chemical Physics Letters 265 (1997) 379–384
[85] C. Journet, W.K. Maser, P. Bernier, A. Loiseau, J.E. Fisher, Nature 388 (1997) 756–758
[86] Junfeng Geng, Charanjeet Singh, S. douglas, S.P. Milo, F.G. Brian, Alan H. Windle Chem. Comm. (2002) 2666–2667
[87] Charanjeet Singh, Milo S.P., Ian A. Kinloch, Alan H. Windle, Chemical Physics Letters 372 (2003) 860–865
[88] S.J. Tans, M.H. Devorat, H. Dai, R.E. Smalley, A. Thess, Nature 386(6634) (1997) 474–477
[89] Charanjeet Singh, Kenneth B.K. Teo, Manish Chhowalla, William I. Milne, Encyclopedia of nanoscience and nanotechnology (2003) 1–22
[90] T. Belin, F. Epron, Material Of Science And Engineering B 119 (2005) 105–118
[91] L. Britnell, R. M. Ribeiro, A. Eckmann, R. Jalil, B. D. Belle et al, Science 340 (2013) 1311-1314
[92] K. Roy, M. Padmanabhan, S. Goswami, T. P. Sai, S. Kaushal, and A. Ghosh, Solid State Commun., 35 (2013) 175– 176
[93] R. Zan, Q. M. Ramasse, R. Jalil, T. Georgiou, U. Bangert, and K. S. Novoselov, ACS Nano 7 (2013) 10167
[94] S. Bertolazzi, D. Krasnozhon, and A. Kis, Nano Lett. 7 (2013) 3246
[95] Lili Yu, Yi-Hsien Lee, Xi Ling et al, Nano Lett. 14 (2014) 3055−3063
[96] H. Li, X. Cao, B. Li, X. Zhou, G. Lu, C. Liuman, Q. He, F. Boey, S. S. Venkatramana and H. Zhang, Chem. Commun., 47 (2011) 10070;

[97] F. D. Novaes, R. Rurali and P. Ordejo, ACS Nano 4 (2010) 7596

[98] V. Varshney, S. S. Patnaik, A. K. Roy, G. Froudakis and B. L. Farmer, ACS Nano 4 (2010) 1153.

[99] E. J. H. Lee, L. Zhi, M. Burghard, K. Mullen and K. Kern, Adv. Mater., 22 (2010) 1854

[100]G. K. Dimitrakakis, E. Tylianakis and G. E. Froudakis, Nano Lett., 8 (2008) 3166.

[101]V. C. Tung, L.M. Chen, M. J. Allen, J. K. Wassei, K. Neloson, R. B. Kaner and Y. Yang, Nano Lett., 9 (2009) 1949.

Chapter 2

Experimental

2.1 Graphene Synthesis and Transfer

2.1.1 Graphene Synthesis using CVD Method

The synthesis of the large-area graphene film was achieved using APCVD technique. Commercially available Cu foil with a thickness of $20\mu m$ and purity of 99.99% (Nilaco Pvt. Ltd.) was used for the graphene synthesis in the CVD process. $1.5mg$ of solid camphor was used as the carbon source. In the growth process, Cu foil was heated up to $1020^{\circ}C$ and annealed for $60min$ in H_2 ($100sccm$) atmosphere in a high temperature furnace zone. Camphor was evaporated and introduced to the high temperature furnace by a gas mixture of Ar:H_2 ($98:2sccm$). The graphene growth was completed in $10min$ and the furnace was cooled to room temperature gradually.

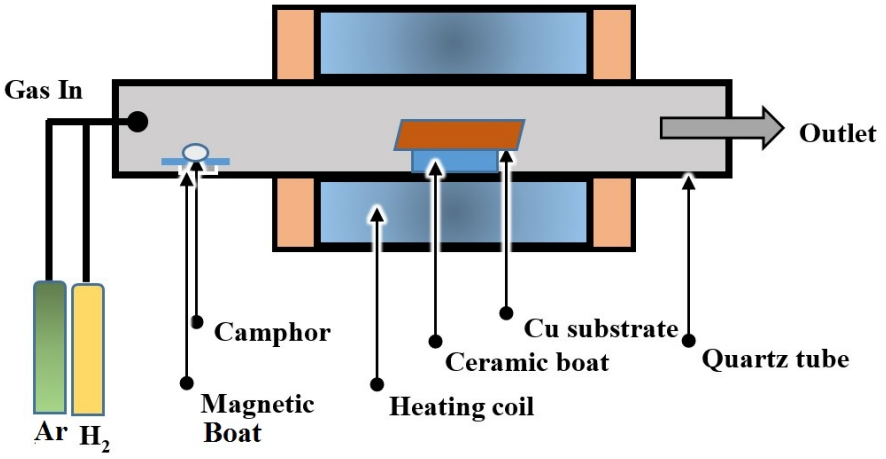

FIGURE 2.1: Schematic of CVD method for graphene synthesis

2.1.2 Graphene transfer by wet chemical method

As synthesized graphene was transferred to SiO_2/Si substrate by coating a PMMA supporting layer. Etching of underneath Cu foil was achieved by using a $50mg/ml$ [$Fe(NO)_3$] solution. PMMA/graphene stack layer was treated with 10% dil. HNO_3 followed by multiple treatment with dil.water. Next, PMMA/graphene stack was transferred to SiO_2/Si substrate. This stack is then dried in oven at $80°C$ for $5min$ and then this coating was dissolved in hot acetone bath at $100°C$ or few hours.

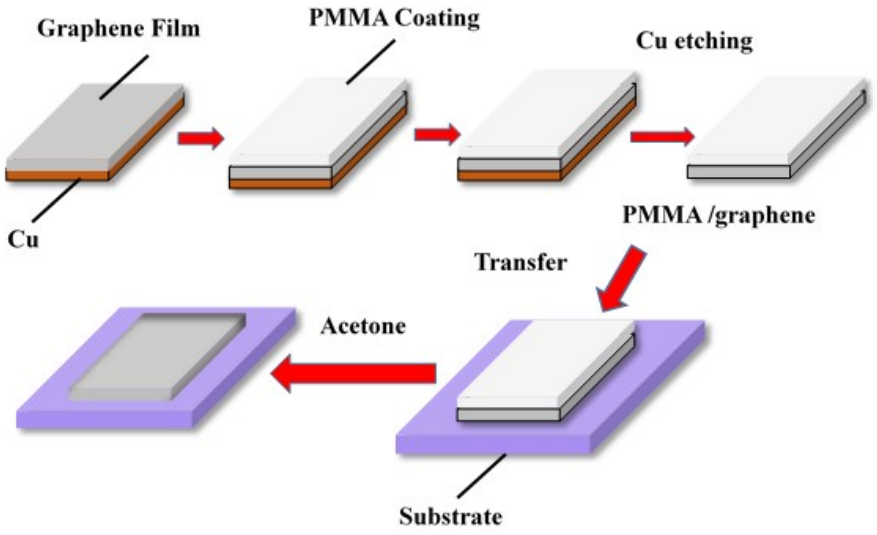

FIGURE 2.2: Schematic of graphene transfer by wet chemical method

2.2 MoS_2 Synthesis and Transfer

Synthesis of MoS_2 comprises of two steps. Coating of MoO_3 by thermal evaporator followed by sulfurization using CVD process. As-synthesized MoS_2 then transferred using conc. NaOH on respective substrates.

Metal Oxide coating by Thermal Evaporator:

MoO_3 (purity $\sim 99.0\%$) and S (purity$\sim 98.0\%$) powder purchased from Wako chemicals were used for synthesis of MoS_2 crystals. MoO_3 thin film with optimized thickness was deposited on a SiO_2/Si substrate by thermal evaporation.

Sulfurization of Metal Oxide by CVD Method:

The MoO_3 thin film coated on SiO_2/Si substrate was placed in a CVD furnace under the flow of $80sccm$ Ar and $20sccm$ H_2 mixture, whereas S powder was kept at room temperature zone. When the hot zone reached to desired temperature ($\sim 650°C$), S powder was evaporated at

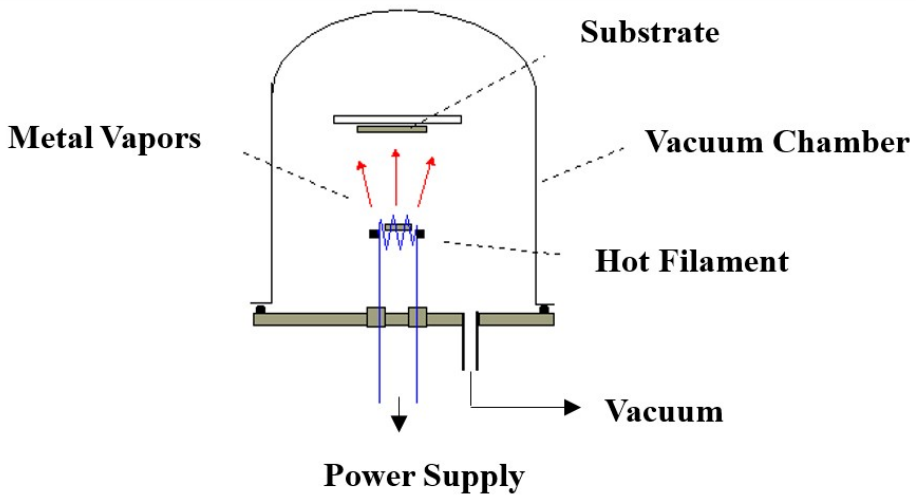

FIGURE 2.3: Thermal Evaporation Set up for MoO_3 deposition

$300°C$. Subsequently, the furnace heater was turned off after finishing the S powder evaporation, and the sample was left in the chamber to cool down.

MoS_2 Transfer:

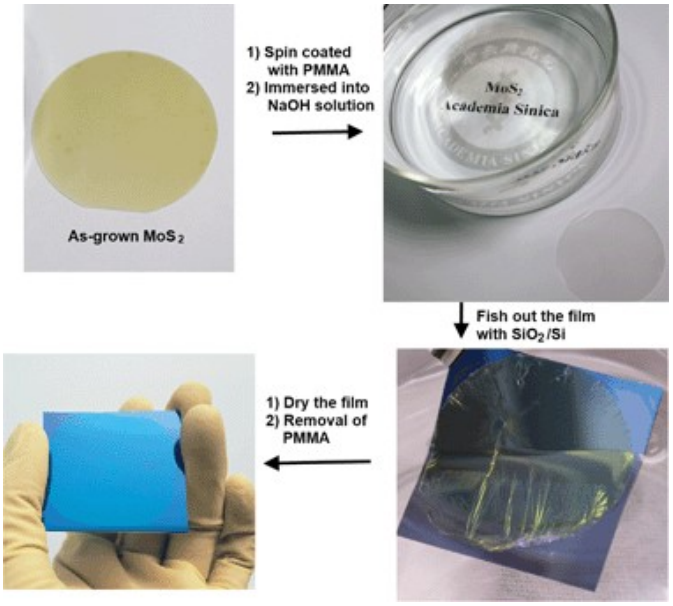

FIGURE 2.4: Schematic for the transfer of as-synthesized MoS_2 layer using NaOH

To transfer as-grown MoS_2 onto fresh SiO_2 /Si substrates, the MoS_2 film was coated with a layer of PMMA by spin-coating ($3000rpm$ for $60s$), followed by baking at $100°C$ for $10min$. After that, the PMMA-capped MoS_2 was then put into a NaOH (2M) solution at $100°C$ for 30 min. The PMMA-supported MoS_2 film was then transferred to DI H_2O to remove the etchant and residues. A fresh SiO_2/Si substrate was then used to fish out the PMMA-capped MoS_2 film,

followed by drying on a hot-plate ($100°C$ for 10 min). The PMMA was removed by acetone, IPA, followed by DI H_2O and chloroform rinsing. (refer FIGURE 2.4)

2.3 VACNTs Synthesis by CVD Method

Highly dense VACNTs forest was grown by the same APCVD process and carbon precursor. Solid camphor was mixed with ferrocene (1 wt %) and was put in the low temperature zone of the CVD furnace. The as synthesized graphene on Cu and transferred graphene on quartz substrate were loaded into the quartz tube furnace, which was heated to a temperature of $750°C$ under the flow of Ar ($80sccm$) and H_2 ($10sccm$) gas mixture. Heating the substrates to the growth temperature, camphor- ferrocene mixture was introduced in the growth zone by the Ar:H_2 carrier gas mixture. The growth period of CNTs was 15 min and then the furnace was cooled down to room temperature under the Ar:H_2 flow. The height and density of the CNTs forest can be controlled by the quantity of camphor-ferrocene mixture and growth duration respectively.

2.4 Device Fabrication

2.4.1 Graphene-CNTs Hybrid

Graphene-CNTs hybrid fabrication process includes steps as shown in figure 2.5 below. First, graphene was synthesized on cu foil using CVD method followed by transfer on quartz substrate. Next, Graphene/quartz membrane is used for the synthesis of VCNTs using same CVD method. Furthermore, $25nm$ of Au contact was deposited using thermal evaporation technique to study the electrical properties.

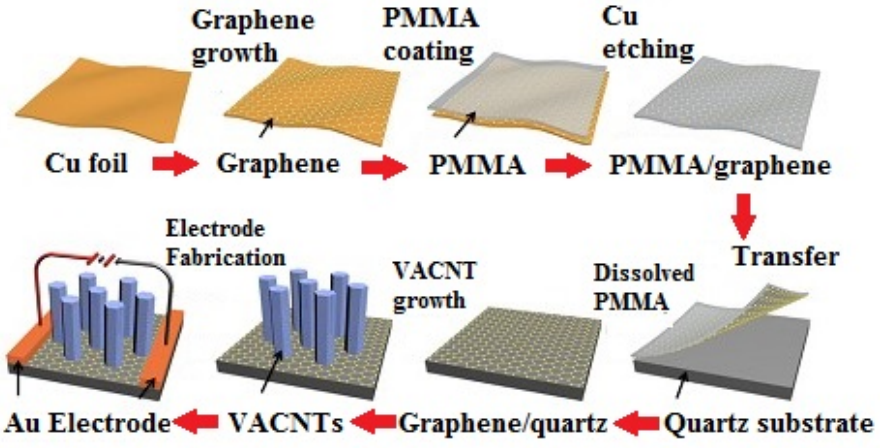

FIGURE 2.5: Schematic for the Graphene-CNTs Hybrid fabrication

2.4.2 Graphene-MoS_2 Hybrid

For the Graphene-MoS_2 non-volatile memory device fabrication transferred graphene on Si/SiO_2 was used as the substrate and MoS_2 was transferred on this substrate using PMMA coating method. Au contact was coated as in the case of previous hybrid structure. FIGURE 2.6 shows graphene-MoS_2 hybrid structure.

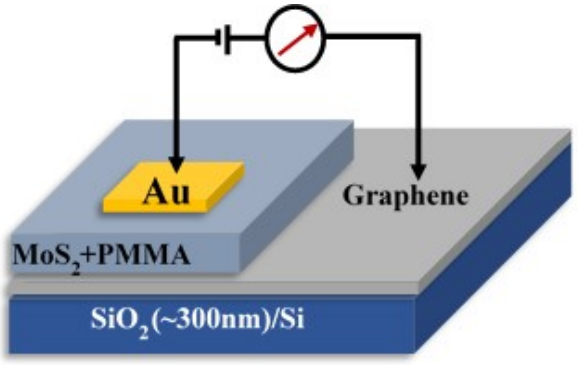

FIGURE 2.6: Schematic for the Graphene- MoS_2 Hybrid fabrication

2.5 Graphene Transfer on Flexible CA Substrate

A Graphene film synthesized by APCVD technique on Cu foil and using solid Camphor was used as the carbon source in these studies. The Graphene film was synthesized at $1020°C$ with a gas mixture of H_2 and Ar as 2.5 and 98 sccm, respectively. In the transfer process, the CVD synthesized continuous graphene film on Cu foil was put on the CA substrate, which was hot pressed at around $\sim 200°C$. Since materials like CA, PVC and PTFE have low glass transition temperature (Tg), they can be molded during hot press to attach on to the graphene coated Cu foil. FIGURE 2.7 shows a schematic diagram of the polymer-free graphene transfer technique onto moldable substrates.

Subsequently, the stacked CA/graphene/Cu was placed in a [$Fe(NO_3)_3$] solution of $10mg/ml$. The graphene remain attached to the surface of CA substrate, after complete etching of the Cu foil. However, some of the [$Fe(NO_3)_3$] solution or Cu residues remain on the graphene/CA substrates. The remaining metal impurities were removed by HNO_3 acid solution (10% diluted HNO_3). Finally the samples were rinsed in DI H_2O and dried in vacuum chamber.

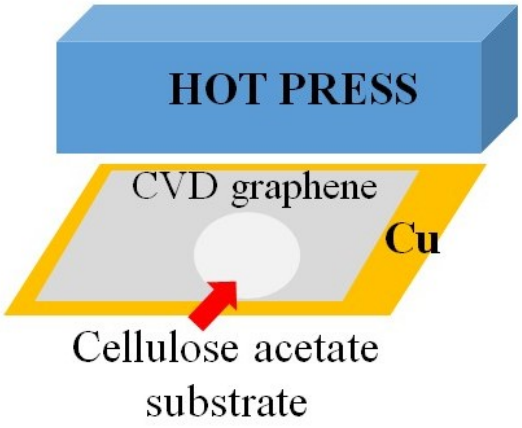

FIGURE 2.7: Schematic diagram of the hot press technique for large-area CVD graphene transfer process onto moldable substrates without using PMMA supporting layer.

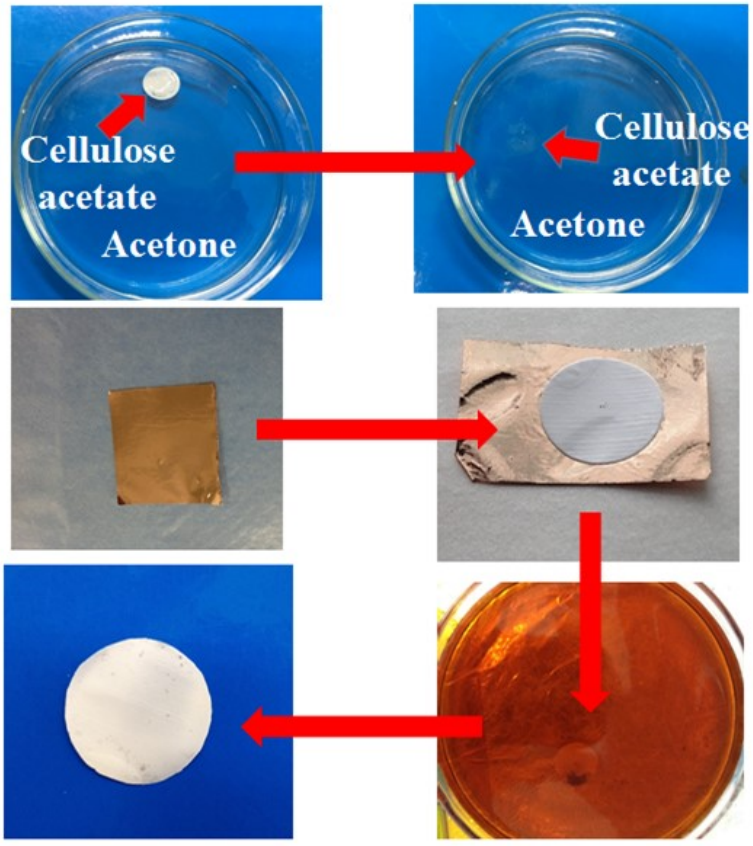

FIGURE 2.8: Schematic diagram of the hot pressed graphene on CA by chemical etching process.

2.6 N-doped Graphene Synthesis

The N-doped graphene was synthesized by the APCVD process using a quartz tube of length $80cm$ and an internal diameter of $50mm$. Cu foil (Nilaco Corp.) of thickness $20\mu m$ with 99.98% purity was taken as the catalytic substrate. The molecular structure of the solid precursors and schematic of the APCVD process are presented in FIGURE 2.9 The Cu foil was cleaned by acetone and placed in a quartz tube with a flow of $100sccm$ hydrogen for annealing at $1015°C$. Solid camphor (carbon source)with Triazine,Melamine and PAN (N source) were used as the feedstock and placed in a ceramic boat inside the lower temperature zone. Once the high temperature zone reaches $1015°C$, the lower temperature zone containing the feedstock was heated up to $600°C$. The growth was carried out with the flow of Ar and H_2 $(98 : 2.5sccm)$ gas mixture. After the growth, the sample was cooled down to room temperature.

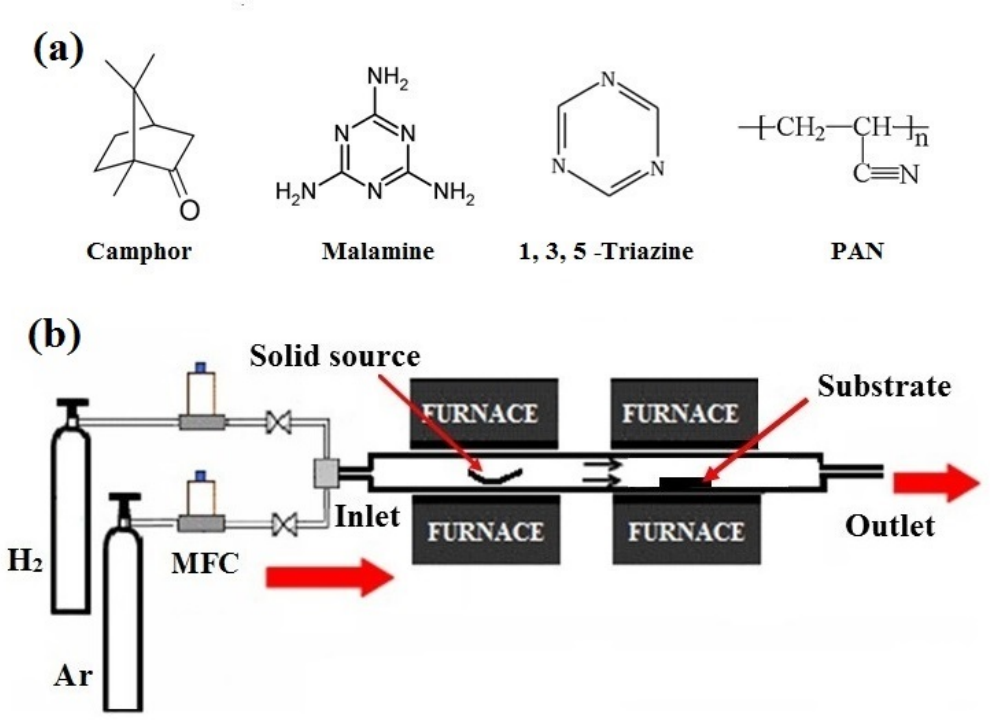

FIGURE 2.9: (a) Molecular structure of the solid precursors and (b) Schematic of the APCVD process for synthesis of N-doped graphene.

Chapter 3

Polymer-free graphene transfer on moldable cellulose acetate based paper by hot press technique

3.1 Introduction

Exceptional electrical, mechanical, optical, and thermal properties makes graphene a potential candidate for wide range of applications [1-4]. In this direction, synthesis of high quality large-area graphene by CVD process on transition metal substrates has been widely investigated [5-9]. The CVD synthesized graphene on metal substrates needs to transfer onto an insulating or semiconducting substrate for practical device fabrication [10-15]. In a transfer process, the compatibility of the substrate material and its processing significantly affect the quality of the transferred graphene. Normally, graphene transfer process has been developed for SiO_2 coated Si, glass and flexible plastic substrates for transistors, photoelectronics devices and transparent conductor applications [11, 16-21]. Face-to-face transfer of graphene has been demonstrated for limited rigid SiO_2/Si and quartz substrates with reduced transfer defects [22]. With respect to flexible device applications, graphene has been transferred onto plastic based substrates by wet-etching process. In many of the graphene transfer techniques, PMMA has been used as a supporting layer for the graphene film on metal surface [16]. Usually, the PMMA is dissolved in acetone or other organic solvents to coat a thin layer and is removed after the transfer process. However, many of the substrate materials may not be compatible with the PMMA supporting layer and may require a polymer-free transfer process. At the same time, the polymer residue significantly affects the intrinsic properties of the synthesized graphene film [22, 23]. Thus, polymer-free transfer process of graphene to obtain clean, wrinkle and damage-free graphene is of a significant challenge [24-26]. Recently, heat and pressure sensitive facial transfer process

has attracted significant attention to achieve polymer-free clean transfer of graphene [27-30]. The transfer process significantly depends on the processability of the substrate materials. CA based substrates are of great interest for flexible, lightweight, low cost and ecofriendly electronics and various other applications [31-33]. CA has significant applications as filter, barrier, separator and component in coating, cosmetic containers and packaging. Similarly, PVC, PTFE and other moldable materials are used in several fields [20, 34]. The PMMA solution can penetrate in micron sized pores of this substrates, thereby affecting the inherent properties of the materials. To avoid this, polymer-free transfer of graphene on CA based flexible and other moldable substrates is desirable. In this report, we demonstrate an innovative large-area graphene transfer technique unlike the state-of- the- art approach, without using any polymer supporting layer in the process.

3.1.1 Materials and Methods

3.1.1.1 Graphene Synthesis and Transfer on CA

Graphene synthesis and its transfer on CA have been carried out as explained in Chapter 2 section 2.1.1 and 2.5 respectively.

3.1.2 Results and Discussion

3.1.2.1 Optical Microscopy Study

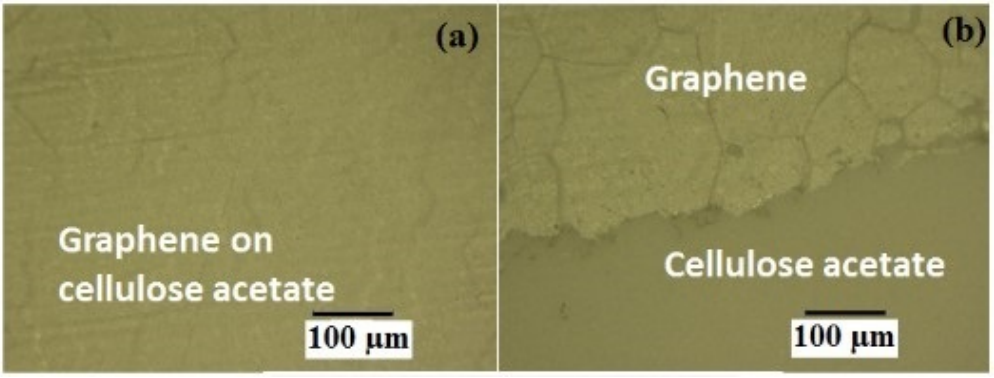

FIGURE 3.1: Optical microscope image at (a) center and (b) edge of the transferred graphene film.

FIGURE 3.1(a)-(b) shows optical microscope images of graphene film transferred onto CA substrate. The graphene film remains continuous on the CA paper without deformation, similar to the graphene film transferred with a PMMA supporting layer. Some of the domain boundaries

are visible at the edge of the transferred graphene film as shown in FIGURE 3.1(b). The continuity of the graphene film can be significant for applications such as the conducting layer on CA paper or for filtration purpose.

3.1.2.2 AFM Study

AFM studies were carried out with a JSPM-5200 scanning probe microscope. FIGURE 3.2(a) shows the AFM image of the as-obtained CA based substrate. The AFM study shows a rough surface of the CA substrate. FIGURE 3.2(b) shows AFM image of the graphene coated CA. A much smoother substrate surface was obtained with the graphene coating. Consequently, a transparent conducting coating is obtained on the insulating CA paper by transferring the CVD graphene film.

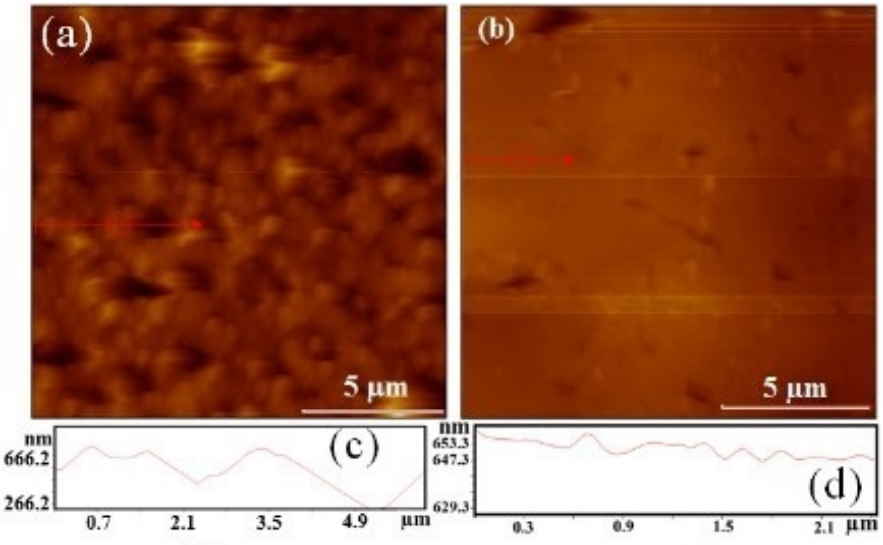

FIGURE 3.2: AFM image of (a) as-obtained and (b) graphene coated CA based substrate. Roughness profile of (c) pristine CA and (d) graphene coated CA surface.

FIGURE 3.2(c)-(d) shows the roughness profile of CA surface with and without coating of the graphene film, respectively. The roughness at the selected region (red arrow mark of FIGURE 3.2(c)-(d)) of bare and graphene coated CA surface is found to be $\sim 142.9nm$ and $\sim 6.69nm$, respectively. This shows that the surface roughness of the CA based substrate significantly reduces with graphene coating.

3.1.2.3 Raman Spectroscopy Study

FIGURE 3.3(a)-(b) show the Raman spectra of the as-synthesized graphene film at two different points on the Cu foil. Raman peaks were observed at 1584 and $2695cm^{-1}$, corresponding to graphitic G and second order 2D band, respectively. The I_G/I_{2D} peak intensity ratio is found

to be different at various positions, corresponding to the presence of monolayer and few-layer graphene.

Raman study was also carried out for the transferred graphene film on CA substrate as shown in FIGURE 3.3(c). The presence of graphene was confirmed by comparing the Raman features of bare and graphene transferred substrate. The CA based material used as the substrate shows Raman features, at $857, 1670$ and $2972cm^{-1}$.

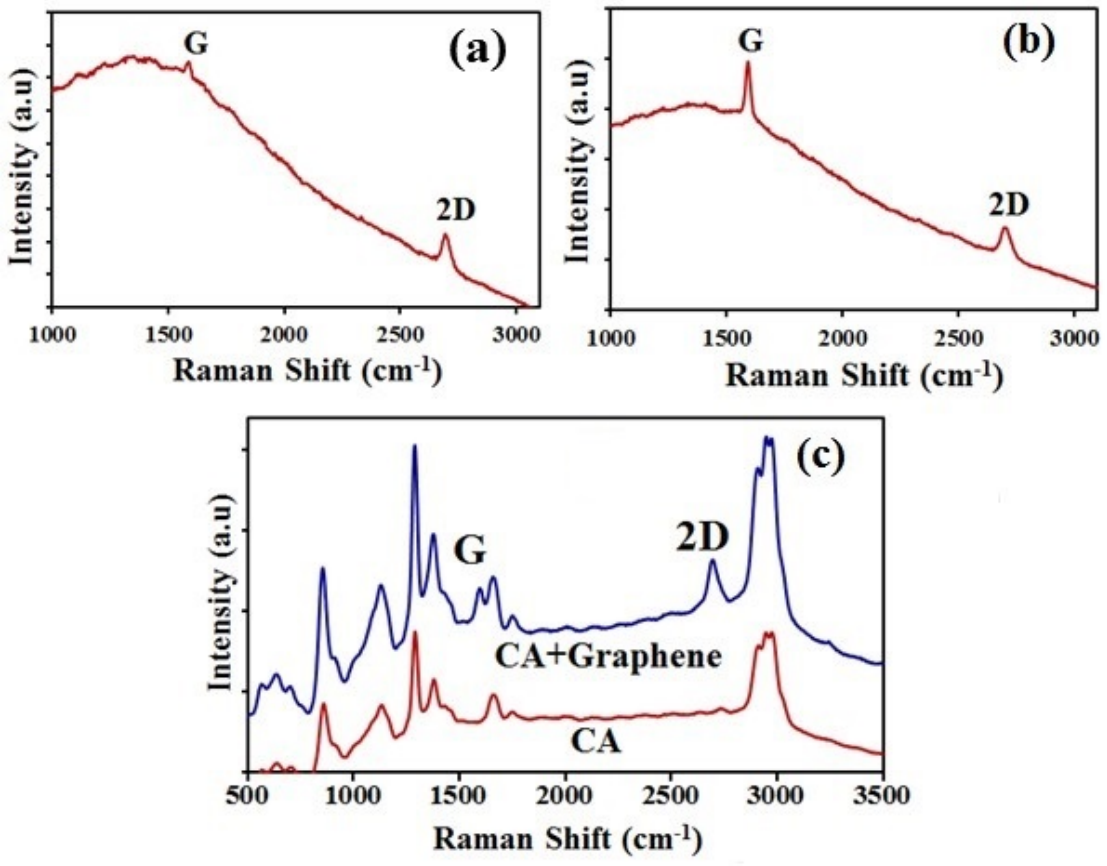

FIGURE 3.3: (a) and (b) Raman spectra of as-synthesized graphene film (c) Raman features of transferred CVD graphene film and CA substrate.

For the graphene transferred sample, the G peak is observed at $1590cm^{-1}$ as the shoulder of one of the CA Raman peak. However, a strong 2D peak of graphene can also be observed, which is completely absent in the base CA substrate. The presence of G and 2D features of graphene in the transferred sample in contrast to the base CA substrate confirms the presence of graphene. Raman peaks corresponding to the graphene film can be observed throughout the coated area of CA. In the demonstrated process, monolayer and few-layer graphene film can be transferred onto the moldable substrates, depending on the starting graphene on Cu foil synthesized by the APCVD process.

3.1.2.4 SEM Study

FIGURE 3.4 shows an SEM image of the conducting graphene film on CA based substrate, which is similar to the optical microscope image, where the domain boundaries of the graphene coating can be observed.

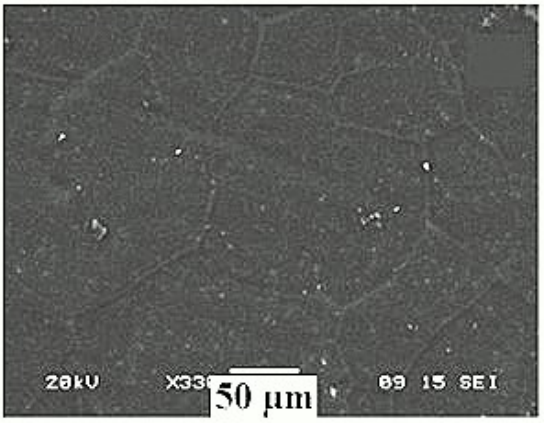

FIGURE 3.4: SEM image of the conducting graphene film on CA based substrate.

In a good transfer process, we do not observe presence of any hole as the graphene film remains intact and continuous. Additionally, the graphene film is much clearer than that of a conventional approach.

3.1.2.5 I-V Study of Graphene Film on CA Substrate

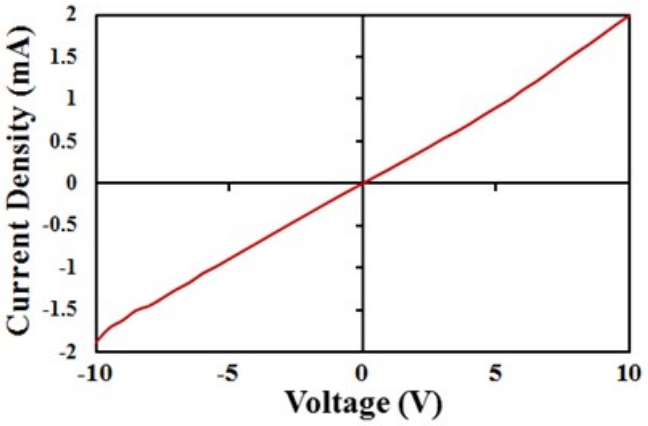

FIGURE 3.5: I-V characteristics of the graphene film on insulating CA substrate.

FIGURE 3.5 shows the I-V characteristics of the graphene film on CA substrate as measured by two probes technique. The measurement shows a typical linear I-V characteristic without any current saturation at higher bias voltage ($20V$). The linear I-V curve indicates similar electrical characteristics of the graphene as compared to those measured on various other substrates.

Sheet resistance of the graphene film on CA paper was measured by four probe technique using $RT - 70V/RG - 7C$ of Napson Corporation. The sheet resistance of the graphene film is measured as $\sim 2k\Omega/\square$ by a four probe technique. The conducting CA paper with coating of graphene film can be successfully used as the building block of various electronics device fabrication techniques.

3.2 Conclusion

We have demonstrated the transfer process of CVD synthesized large-area graphene film on to flexible CA substrate by a hot press technique. The CA based substrate was not compatible with acetone and PMMA supporting layer in a conventional transfer process. Nevertheless, the moldable CA substrate was simply hot pressed onto the graphene synthesized Cu foil. The base Cu foil was etched by a Cu etchant to obtain the graphene coating directly on the CA substrate. A clean, continuous and damage-free graphene was transferred on the CA substrate as confirmed by the Raman, optical microscopy, SEM and AFM analysis. The graphene film on CA substrate is highly conducting ($R_s \sim 2k\Omega/\square$) as measured by electrical measurements, suggesting that it can be used as building block for paper based electronic devices. The developed process can be significant for graphene transfer on moldable substrate materials with the advantage of not using polymer and organic solvents.

References

[1] A. K. Geim, K. S. Novoselov, Nature Mater. 6 (2007) 183-191

[2] S. V. Morozov, K. S. Novoselov, M. I. Katsnelson, F. Schedin, D. C. Elias, J. A. Jaszczak, A. K., Phys. Rev. Lett. 100 (2008) 016602

[3] R. R. Nair, P. Blake, A. N. Grigorenko, K. S. Novoselov, T. J. Booth, T. Stauber, N. M. R. Peres, A. K., Science 320 (2008) 1308

[4] C. Lee, X. Wei, J. W. Kysar and J. Hone, Science 321 (2008) 385-388

[5] K. S. Kim, Y. Zhao, H. Jang, S. Y. Lee, et al, Nature 457 (2009) 706-710

[6] X. S. Li, W. W. Cai, J. H. An, S. Kim, et al, Science 324 (2009) 1312-1314

[7] Z. Sun, Z. Yan, J. Yao, E. Beitler, Y. Zhu, J. M. Tour,. Nature 468 (2010) 549-552

[8] X. Li, C. W. Magnuson, A. Venugopal, R. M. Tromp, J. B. Hannon, E. M. Vogel, L. Colombo, R. S. Ruoff, , J. Am. Chem. Soc. 133 (2011) 2816-2819

[9] J. H. Lee, E. K. Lee, W. J. Joo, Y. Jang, B. S. Kim, J. Y. Lim, et al, Whang, Science 344 (2014) 286-289

[10] A. Reina, X. Jia, H. John, D. Nezich, H. Son, V. Bulovic, M. S. Dresselhaus, J. Kong, Nano Lett. 9 (2009) 30-35

[11] S. Bae, H. Kim, Y. Lee, X. Xu, J. S. Park, Y. Zheng, J. Balakrishnan et al, Nat. Nanotechnol. 5 (2010) 574-578

[12] Y. Wang, Y. Zheng, X. Xu, E. Dubuisson, Q. Bao, J. Lu, K. P. Loh, ACS Nano 5 (2011) 9927-9933

[13] E. H. Lock, M. Baraket, M. Laskoski, S. P. Mulvaney et al, Nano Lett. 12 (2012) 102-107

[14] X. Liang, B. A. Sperling, I. Calizo, G. Cheng, et al, ACS Nano 5 (2011) 9144-9153

[15] P. Gupta, P. D. Dongare, S. Grover, S. Dubey, H. Mamgain, A. Bhattacharya, M. M., Scientific report 4 (2014) 3882

[16] Z. Yan, J. Lin, Z. Peng, Z. Sun, Y. Zhu, L. Li, C. Xiang, E. L. Samuel, C. Kittrell, J. M. Tour, ACS Nano 6 (2012) 9110-9117

[17] Y. Y. Wang, P. J. Burke, A large-area and contamination-free graphene transistor for liquid-gated sensing applications, Appl. Phys. Lett 103 (2013) 052103

[18] J. Lee, Y. Kim, H. J. Shin, C. S. Lee, D. Lee, S. Lee et al, ACS Appl. Mater. Interfaces 6 (2014) 12588-12593

[19] Y. Han, L. Zhang, X. Zhang, K. Ruan, L. Cui, Y. Wang, L. Liao, Z. Wang, J. Jie, J. Mater. Chem. C 2 (2014) 201-207

[20] L. G. P. Martins, Y. Song, T. Zeng, M. S. Dresselhaus, J. Kong, P. T. Araujo, Proc. Natl. Acad. Sci. 110 (2013) 17762-17767

[21] L. G. D. Arco, Y. Zhang, C. W. Schlenker, K. Ryu, M. E. Thompson, C. Zhou, ACS Nano 4 (2010) 2865-2873

[22] L. Gao, G. X. Ni, Y. Liu, B. Liu, A. H. C. Neto, K. P. Loh, Face-to-face transfer of wafer-scale graphene films, Nature 505 (2014) 190-194

[23] L. Gao1, W. Ren1, H. Xu, L. Jin, Z. Wang, T. Ma, L. P. Ma, Z. Zhang, Q. Fu, L. M. Peng, X. Bao, H. M. Cheng, Nature Commun. 3 (2012) 699

[24] Y. C. Lin, C. Jin, J. C. Lee, S. F. Jen, K. Suenaga, P. W. Chiu, ACS Nano 5 (2011) 2362-2368

[25] W. H. Lin, T. H. Chen, J. K. Chang, J. I. Taur, Y. Y. Lo, W. L. Lee, C. S. Chang, W. B. Su, C. I. Wu, ACS Nano 8 (2014) 1784-1791

[26] L. Song, L. Ci, W. Gao, P. M. Ajayan, ACS Nano 3 (2009) 1353-1356

[27] T. L. Chen, D. S.Ghosh, V. Mkhitaryan and V. Pruneri, ACS Appl. Mater. Interfaces 5 (2013) 11756-11761

[28] J. Kang, S. Hwang, J. H. Kim, M. H. Kim, J. Ryu, S. J. Seo, B. H. Hong, M. K. Kim, J. B. Choi, ACS Nano 6 (2012) 5360-5365

[29] J. D. Caldwell, T. J. Anderson, J. C. Culbertson, G. G. Jernigan et al, ACS Nano 4 (2010) 1108-1114

[30] E. H. Lock, S. C. Hernández, T. J. Anderson, S. W. Schmucker et al, Surface and Coatings Technology, 241 (2014) 118-122

[31] H. Zhu, Z. Xiao, D. Liu, Y. Li, N. J. Weadock, Z. Fang, J. Huang, L. Hu,. Sci. 6 (2013) 2105-2111

[32] D. Gaspar, S. N. Fernandes, A. G. de Oliveira, J. G. Fernandes et al, Nanotechnology 25 (2014) 094008

[33] A. Amaral, C. N. de Carvalho, P. Brogueira, G. Lavareda, L.V. Melo, M. H. Godinho, Mater. Sci. Eng. B 118 (2005) 183186

[34] D. R. Hines, S. Mezhenny, M. Breban, E. D. Williams, V. W. Ballarotto, G. Esen, A. Southard, M. S. Fuhrer, Appl. Phys. Lett. 86 (2005) 163101

Chapter 4

Synthesis of a three dimensional structure of vertically aligned carbon nanotubes and graphene from single solid carbon source

4.1 Introduction

Graphene is the most important building block of many other carbon allotropes such as, fullerene, CNTs and graphite [1]. Graphene possess excellent electrical, mechanical, thermal and optical properties at room temperature [2-5]. Similarly, CNTs (rolled graphene sheet) show extraordinary physical properties arising from the unique 1D structure [6-9]. This outstanding properties of graphene and CNTs have been exploited for fabrication of high mobility FET, transparent conductors, field emitters, energy storage devices [10-23]. Apart from the individual properties and applications of carbon materials, a hybrid structure can have significant technological advantages. Fullerene-CNTs, fullerene-graphene and graphene-CNTs hybrid systems have been reported to combine the individual properties in various applications [24-27]. Graphene and CNTs 3D hybrid structure can be useful for the application in interconnects, flexible nanoelectronics and flexible field emission devices. Individual synthesis process of high quality CNTs and large-area graphene film by the CVD technique has been extensively investigated [28-32].

VACNTs have been grown on various insulating substrates such as SiO_2/Si, Al_2O_3 and quartz by the CVD process. However, the selection of the substrate significantly affects the electrical and thermal transport properties in the perpendicular direction of 1D CNTs [33]. A 3D integrated structure of CNTs and a few-layers graphene film has been developed by Sato et al. of Fujitsu

Corp. [34]. The catalytic growth of VACNTs with graphene-supported metal particles using graphene as a base substrate also can be significant. The transfer of CVD graphene film onto an arbitrary substrate provides more flexibility for CNTs growth in wide range of applications. Recently, Lee et al. reported an approach to grow VAMWCNTs on reduced graphene oxide platelets and proposed its application as a flexible field emission device [35]. Various other applications for these composite structures have been proposed, such as efficient heat radiators and wiring for very large scale integrated circuits. Also, Jeong et al. have reported a flexible room temperature NO_2 gas sensor consisting of a VACNTs/reduced graphene hybrid film supported by a polyimide substrate [36]. Rao et al. demonstrated the synthesis of CNTs forest on a suspended monolayer graphene and thereby extending the class of substrates for CNTs growth [37].

In context to the previous reports, we demonstrate a synthesis process of graphene-CNTs hybrid structure using a single solid carbon source in an APCVD. Graphene growth on Cu foil is achieved using camphor as the carbon source; whereas VACNTs are obtained by adding a small amount of ferrocene ($1wt\%$) to the camphor. Raman spectroscopy, optical and scanning electron microcopy studies are performed to confirm the out-of-plane growth of CNTs from the transferred graphene film. Contact resistance of synthesized VACNTs- graphene system is obtained by I-V measurements taking into account the various resistive contacts in the 3D structure.

4.1.1 Materials and Methods

4.1.1.1 Graphene Synthesis and Transfer

Graphene synthesis and its transfer have been carried out as explained in Chapter 2 section 2.1.1 and 2.5 respectively.

4.1.1.2 Synthesis of CNTs on graphene

Synthesis of CNTs on graphene has been carried out as explained in Chapter 2 section 2.3.

4.2 Results and Discussion

The structural morphology of the as-synthesized and transferred graphene film was investigated by Raman and optical microscopy studies. Both monolayer and few-layer graphene films can be synthesized by the developed APCVD process. In this study, few-layer graphene films were grown to be compatible with CNTs growth on graphene film, thereby creating a highly conducting 3D structure.

4.2.1 Optical Microscopy Study

The morphological structural views of the synthesized materials were obtained by the digital optical microscope VHX-500. FIGURE 4.1(c)-(d) shows optical microscope images of the as-synthesized and transferred graphene films. The optical image of the as-synthesized graphene film on Cu foil shows the grain boundaries, domain structure and formation of a continuous graphene film.

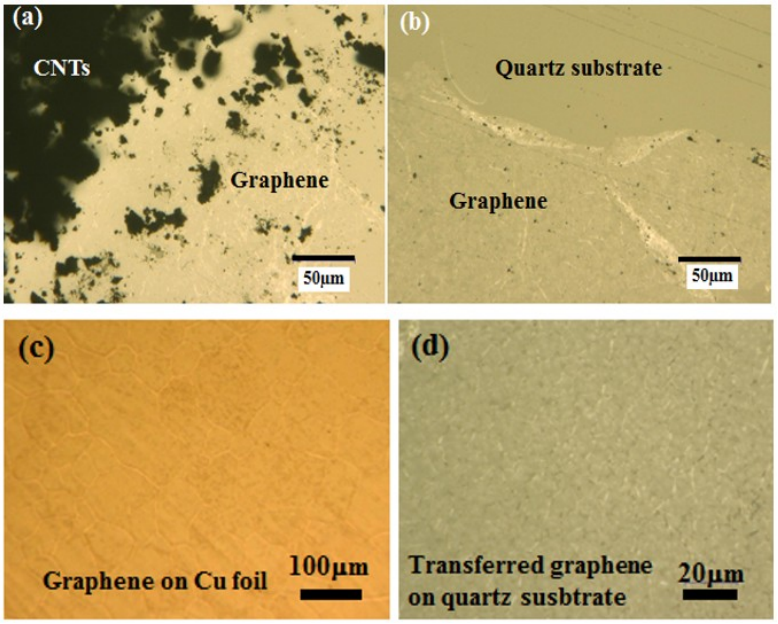

FIGURE 4.1: Optical microscope images of (a) synthesized CNTs on transferred graphene film and (b) masked graphene region during CNTs growth process, confirming that the film remain intact (c) The as-synthesized and (d) transferred graphene film.

Similarly, the transferred graphene film remain continuous, however wrinkles formation was also observed due to difference in the thermal coefcients of Cu foil and graphene film. FIGURE 4.1(a) shows an optical microscope image of the synthesized CNTs on the transferred graphene film at the edge of the masked graphene film. Some of the CNTs are scattered at the edge due to piling up after removing the mask. As indicated in FIGURE 4.1(a), the black part shows highly dense CNTs growth, where the graphene film remains intact. FIGURE 4.1(b) shows a much clear view of the underlying graphene film at the edge of the mask. The transferred graphene film is used as the base for CNTs growth from the same camphor precursor with the addition of 1 wt % of ferrocene molecules. The use of same carbon source in the APCVD process to grow graphene and CNTs can lead to symmetry in the growth dynamics, thereby developing a seamless 3D structure.

4.2.1.1 Raman Spectroscopy Study

Raman spectra were obtained using NRS 3300 laser Raman spectrometer with a laser excitation energy of 532.08 nm wavelength from a green laser. FIGURE 4.2(a) shows Raman spectra of as-synthesized graphene film on the polycrystalline Cu foil. An intense graphitic G and a second order double-resonance 2D peak were observed at 15842 and $2695cm^{-1}$, respectively. In contrary, there is no apparent defect related D peak in the synthesized graphene film. The intensity ratios of the 2D and the G peak (I_{2D}/I_G) are found to be in the range of 1.2 to 0.7, attesting presence of bi-layer and few-layer graphene in the deposited continuous film. Similarly, FIGURE 4.2(b) shows Raman spectra of transferred graphene on the quartz substrate. Raman peaks for bi-layer and few-layer graphene were also detected in the transferred film. However, a low intense D peak appeared around $1330cm^{-1}$ after chemical etching and transferring the graphene film on to the quartz substrate. The (I_{2D}/I_G) ratios for the transferred graphene film are also found to be in the range of 1.02 to 0.75 , as that of synthesized graphene on Cu foil. The wrinkle formation as shown in FIGURE 4.2(b), as well as etchant and mechanical impact during transfer process can contribute to the small increase in D peak. However, the overall structure and quality of transferred graphene film did not change significantly.

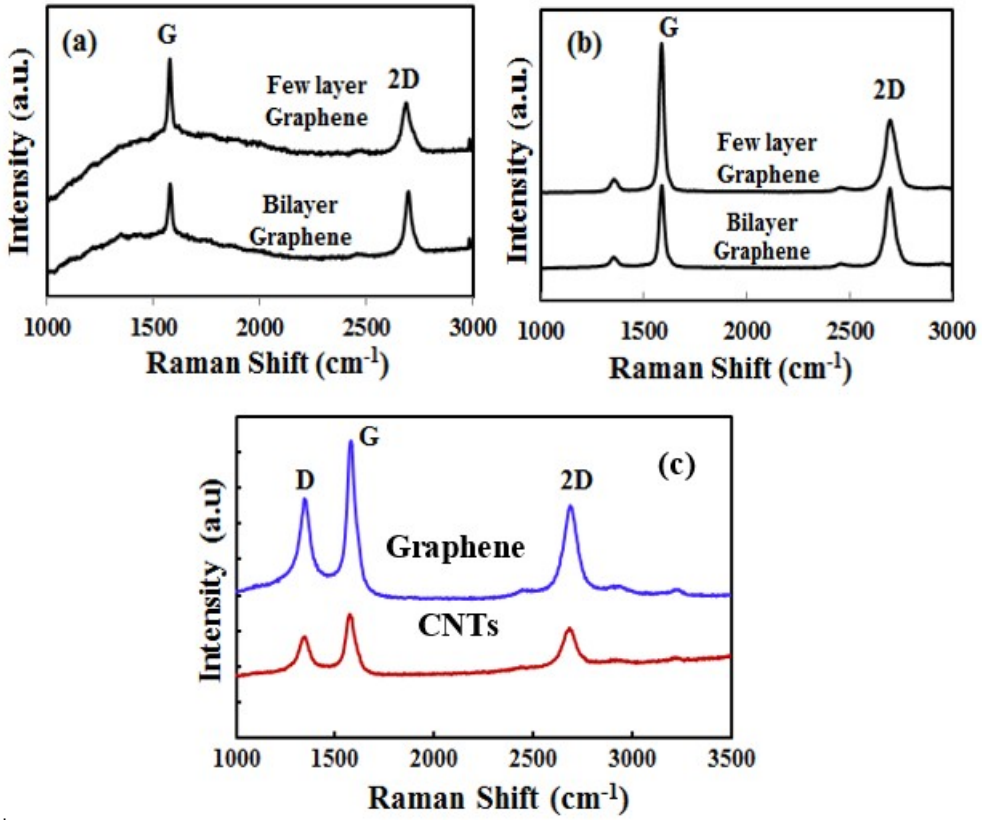

FIGURE 4.2: Raman spectra of bi-layer and few-layer graphene for (a) as-synthesized on polycrystalline Cu foil and (b) transferred to a quartz substrate. (c) Raman spectra of underlying graphene film and the as-synthesized CNTs.

FIGURE 4.2(c) shows the Raman spectra of the as-synthesized CNTs structure on the transferred graphene film. The graphitic G and second order resonance 2D peaks are observed at 1582 and $2695cm^{-1}$, respectively. Again, the defect related D peak is observed at $1342cm^{-1}$, corresponding to the CVD synthesized MWCNTs. At the same time, intensity of the D peak for underlying graphene film also increases as compared to the transferred film. Increase in the D peak intensity for the graphene film can be explained by considering the distortion of sp^2 carbon atoms due to thermal stress and oxidation during the high temperature CNTs growth process. Still, high graphitization of the graphene film with its original structure was not significantly changed. Again, it has been demonstrated that with using 13C isotope graphene, the raman peaks can be visualized separately for graphene and CNTs [37]. However, in our symmetric growth process with identical precursor material, shift in Raman peaks for graphene and CNTs are not observed.

4.2.1.2 SEM Study

SEM studies of the graphene film and CNTs were carried out with the Hitachi S-4300 at an accelerating voltage of $20kV$. FIGURE 4.3(a) shows the SEM image of the synthesized VAMWCNTs on graphene film using mixture of solid camphor and ferrocene molecules. In the synthesis technique, only 1 wt % of ferrocene is adding to the camphor, the lower catalyst concentration in the feedstock enables MWCNTs growth with low metal impurity. Whereas, in various other processes high catalyst concentration in the feedstock leads to high metal-impurity and so the post-deposition purification becomes unavoidable. The growth process involves simultaneous pyrolysis of solid camphor and ferrocene mixture in a high temperature ($750°C$) furnace to obtain the VAMWCNTs.

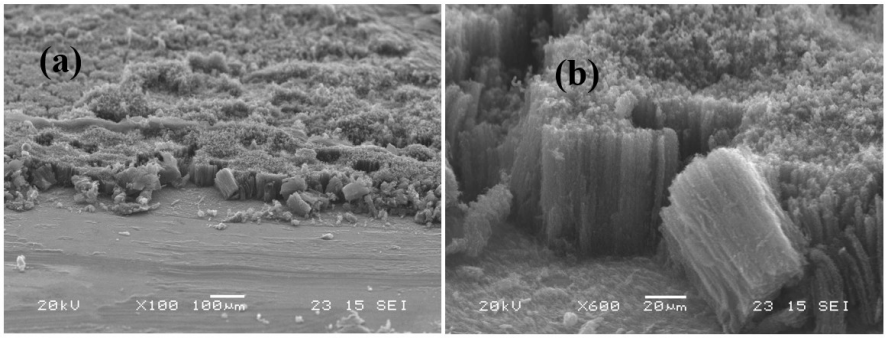

FIGURE 4.3: SEM images of (a) CNTs forest grown from the solid camphor on transferred graphene film and (b) its higher magnified image confirm the vertical.

The nucleation and growth of CNTs occur on vapor phase catalyst sites [30], which can be significant in keeping the graphene film undamaged without the formation of metal nanoparticles. FIGURE 4.3(b) shows a magnified SEM image of the VAMWNTs synthesized on the graphene

film. We have scratched at one edge of the graphene-CNTs sample to observe the vertical alignment of the CNTs bundle. Some of the bundles pilled of during scratching, otherwise, CNTs structure is robust on the basal graphene film. A highly dense structure of VACNTs with a length of around $80\mu m$ can be observed at the edge. The vertical column of the CNTs bundle consists of numerous nanotubes self-organized into a densely packed structure. The observed structure of the synthesized material can be significant for high thermal and electrical conductivity.

4.2.1.3 TEM Study

FIGURE 4.4(a) shows a TEM image of the synthesized graphene sheet on the polycrystalline Cu foil. Inset of the figure shows SAED pattern of the graphene sheet. Multiple spots are observed in the SAED pattern; this may be due to overlap of two graphene sheets or owing to rotational stacking fault. Most of the graphene sheets on the TEM grid showed single crystal SAED patterns, while the relative orientation of the single crystals differed considerably.

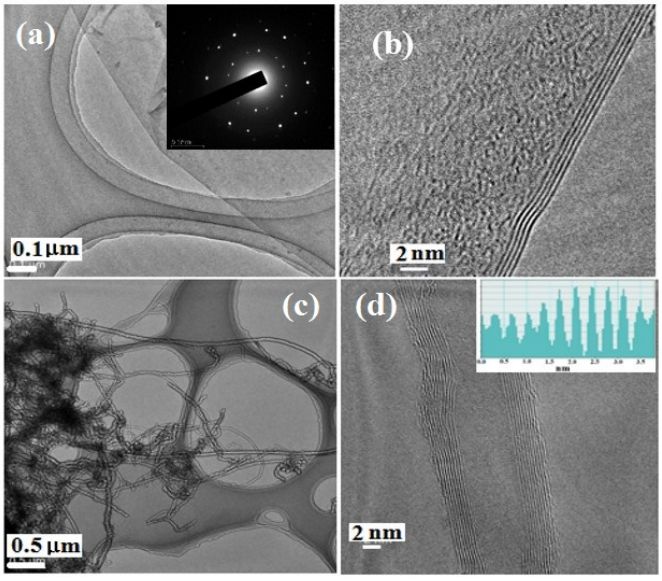

FIGURE 4.4: (a) TEM image of synthesized graphene on polycrystalline Cu foil. Inset of the figure shows SAED pattern of the graphene sheet. Most of the graphene sheets on TEM grid showed single crystal SAED patterns. (b) HRTEM image at the folded edge of a graphene sheet, presenting the formation of few-layer graphene. (c) TEM of synthesized CNTs using the camphor-ferrocene feedstock with a diameter distribution of 10-50 nm. (d) HRTEM image of a CNT presenting more than 10 layers of graphene rolled-up to form MWCNT structure.

FIGURE 4.4(b) shows a High Resolution TEM (HRTEM) image at the folded edge of a graphene sheet, presenting formation of few-layers graphene. The synthesis of monolayer graphene and few-layer graphene can be controlled in the developed process with change in the camphor injection rate and growth duration. The TEM results for the formation of few-layers graphene can be correlated with the Raman studies. Similarly, FIGURE 4.4(c) shows a TEM of the CNTs synthesized using the camphor- ferrocene feedstock. Diameter distribution of the CNTs

is observed to be in the range of $10 - 50nm$. FIGURE 4.4(d) shows HRTEM image of a CNT displaying more than 10 layer of graphene rolled-up to form MWCNT structure. The rolled graphene sheets form a tube structure with a diameter of $10nm$ for the inner hole. As explained previously the ferrocene molecules act as vapor phase catalyst for CNTs growth with decomposition along with the solid camphor feedstock. The sp^2 hybridized graphene film acts as a seeding base for the CNTs growth. The transferred graphene film shows a sheet resistance (Rs) of $108\Omega/\square$ as measured by the four probe technique.

4.2.1.4 IV Study of CNTs-Graphene Hybrid

I-V characteristics of the transferred graphene film and CNTs-graphene hybrid structure were measured at room temperature ($250°C$) using a series 2400 Source Meter Keithley. FIGURE 4.5(a) presents a schematic diagram of the graphene film on an insulating substrate for I-V characteristic measurements.

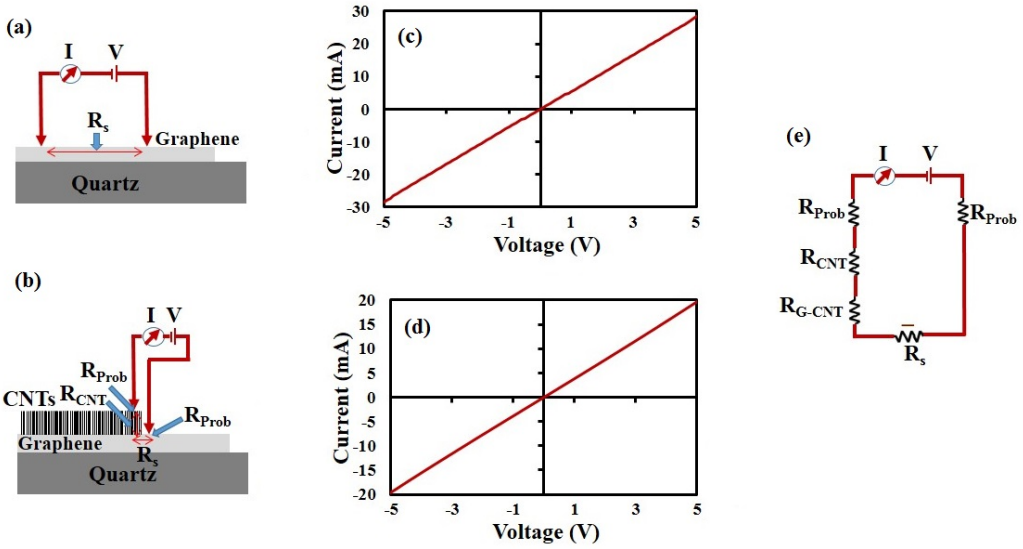

FIGURE 4.5: (a) Schematic diagram of graphene film on an insulating substrate for I-V characteristic measurement (b) I-V characteristic of the graphene film without any metal contact (c) Schematic diagram of VAMWCNTs-graphene 3D structure on quartz for I-V measurement (d) I-V characteristic of the VAMWCNTs-graphene measured by putting a probe on the top CNTs and the other probe on bottom graphene contact (e) Possible contact and sheet resistances in the 3D structure

The device shows a linear I-V characteristic as shown in figure 4.5(b), signifying metallic behavior of the graphene film. In previous studies, contact resistance of VACNTs on graphene coated Cu foil was explored [37]. However, only the VACNTs forest directly on Cu substrate also can show very low contact resistance. In this context, exploring the contact and sheet resistances of VACNTs on graphene is quite essential for realizing a VACNTs-graphene 3D system [39]. Hence, we consider a transferred graphene film on quartz substrate integrating with VACNTs to investigate contact resistance at VACNTs-graphene interface. Figure 4.5(c) shows a

schematic diagram of the VAMWCNTs-graphene 3D structure on quartz for electrical conductance measurements. FIGURE 4.5(d) shows the I-V characteristic of the 3D structure measured by putting a probe on the top CNTs and the other probe on bottom graphene contact. I-V characteristic shows liner behaviour with an applied bias voltage of 5 V, similar to an ohmic contact. A contact resistance of 255Ω is obtained in the VAMWCNTs-graphene 3D material system.

The obtained contact resistance can be explained from the individual contributions of resistance at the probe (Rprob), that at total resistance. Therefore, the observed contact resistance can be influenced by various other factors, rather than only CNTs-graphene interface. This finding shows that highly conducting 3D structure of VAMWCNTs-graphene can be synthesized from single solid precursor. Further studies are required in nanoscale order to observe and confirm the formation of a seamless junction interface with directly grown CNTs on graphene film.

4.3 Conclusion

In summary, we have demonstrated a symmetric synthesis process of a VAMWCNTs-graphene 3D structure using single solid carbon source. Graphene growth on Cu foil was achieved using solid camphor as the carbon source; whereas VAMWCNTs were obtained by adding a small amount of ferrocene ($1wt\%$) in the camphor feedstock with minimum contamination from the iron catalyst. CNTs growth occurs on vapor phase catalyst sites, which can be significant in keeping the graphene film undamaged without depositing metal nanoparticles. Optical microscopy and SEM studies confirmed out-of-the plane growth of the CNTs on the transferred graphene film. TEM studies were performed to confirm the structure of CNTs and graphene in the 3D system. The carbon material structure varies significantly from the same feedstock with the addition of catalytic ferrocene molecules and controlled growth process. In the developed process, sp^2 hybridized graphene film acted as a seeding base substrate for the VAMWCNTs growth. I-V measurements were carried out to investigate in plane and out of plane electrical characteristics of the 3D system. The VAMWCNTs-graphene structure showed a contact resistance of 255Ω, wherein resistance at the probe, graphene-CNTs interface, sheet resistance and CNTs bundle resistance have also contributed. Achieving a seamless contact of CNTs-graphene film can be significant for low contact resistance and thereby practical device applications.

References

[1] A. K. Geim and K. S. Novoselov, Nat. Mater. 6 (2007) 183-191

[2] A. K. Geim and P. Kim, Sci. Am., 298 (2008) 90-97

[3] R. R. Nair, P. Blake, A. N. Grigorenko, K. S. Novoselov, T. J. Booth, T. Stauber, N. M. R. Peres and A. K. Geim, Science 320 (2008) 1308

[4] C. Lee, X. Wei, J. W. Kysar and J. Hone, Science 321 (2008) 385-388

[5] A. A. Balandin, S. Ghosh, W. Bao, D. Teweldebrhan, F. Miao and C. N. Lau., Nano Letter 8 (2008) 8 902-907

[6] S. Iijima, Nature 354 (1991) 56-58

[7] S. J. Tans, A. R. M. Verschueren and C. Dekker, Nature 393 (1998) 49-52

[8] P. Kim, L. Shi, A. Majumdar and P. L. McEuen, Phys. Rev. Lett. 87 (2001) 215502

[9] J. Hone, M. Whitney, C. Piskoi and A. Zettl, Phys. Rev. B. 59(1999) R2514- R2516

[10] R. H. Baughman, A. A. Zakhidov and W. A. de Heer, Science 297 (2002) 787-792

[11] W. B. Choi, D. S. Chung, J. H. Kang, H. Y. Kim, Y. W. Jin, I. T. Han, Y. H. Lee, J. E. Jung, N. S. Lee, G. S. Park and J. M. Kim, Appl. Phys. Let. 75 (1999) 3129-3131

[12] Y. B. Zhang, S. P. Lau, L. Huang and M. Tanemura, Appl. Phys. Lett. 86 (2005) 123115-1-3

[13] S.V. Morozov, K. S. M. I. Novoselov, Katsnelson, Phys. Rev. Lett. 100 (2008) 016602

[14] K. I. Bolotin, K. J. Sikes, Z. Jiang, M. Klima, G. Fudenberg, J. Hone, P. Kim and H. L. Stormer, Solid State Commun. 146 (2008) 351-355

[15] L. Britnell, R. V. Gorbachev, R. Jalil, B. D. Belle et al, Science 335 (2012) 947-950

[16] S. Bae, H. K. Kim, Y. Lee, X. Xu, J. Park, Y Zheng et al, Nat. Nanotechnol. 5 (2010) 574-578

[17] G. Kalita, M. Masahiro, H. Uchida, K. Wakita and M. Umeno, Mater. Lett. 64 (2010) 2180-2183

[18] A. Cao, P. L. Dickrell, W. G. Sawyer, M. N. Ghasemi-Nejhad and P. M. Ajayan, Science 310 (2005) 1307-1310

[19] X. Yang, C. Cheng, Y. Wang, L. Qiu and D. Li, Science 341 (2013) 534-537.

[20] Z. Guo, J. Wang, F. Wang, D. Zhou, Y. Xia and Y. Wang, Adv. Funct. Mater. 23 (2013) 4840-4846

[21] K. P. Loh, Q. L. Bao, G. Eda and M. Chowalla, Nat. Chem. 2 (2010) 1015-1024

[22] P. Avouris, Z. Chen and V. Perebeinos, Nat. Nanotechnol. 2 (2007) 605-615

[23] M. Zhang, S. Fang, A. A. Zakhidov, S. B. Lee, A. E. Aliev, C. D. Williams, K. R. Atkinson, R. H. Baughman, Science 309 (2005) 1215-1219

[24] G. Kalita, S. Adhikari, H. R. Aryal, M. Umeno, R. Afre, T. Soga and M. Sharon, Appl. Phys. Lett. 92 **(**2008) 063508

[25] Y. Zhang, L. Ren, S. Wang, A. Marathe, J. Chaudhuri and G. Lic, J. Mater. Chem. 21 (2011) 5386-5391

[26] D. H. Lee, J. E. Kim, T. H. Han, J. W. Hwang, S. Jeon, S. Y. Choi, S. H. Hong, W. J. Lee, R. S. Ruoff and S. O. Kim, Adv. Mater. 22 (2010) 1247-1252

[27] A. Rodriguez-Manzo, F. Banhart, M. Terrones, H. Terrones et al Proc. Natl. Acad. Sci. 106 (2009) 4591-4595

[28] K. Hata, D. N. Futaba, K. Mizuno, T. Namai, M. Yumura and S. Iijima, Science 306 (2004) 1362-1364

[29] J. Prasek, J. Drbohlavova, J. Chomoucka, J. Hubalek, O. Jasek, V. Adamc and R. Kizek, J Mater. Chem. 21 (2011) 15872-15884

[30] M. Kumar and Y. Ando, J. Nanosci. Nanotech. 10 (2010) 3739–3758

[31] K. S. Kim, Y. Zhao, H. Jang, S. Y. Lee, J. M. Kim, K. S. Kim, J. H. Ahn, P. Kim, J. Y. Choi and B. H. Hong, Nature 457 (2009) 706-710

[32] X. S. Li, W. W. Cai, J. H. An, S. Kim, J. Nah, D. X. Yang et al, Science 324 (2009)1312-1314

[33] S. Talapatra, S. Kar, S. K. Pal, R. Vajtai, L. Ci, P. Victor, M. M. Shaijumon, S. Kaur, O. Nalamasu and P. M. Ajayan, Nat. Nanotechnol. 1 (2006) 112-116

[34] D. Kondo, S. Sato and Y. Awano, Appl. Phys. Express 1(2008) 074003

[35] D. H. Lee, J. A. Lee, W. J. Lee and S. O. Kim, Small 7 (2011) 95-100

[36] H. Y. Jeong, D. S. Lee, H. K. Choi, D. H. Lee, J. E. Kim, J. Y. Lee, W. J. Lee, S. O. Kim and S. Y. Choi, Appl. Phys. Lett. 96 (2010) 213105

[37] R. Rao, G. Chen, L. M. R. Arava, K. Kalaga, M. Ishigami, T. F. Heinz, P. M. Ajayan, and A. R. Harutyunyan, Scient. Report 3(2013) 1891

[38] G. Kalita, K. Wakita and M. Umeno, Physica E 43 (2011) 1490-1493

[39] Y. Jiang, P. Wang and L. Lin, Nanotechnology 22 (2011) 365704

[40] N. Chiodarelli, S. Masahito, Y. Kashiwagi, Y. Li, K. Arstila et al, Nanotechnology 22 (2011) 085302.

Chapter 5

Fabrication of poly (methyl methacrylate)-MoS_2/graphene heterostructure for memory device application

5.1 Introduction

Substantial interest has been given to 2D materials after the discovery of graphene, considering the fascinating electronic properties for novel device applications [1-4]. Besides graphene related materials, quasi 2D TMDCs are gaining a lot of attention due to the wide range of band gap for practical electronic device applications [5-8]. Among various TMDCs, MoS_2 is of great interest for next generation FETs and optoelectronic devices owing to wide range of band gap the presence of a direct band gap ($1.85eV$ direct band gap in a monolayer and $\sim 1.29eV$ indirect band gap in bulk)[5, 9-11]. Monolayer and few-layer MoS_2 have been applied in the fabrication of FETs, sensors, phototransistors, and energy storage devices [11-17]. Excellent on/off ratio ($\sim 10^8$) in a FET device with high carrier mobility has been obtained due the presence of direct band gap [12]. Recently, a heterojunction of graphene and MoS_2 has been fabricated by extracting the metallic and semiconducting properties of the respective materials[18-19]. A multifunctional photoresponsive memory device has been created with a graphene-MoS_2 hybridized structure [20]. Non-volatile memory device based on FET device has also been fabricated with graphene, hexagonal boron nitride and MoS_2 stacked 2D materials [21, 22].

Bearing the rapid development of 2D materials in mind for next generation device applications, several methods have been discovered to derive or synthesize MoS_2 layers [5, 11, 23-28]. There

have been efforts to produce monolayer and few-layer MoS_2 by micromechanical exfoliation process as well [5-11]. MoS_2 layers have also been fabricated with intercalation-assisted and solution-based chemical exfoliation process [23-24]. On the other hand MoS_2 sheets were synthesized using hydrothermal method, physical vapor deposition, electrochemical synthesis and CVD techniques [25-26]. Similarly, large-area uniform growth of MoS_2 layer has been achieved by sulfurization of Mo and MoO_3 [27-28]. Controlled synthesis of MoS_2 crystals in a large-area is one of the important aspects for its integration in photovoltaic, phototransistors and memory device applications. In contrast to previous reports, we demonstrate the synthesis of elongated hexagonal and rhombus shaped MoS_2 crystals by sulfurization of MoO_2 thin film and fabrication of a PMMA-MoS_2/graphene heterostructure memory device. In the fabricated device, the PMMA layer plays the dual role of being the supporting layer for the transfer process and as an insulating dielectric in the memory device. The developed material system and the observational study of its bi-stable electrical switching effect can be significant for the development of a future generation of non-volatile memory devices.

5.2 Materials and Methods

5.2.1 Graphene Synthesis

Graphene synthesis has been carried out as explained in Chapter 2 section 2.1.1.

5.2.2 MoS_2 Synthesis

MoS_2 synthesis has been carried out as explained in Chapter 2 section 2.2.2.

5.2.3 MoS_2 Transfer on Graphene and Device Fabrication

MoS_2 transfer on graphene and device fabrication have been carried out as explained in Chapter 2 section 2.2.3.

5.3 Results and Discussion

The synthesized MoS_2 crystals were characterized by Raman and UV-visible absorption spectroscopy. TEM images were taken by JEOL JEM 2100, operated at $200kV$ equipped with an element analyzer. STEM studies of MoS_2 crystals were carried out by JEM-ARM 200F. SEM study was carried out with Hitachi S-4300 operated at an acceleration voltage of $20kV$.

The MoO_3 film and Au electrode were deposited by thermal evaporation technique using ULVAC VPC-260F. I-V characteristic measurements were carried out using two probe system and Keithley 2401 Source Meter.

5.3.1 Optical Microscopy Study

Optical microscopy studies of the graphene and the fabricated heterostructure were carried out with VHX-500 digital microscope. FIGURE 5.1(a) shows an optical image at the edge of the transferred graphene film. From the color contrast, the graphene film can be directly identified on the SiO_2/Si substrate. The synthesized MoS_2 crystals coated with PMMA solution was then transferred on to the high quality graphene. FIGURE 5.1(b) shows an optical microscope image of the transferred PMMA-MoS_2 on the graphene film. The layer-by-layer transferred PMMA-MoS_2 on graphene can form a close contact hybridized heterostrucure with strong van der Waals interaction.

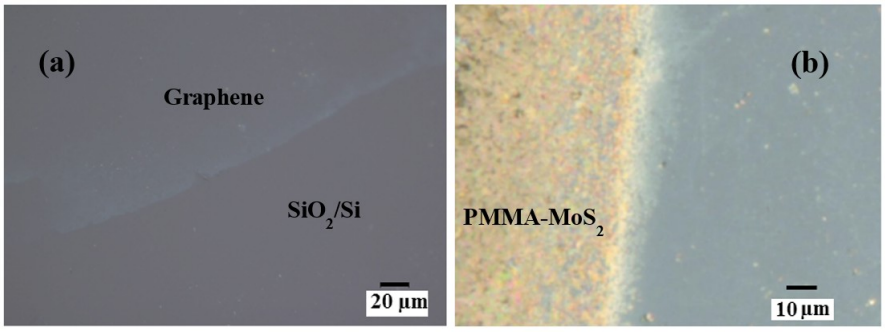

FIGURE 5.1: Optical microscope image (a) at the edge of the transferred graphene film and (b) of the transferred PMMA-MoS_2 on the graphene film.

5.3.2 Raman and UV-Visible Spectroscopy Study

Raman studies of MoS_2 crystals and graphene film were carried out with NRS 3300 laser Raman spectrometer with a laser excitation energy of $532.08nm$. FIGURE 5.2(a) shows a Raman spectra of the graphene film. Graphitic G and second order 2D Raman peaks are observed at 1589 and $2700cm^{-1}$, respectively. The ratio of G to 2D peak intensity (I_G/I_{2D}) is found to be around 1.12, signifying the presence of more than single layer graphene. FIGURE 5.2(b) shows Raman spectra of the as-synthesized MoS_2 layer by the S reaction process of the MoO_3 thin film. Two characteristic peaks at 409.8 and $385.6cm^{-1}$ are observed corresponding to A_{1g} mode associated with out of plane vibration of S atoms and E_{2g} mode related to in-plane vibration of Mo and S atoms.

Broadening of the Raman peaks is considered to be due to phonon confinement, as well as signifying smaller lateral size of the synthesized MoS_2 crystals.

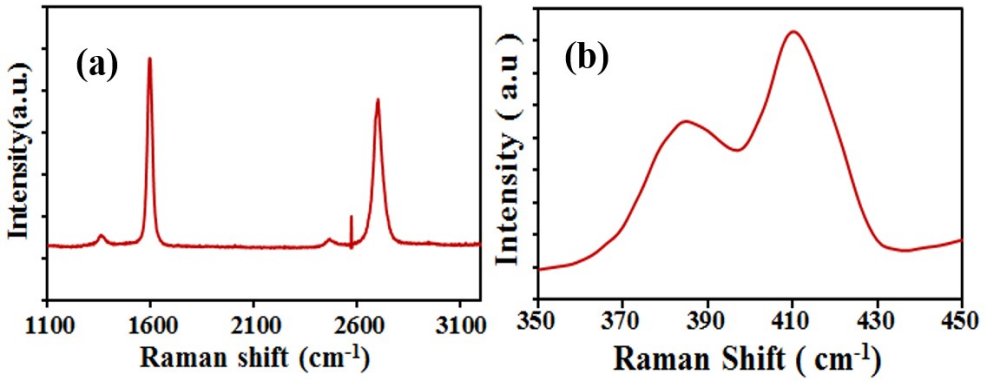

FIGURE 5.2: Raman spectra of (a) the transferred graphene (a) as-synthesized MoS_2 crystals by sulfur reaction process of thermally evaporated MoO_3 film

The frequency difference between the A_{1g} and $E^1{}_{2g}$ mode is found to be $24.2cm^{-1}$, corresponding to the growth of few-layer structure. On the other hand, the frequency difference has been found to be around $20.4cm^{-1}$ for a CVD synthesized monolayer MoS_2 [29]. UV-visible absorption spectroscopy was carried out with JASCO V-670K spectrophotometer.

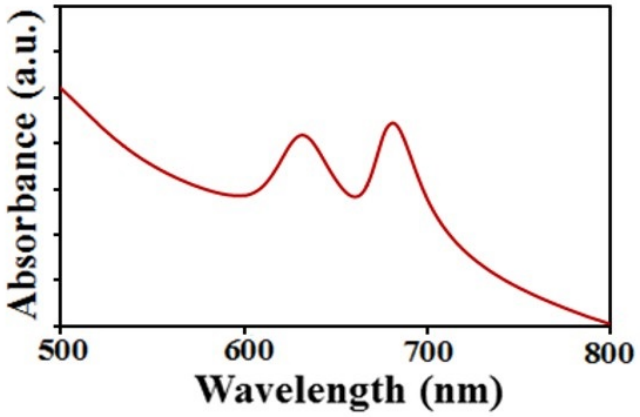

FIGURE 5.3: UV-visible spectra of the transferred MoS_2.

FIGURE 5.3 shows UV-visible spectra of the transferred MoS_2 film on a glass substrate. Two prominent absorption peaks are observed at 628 and $680nm$ corresponding to direct excitonic transitions. It has been reported that the peak positions of the absorption spectra corresponding to the direct excitonic states can vary with the change in number of layers [8]. For monolayer and few-layer MoS_2, the two exciton peaks show blue-shift due to quantum confinement effect as the thickness of the crystal decreases [30].

5.3.3 SEM Study

FIGURE 5.4 shows a top-view SEM image of the PMMA-MoS_2 hybrid structure. The PMMA coating can hold MoS_2 crystals together and at the same time act as the dielectric interface

for the memory device. The dual role of PMMA in the MoS_2 crystals and CVD graphene based memory device has not been explored. Hence, it is an interesting aspect of the developed material system, which can be integrated for the memory device application.

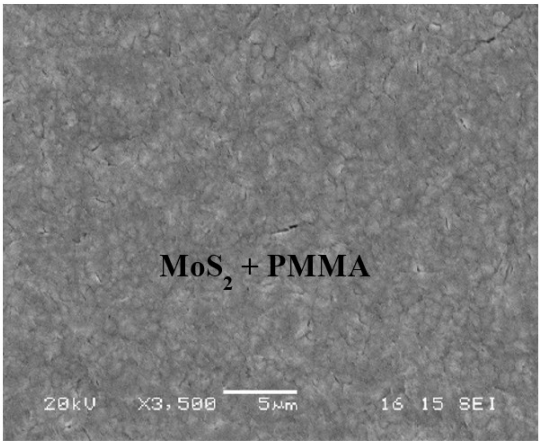

FIGURE 5.4: SEM image of the PMMA-MoS_2 hybrid structure

5.3.4 TEM Study

The crystallinity and structural morphology of the synthesized MoS_2 crystals were investigated by TEM studies. FIGURE 5.5(a)-(b) show the TEM bright-field images of the as-synthesized MoS_2, presenting elongated-hexagonal and rhomboidal shape of the crystals.

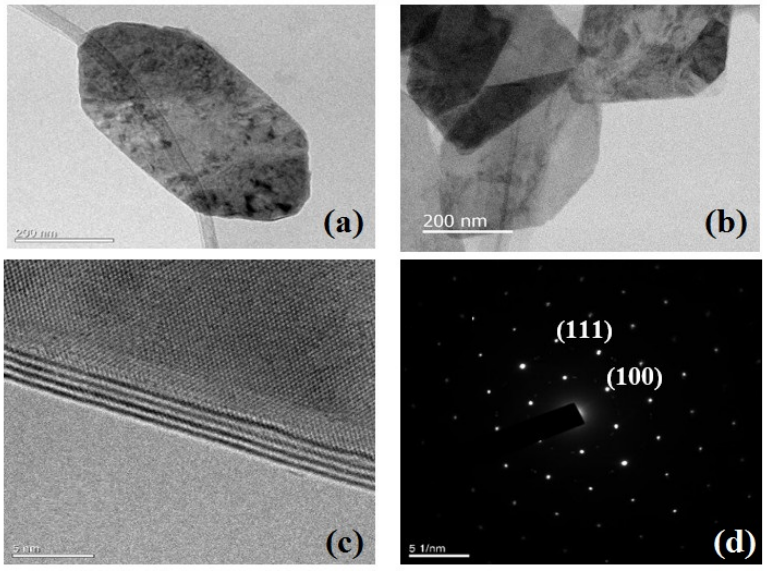

FIGURE 5.5: TEM bright-field images of synthesized MoS_2, presenting (a) elongated-hexagonal and (b) rhomboidal shapes (c) few-layer structure with a layer spacing of about $\sim 0.65nm$(d) SAED pattern taken from the MoS_2 crystal, presenting the hexagonal symmetric structure

Previously, similar rhomboidal shaped MoS_2 flakes have been grown using a MoO_2 microcrystals as a template; however formation of elongated-hexagonal flakes were not observed [31]. FIGURE 5.5(c) shows layer numbers of a hexagonal flake as obtained at the folded edge. The MoS_2 crystal with four layers shows a layer spacing of about $0.65nm$. FIGURE 5.5(d) shows SAED pattern taken from the MoS_2 crystal, revealing the hexagonal symmetric structure. The SAED pattern also shows the (100) and (110) lattice planes of the MoS_2 crystals. Recently, large-area MoS_2 thin layer has been synthesized by two step thermal reduction and sulfurization process of the MoO_3 thin film [32].

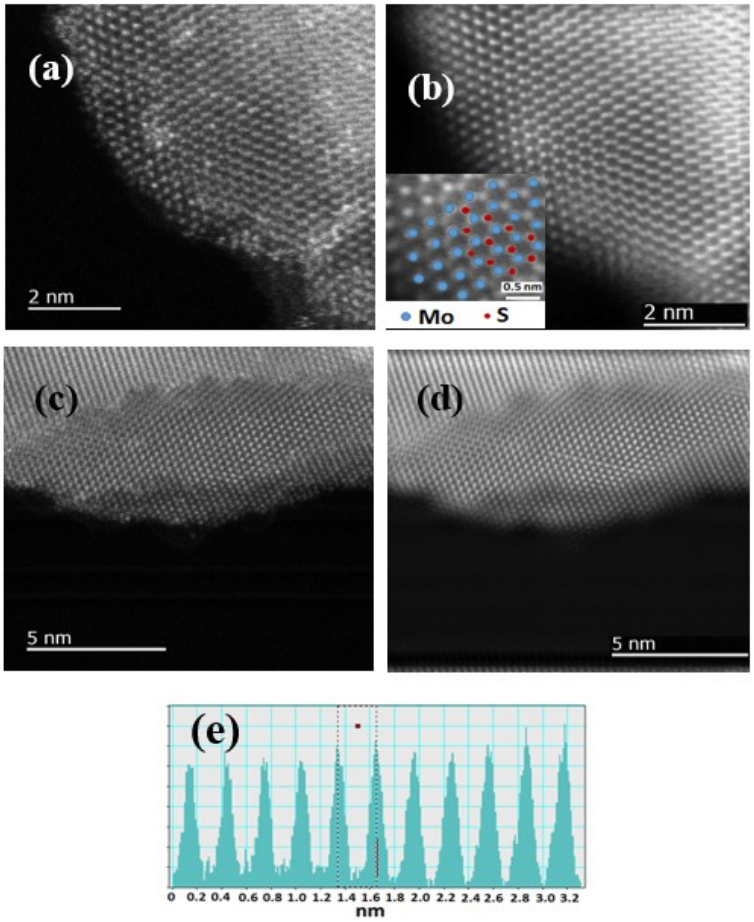

FIGURE 5.6: (a) HAADF image of a MoS_2 crystal at the edge. (b) Fourier-filtered image corresponding to the HAADF image, presenting better view of the lattice structure. In the inset of the figure, the atomic arrangement of Mo and S atoms to form a MoS_2 layer is presented (c) Cross-section HAADF image of few-layer MoS_2 crystal. (d) Corresponding Fourier-filtered image of the cross-section HAADF image (e) Line profile across the filtered image as marked in (d)

In contrast to a previous finding, we demonstrate the synthesis of hexagonal and rhombus shaped MoS_2 crystals with a sulfurization process of the MoO_3 thin film. The structural morphology was further analyzed with aberration corrected STEM-HAADF, also known as Z-contrast imaging. At the edge of a MoS_2 crystal, we can observe the atomic structure of a single layer as shown in FIGURE 5.6(a). The Mo and S atoms can be directly identified from the contrast

of the image, signifying highly ordered and crystalline MoS_2 layer. FIGURE 5.6(b) shows a Fourier-filtered image corresponding to the HAADF image, presenting a better view of the lattice structure of the MoS_2 layer The Mo atoms show higher contrast than that of S atoms. In the inset of the figure, we present the atomic arrangement of Mo and S atoms to form a MoS_2 layer. FIGURE 5.6(c) shows cross-section HAADF image of the synthesized few-layer MoS_2 crystal, presenting a high quality lattice structure. FIGURE 5.6(d) shows the corresponding Fourier-filtered image of the cross-section HAADF image, where direct evaluation of the lattice constant is possible. FIGURE 5.6(e) shows line profile across the filtered image as marked in FIGURE 5.6(d). A lattice constant around $\sim 0.312nm$ is estimated from the line profile for the MoS_2 crystal.

FIGURE 5.7 shows the transfer process of the synthesized graphene and MoS_2 crystals for the fabrication of a heterojunction memory device. High quality graphene synthesized on Cu foil by the solid precursor based CVD process was transferred onto a SiO_2/Si substrate.

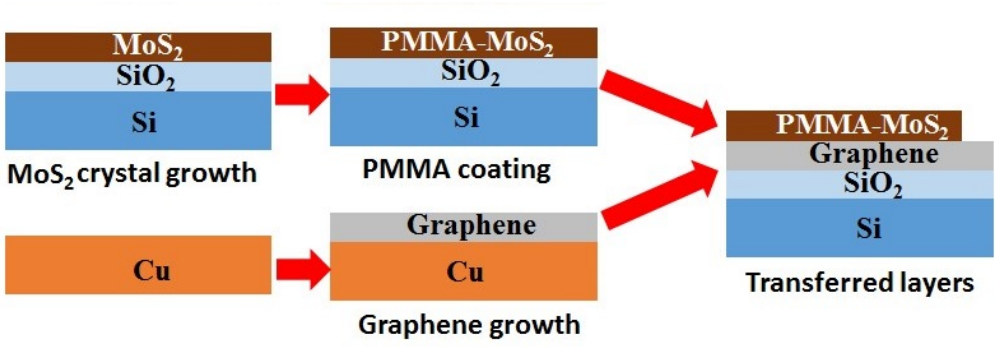

FIGURE 5.7: Transfer process of the synthesized graphene and MoS_2 crystals for the fabrication of heterojunction memory device

5.3.5 I-V Study of PMMA-MoS_2/Graphene Heterostructure

FIGURE 5.8(a) shows a schematic diagram of the fabricated PMMA-MoS_2/graphene heterostructure as a memory device. In the fabricated device, the PMMA-MoS_2 hybrid structure is the functional material, whereas the continuous CVD graphene film acts as the electrode. FIGURE 5.8(b) shows a typical IV characteristic of the PMMA-MoS_2/graphene heterojunction device. Increasing the applied potential (V) from 0 to 5 V,the current increases gradually (stage I), while an abrupt increase in current occurred from $0.052mA$ to $0.127mA$ (stage II). This indicates the transition of the device from HRS to LRS. The fabricated heterojunction shows good stability in the LRS during the subsequent voltage sweep in stages III and IV, signifying a nonvolatile memory effect.

Repeated measurements also show identical device characteristics in the developed heterostructure material system. Again, a device fabricated with higher amount of PMMA solution drop

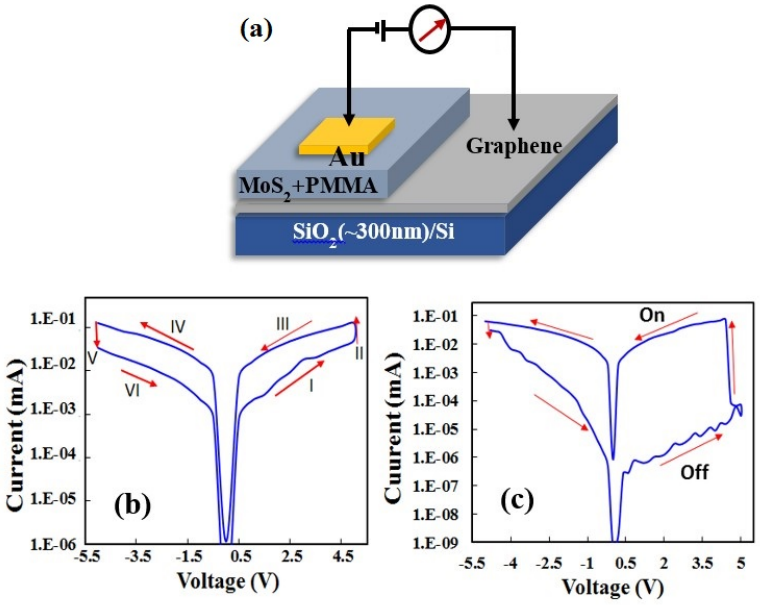

FIGURE 5.8: (a) Schematic diagram of the fabricated PMMA-MoS_2/graphene heterostructure as a memory device (b) and (c) Typical I-V characteristic of the PMMA-MoS_2/graphene heterojunction device varying the amount of PMMA solution coated on the MoS_2 film

casted on the MoS_2 crystals shows much higher on/off ratio as shown in FIGURE 5.8(c). Abrupt increase in current is observed from stage I to stage II with an on/off ratio as high as 2.5E3, which is higher than that of the device fabricated with MoS_2 powder and shows charge trapping and de-trapping behaviour of MoS_2 in the PMMA blend. The HOMO and LUMO level of PMMA is not well known, however it shows an energy of around $5.6eV$ [33]. Again, Few-layer MoS_2 has low electron affinities of around $\sim 3.0eV$, with a bandgap in the range of 1.4 to $1.8eV$. Hence, it will create a large barrier for electron and hole injection with the applied potential. Charge transfer can occur between the PMMA and MoS_2 in the hybridized structure, subsequently trapping the charge in the MoS_2 crystals due to its lower energy level and quantum confinement effect.

The observed memory device characteristics can be explained by this charge trapping mechanism in the PMMA-MoS_2/graphene heterostructure. In the demonstrated device, the top electrode and the PMMA-MoS_2 functional material composition is still un-optimized, which provides an ample opportunity for fabrication of an efficient memory device. This nonvolatile rewritable feature of the fabricated PMMA-MoS_2/graphene heterojunction device can be used as electrically bi-stable material in flash memory devices. The demonstrated MoS_2 crystal synthesis process and their integration to fabricate heterojunction memory device can be a significant prospect for memory device applications.

5.4 Conclusion

In summary, the synthesis of elongated hexagonal and rhombus shaped MoS_2 crystals by sulfurization of thermally evaporated MoO_3 thin film has demonstrated. TEM and STEM-HAADF studies were performed to reveal the atomic level structure of the synthesized high quality MoS_2 crystals. A hybridized structure of graphene and MoS_2 was fabricated with a layer-by-layer transfer process to configure a memory device. The PMMA layer used for the transfer process of MoS_2 film performed a dual role of supporting and insulting dielectric layer in the fabricated memory device. The memory device was configured with PMMA-MoS_2 and CVD graphene as the functional and electrode materials, respectively. Typical bi-stable electrical switching and nonvolatile rewritable memory effect was observed in the fabricated PMMA-MoS_2/graphene heterostructure. An on/off ratio as high as 2.5E3 was obtained in the fabricated PMMA-MoS_2/graphene memory device. The memory characteristic of the fabricated device is attributed to the charge trapping and de-trapping behavior of MoS_2 in the presence of PMMA. The developed material system and the demonstrated memory device fabrication process can be a significant platform for next generation data storage applications.

References

[1] A. K. Geim and K. S. Novoselov, Nat. Mater. 6 (2007) 183

[2] K. I. Bolotin, F. Ghahari, M. D. Shulman, H. L. Stormer, and P. Kim, Nature 462 (2009) 196

[3] Y. Lin, A. Valdes-Garcia, S. Han, D. Farmer, I. Meric, Y. Sun, Y. Wu, C. Dimitrakopoulos, A. Grill, P. Avouris, and K. Jenkims, Science 332 (2011) 1294

[4] C. Zhi, Y. Bando, C. Tang, H. Kuwahara, and D. Olberg, Adv. Mater. 21 (2009) 2889

[5] K. F. Mak, C. Lee, J. Hone, J. Shan, and T. F. Heinz, Phys. Rev. Lett. 105 (2010) 136805

[6] N. Coleman, M. Lotya, A. O'Neill, S. Bergin, P. King, U. Khan, K. Young, A. Gaucher, S. De, and R. Smith, Science 331 (2011) 568

[7] B. Radisavljevic, A. Radenovic, J. Brivio, V. Giacometti, and A. Kis, ACS Nano 5 (2011) 9934. [8] A. Splendiani, L. Sun, Y. Zhang, T. Li, J. Kim, C. Y. Chim, G. Galli, and F. Wang, Nano Lett. 10 (2010) 1271

[9] M. Shanmugam, C. A. Durcan, and B. Yu, Nanoscale 4 (2012) 7399

[10] H. Liu and P. D. Ye, IEEE Electron Device Lett. 33 (2012) 546

[11] B. Radisavljevic, A. Radenovic, J. Brivio, V. Giacometti, and A. Kis, Nat. Nanotechnol. 6 (2011) 147

[12] Y. Zhang, J. Ye, Y. Matsuhashi, and Y. Iwasa, Nano Lett. 12 (2012) 1136

[13] Y. Cai, G. Zhang, and Y. W. Zhang, J. Am. Chem. Soc. 136 (2014) 6269

[14] H. Li, Z. Yin, Q. He, H. Li, X. Huang, G. Lu, D. W. H. Fam, A. Y. Tok, Q. Zhang, and H. Zhang, Small 8 (2012) 63

[15] Z. Y. Yin, H. Li, H. Li, L. Jiang, Y. M. Shi, Y. H. Sun, G. Lu, Q. Zhang, X. D. Chen, and H. Zhang, ACS Nano 6 (2012) 74

[16] J. Xiao, D. Choi, L. Cosimbescu, P. Koech, J. Liu, and J. P. Lemmon, Chem. Mater. 22 (2010) 4522

[17] H. S. Lee, S. W. Min, Y. G. Chang, M. K. Park, T. Nam, H. Kim, J. H. Kim, S. Ryu, and S. Im, Nano Lett. 12 (2012) 3695

[18] A. K. Geim and I. V. Grigorieva, Nature 499 (2013) 419

[19] H. J. Chuang, X. Tan, N. J. Ghimire, M. M. Perera, B. Chamlagain, M. M. C. Cheng, J. Yan, D. Mandrus, D. Tomanek, and Z. Zhou, Nano Lett. 14 (2014) 3594

[20] K. Roy, M. Padmanabhan, S. Goswami, T. P. Sai, G. Ramalingam, S. Raghavan, and A. Ghosh, Nat. Nanotechnol. 8 (2013) 826

[21] S. Bertolazzi, D. Krasnozhon, and A. Kis, ACS Nano 7 (2013) 3246.

[22] M. S. Choi, G. H. Lee, Y. J. Yu, D. Y. Lee, S. H. Lee, P. Kim, J. Hone, and W. J. Yoo, Nat. Commun. 4 (2013) 1624

[23] K. G. Zhou, N. N. Mao, H. X. Wang, Y. Peng, and H. L. Zhang, Angew. Chem. Int. Ed. 50 (2011) 10839

[24] H. S. S. M. Ramakrishna, A. Gomathi, A. K. Manna, D. J. Late, R. Datta, S. K. Patil, and C. N. R. Rao, Angew. Chem. Int. Ed. 49 (2010) 4059

[25] S. Helveg, J. V. Lauritsen, E. Lægsgaard, I. Stensgaard, J. K. Nørskov, B. S. Clausen, H. Topse, and F. Besenbacher, Phys. Rev. Lett. 84 (2000) 95.

[26] Y. H. Lee, X. Q. Zhang, W. Zhang, M. T. Chang, C. T. Lin, K. D. Chang, Y. C. Yu, J. T. W. Wang, C. S. Chang, L. J. Li, and T. W. Lin, Adv. Mater. 24 (2012) 2320

[27] H. Hadouda, J. Pouzet, J. C. Bernede, and A. Barreau, Mater. Chem. Phys. 42 (1995) 291

[28] S. Balendhran, J. Z. Ou, M. Bhaskaran, S. Sriram, Z. Ippolito, E. Kats, S. Bhargava, S. Zhuiykov, and K. Kalantar-zadeh, Nanoscale 4 (2012) 461

[29] Y. Yu, C. Li, Y. Liu, L. Su, Y. Zhang, and L. Cao, Sci. Rep. 3 (2013) 1866

[30] H. Shi, R. Yan, S. Bertolazzi, J. Brivio, B. Gao, A. Kis, S. Jena, H. G. Xing, and L. Huang, ACS Nano 7 (2013) 1072

[31] X. Wang, H. Feng, Y. Wu, and L. Jiao, J. Am. Chem. Soc. 135 (2013) 5304

[32] Y. C. Lin, W. Zhang, J. K. Huang, K. K. Liu, Y. H. Lee, C. T. Liang, C. W. Chu, and L. J. Li, Nanoscale 4 (2012) 6637

[33] Y. J. Yun, C. Pearson, and M. C. Petty, J. Appl. Phys. 105 (2009) 034508

Chapter 6

Synthesis of N-doped graphene from different precursors

6.1 Introduction

Graphene, the 2D honeycomb lattice of sp^2 hybridized carbon atoms is considered to be a next generation material for application in various electronic devices, such as transistors, optoelectronics, sensors, supercapacitors etc. [1-6]. However, the electrical, optical and chemical properties of pristine graphene based materials are limited by the absence of a bandgap [7, 8]. Incorporation of foreign atoms in the sp^2 sites of graphene lattice can be an interesting prospect to tune the intrinsic properties of graphene [9, 10]. Theoretical studies have revealed that substitutional doping of graphene with a heteroatom like nitrogen, boron, etc., can change the Fermi energy and introduce a band gap [11-15]. This doping with heteroatoms creates charged sites in the graphene lattice, and as a result the spin and charge densities are redistributed bringing new functionalities [16]. In this prospect, nitrogen incorporation in graphene by substitution of carbon atoms has been explored significantly to achieve high electron density, n-type doping, increased capacity of battery, high supercapacitance and oxygen-reduction functionalities [16-21]. Thus, various studies have revealed that nitrogen doping can be an exciting platform to tune or introduce novel properties in graphene.

Considering the significant potential, the controlled synthesis of high quality graphene with desired electronic and chemical properties can be the key for future applications. In the last few years, significant development has been made in large-area high quality and individual single crystal domains of graphene synthesized by the CVD technique [22-26]. Synthesis of graphene with substitutional nitrogen doping by a CVD process has also been attracting significant interest [28-32]. CVD process can be the most effective approach to achieve substitutional doping without affecting the crystalline nature of graphene. The incorporation of foreign atoms in

the graphene lattice site is quite significant to observe different properties depending on their concentration and structures. The pyridinic nitrogen doping in graphene can facilitate oxygen reduction reaction activity, while pyrrolic nitrogen contributes to enhancing specific capacitance [18, 32]. Again, it has been reported that a band gap can be observed in graphene with a nitrogen concentration of 2-12% [19, 33]. Recently, several solid and liquid precursor materials have been used for synthesis of N-doped graphene [34-38]. However, details of atomic level study of defects, substitutional doping and grain structure have not been explored for the solid or liquid source-based CVD graphene. Here, we demonstrate a solid source-based CVD process to synthesize N-doped graphene by using different solid precursors and investigate the Atomic percentage of Nitrogen in the same. Three solid materials, namely Melamine, Triazine and PAN have selected for the synthesis of N-doped graphene depending upon their N and C contents. Melting point is also an important factor have to consider while using them in the CVD system.

In following chapter comparative study of N-doped graphene synthesized by above materials has been performed. Raman and XPS have been used to probe the N-doping effects in our experiments.

6.2 Materials and Methods

6.2.1 N-doped Graphene Synthesis

General synthesis process for the N-doped graphene is explained in Chapter 2 section 2.6.

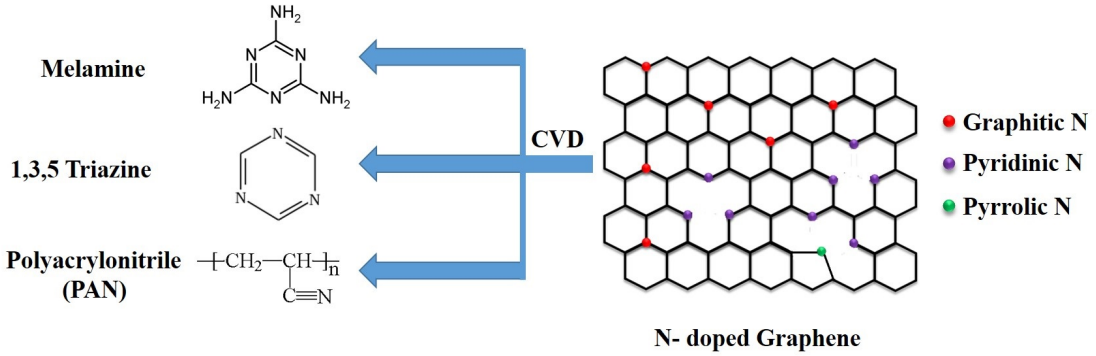

FIGURE 6.1: Schematic for the synthesis of N-doped graphene from different precursors.

APCVD technique is used to synthesize N-doped graphene. Above materials are taken in different ratios and feed into the CVD system. Melamine and Triazine were combined with camphor to get graphene whereas in the case of PAN no camphor was used. Different ratios have been used and optimized to get the highest % of nitrogen in N-doped graphene. $1:3$ ratio of Melamine and Triazine was optimized to get best results. The graphene growth was carried out

at the temperature of $1020°C$. The presence of Nitrogen and atomic % of Nitrogen in the as synthesized graphene was estimated using Raman Spectroscopy and XPS analysis respectively.

Precursor	Ratio	Temperature (^{0}C)		Gas (sccm)		Time (min)		% N
		Anneal	Growth	Anneal	Growth	Anneal	Growth	
M : C	1 : 3	1015		100 H_2	98 : 2 Ar:H_2	60	15 - 30	5.2
T : C	1 : 3							2.6
P : C	3 : 0							0.7

C: Camphor; M: Melamine; T: Triazine; P: PAN

FIGURE 6.2: Experimental parameters for the growth of N-doped graphene from Camphor, Melamine, Triazine and PAN

6.3 Results and Discussion

The synthesized materials were analyzed by Raman and XPS studies. Raman spectra were obtained using NRS 3300 laser Raman spectrometer with a laser excitation energy of $532.08nm$. XPS data were acquired to determine the chemical composition of the graphene film on the Cu foil using the Versaprobe photoelectron spectrometer with photoemission stimulated by a monochromated AlK_α radiation source ($1486.6eV$).

6.3.1 Raman Spectroscopy Study

Raman spectroscopy is another very useful method to characterize N-graphene. The D, G, and 2D bands are the predominant features in the spectrum of N-graphene. They are represented by peaks at around $1320-1360$, $1570-1600$, and $2640-2700cm^1$, respectively. In some studies, the peak called D‘ will appear at $\sim\ 1602-1625cm^1$. Specifically, the G band corresponds to the doubly degenerate E_{2g} phonons at the Brillouin zone. It originates from the first-order Raman scattering process. The 2D and D bands are all induced by the second-order, double-resonance process and related to zone-boundary phonons. The scattering process involve two zone-boundary phonons for 2D mode; it involves one phonon and one defect for the D mode. Different from the D band which requires defects to activate it, the 2D band does not require the activation of defects. Thus, the 2D band is always seen in the Raman spectra of graphene and N-graphene, even when the D band cannot be observed. For the D‘ , it arises from the intravalley, defect-induced, double-resonance process.

The graphene was synthesized from the solid camphor precursor without using the dopant precursor material. The Raman spectra shows a small defect induced D peak, indicating a high

quality graphene growth. The graphitic G and second order 2D Raman peaks were observed at 1596 and $2698cm^{-1}$, respectively. The higher intensity of the 2D peak than that of the G peak ($I_{2D}/I_G \sim 3$) confirm a single layer graphene domain. However, there are more than single layer graphene domains as observed by Raman analysis.

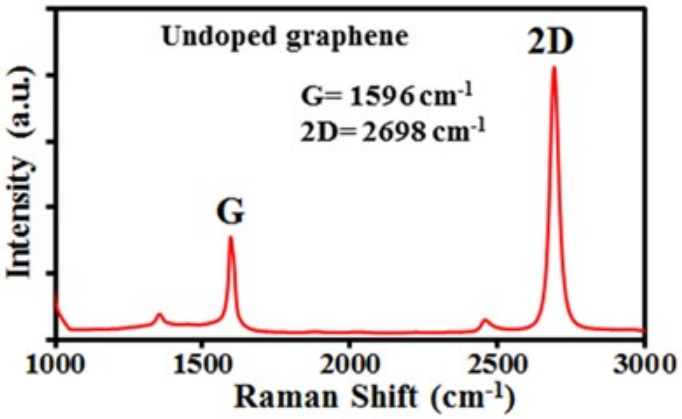

FIGURE 6.3: Raman spectra of un-doped graphene on SiO_2/Si substrate synthesized from Camphor.

6.3.1.1 Melamine

FIGURE 6.4 shows a Raman spectra of the graphene synthesized with $1:3$ ratio of camphor and melamine with similar growth conditions. We can observe significant difference in graphene structure with the addition of melamine, causing the intensity of defect related D peak to increase significantly irrespective of sample positions. The Raman studies confirm presence of defects in the sp^2 hybridized graphene grown on the Cu foil. The induced defects with the introduction of melamine can be attributed to the doping of nitrogen. We observed a blue-shift ($4cm^{-1}$) of the G peak, whereas a red-shift ($5cm^{-1}$) is seen for the 2D peak, considering the Si peak as the base.

6.3.1.2 Triazine

Since Triazine was failed to synthesize N-doped graphene and hence it was then combined with the Camphor in 1:3 ratio. In FIGURE 6.5 presence of N-doped graphene can be seen from raman spectra. High intensity of D peak and presence of D‘ peak confirms the incorporation of N in graphene. The graphitic G and second order 2D Raman peaks were observed at 1596 and $2700cm^{-1}$, respectively. The higher intensity of the G peak than that of the 2D peak confirm presence of few layer graphene domains. There is no shift in G peak but red-shift ($2cm^{-1}$) is seen for the 2D peak.

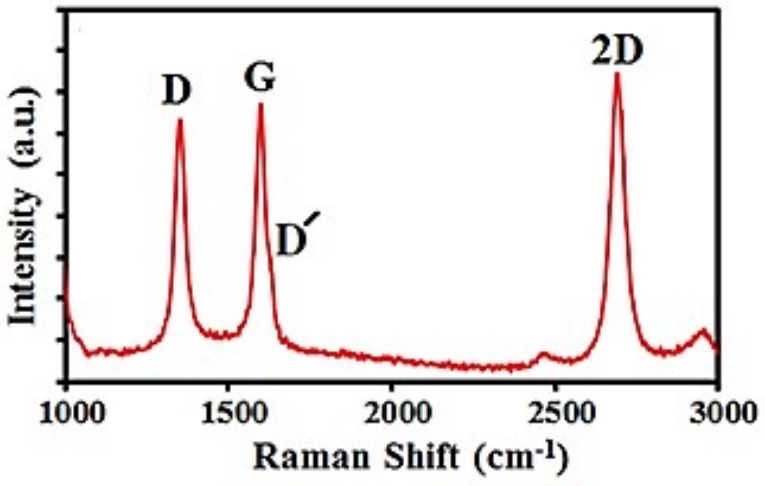

FIGURE 6.4: Raman spectra of N-doped graphene on SiO_2/Si substrate synthesized from Camphor and Melamine with $1:3$ ratio.

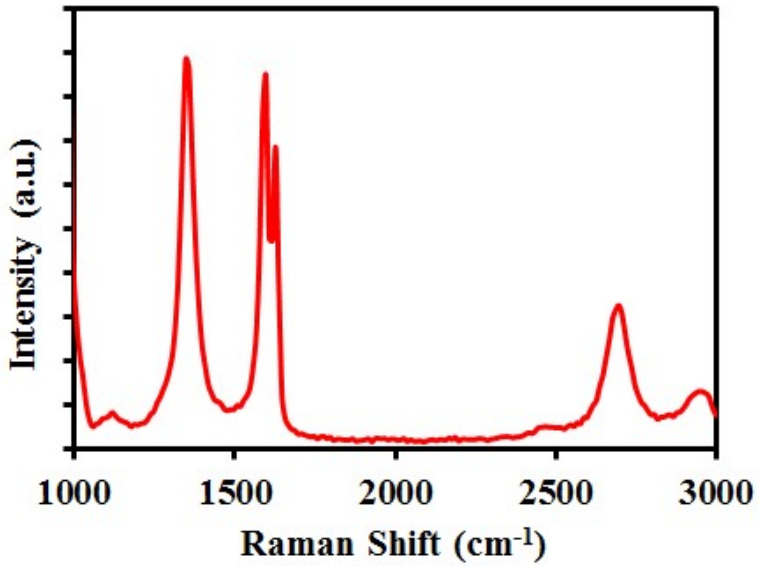

FIGURE 6.5: Raman spectra of N-doped graphene on SiO_2/Si substrate synthesized from Camphor and Triazine with $1:3$ ratio.

6.3.1.3 PAN

Raman spectra obtained from the N-doped graphene synthesized from PAN is given below. In FIGURE 6.6 all peaks related to N-doped graphene can be seen. The Raman studies confirm presence of defects in the sp^2 hybridized graphene grown on the Cu foil. The graphitic G and second order 2D Raman peaks were observed at 1587 and $2695cm^{-1}$, respectively. The defect peak was observed at $1352cm^{-1}$ and another weak so-called D‘ band centered at $1625cm^{-1}$ also appears. All peaks are shifted from the original position in the pristine graphene confirms the doping of graphene. The equal intensity of the G peak to that of the 2D peak confirm presence of bilayer graphene domains.

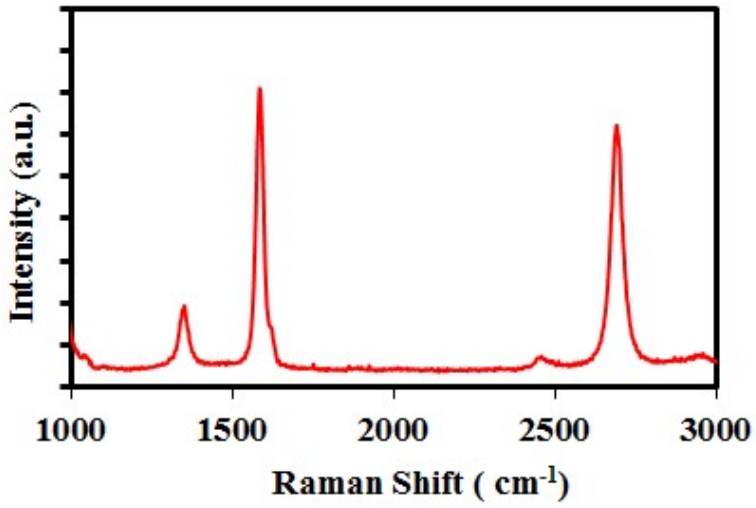

FIGURE 6.6: Raman spectra of N-doped graphene on SiO_2/Si substrate synthesized from PAN.

6.3.2 XPS Study

XPS is the standard technique to study the nitrogen doping effect in graphene. In the XPS spectrum of N-doped graphene, the peaks appearing at about 400 and $284eV$ correspond to the N1s and C1s, respectively. The ratio of peak intensity between N1s and C1s is used to determine the nitrogen content in N-doped graphene. Moreover, the N1s spectrum is used to determine the nitrogen configurations. In the research about N-doped graphene, the N1s spectrum can be deconvoluted to several individual peaks that are assigned to pyridinic N ($398.1 - 399.3eV$), pyrrolic N ($399.8 - 401.2eV$), and graphitic N ($401.1 - 402.7eV$). Apart from these three nitrogen types, peak corresponding to N-oxides of pyridinic N is observed at $\sim 402.8eV$ in several studies.

6.3.2.1 Melamine

In the XPS spectra obtained from the graphene synthesized by melamine and camphor using ratio of $1:3$, a small shoulder peak is observed corresponding to the higher binding energy ($\sim 288.4eV$). This can be attributed to presence of nitrogen containing C-N as well as oxygen containing $C-O$ and $C=O$ bonds. Further, the N 1s spectra was analyzed to evaluate the N content in the graphene samples. In this case we obtained two split N1s peaks with peaks cantered at ~ 398.8 and $406.6eV$. The peak at the higher binding energy (peak cantered at $406.6eV$) signifies the presence of NO_x as observed in the previous case as well [41]. The NO_x related peak arises from the presence of nitrogen atoms in amorphous carbon and other contaminant sites, which can easily react with the surface oxygen.

It should be noted that the graphene samples on the Cu foils were taken out to the atmosphere after the CVD growth and then the XPS analysis was performed. The quantitative analysis shows 5.2 at % of N content in the sample. FIGURE 6.7(b) shows a deconvoluted N1s peak, corresponding to presence of graphitic ($400.8eV$), pyrrolic ($400.5eV$) and pyridinic ($398.6eV$) nitrogen atoms. The deconvoluted spectra suggests that the pyridinic nitrogen content is much higher than that of graphitic and pyrrolic nitrogen. We conclude that the nitrogen observed by XPS analysis is not only incorporated in the graphene lattice, but is also adsorbed on the graphene as contaminant.

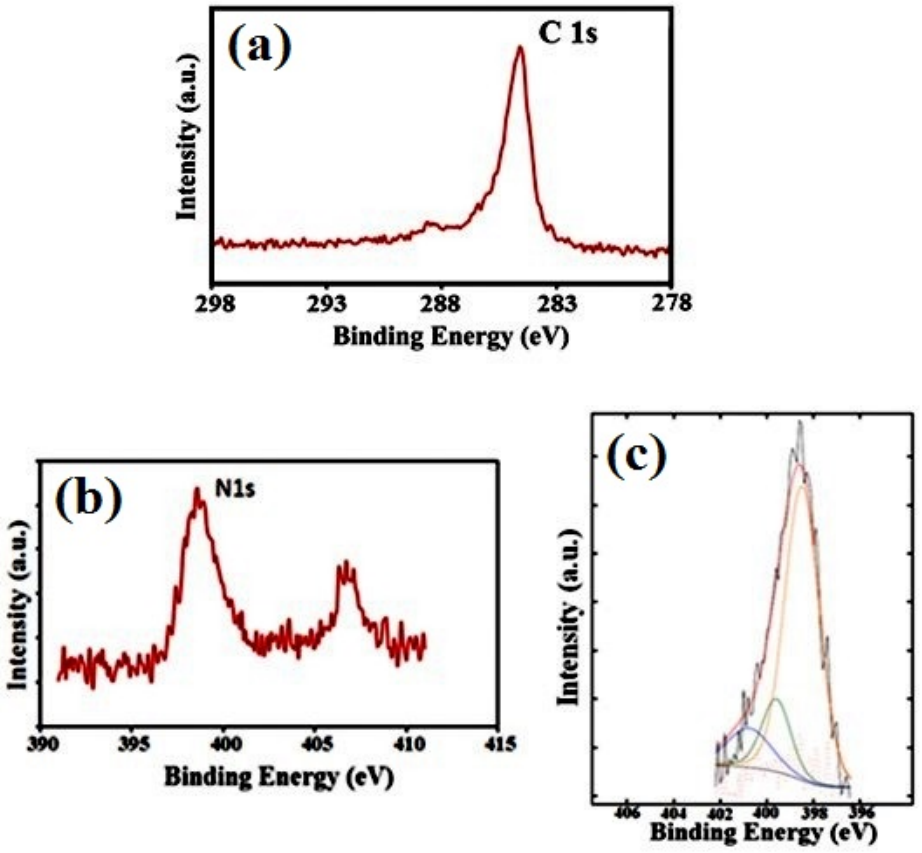

FIGURE 6.7: XPS (a) C1s (b) N1s spectra and (c) deconvoluted N1s peak showing the presence of graphitic ($400.8eV$), pyrrolic ($400.5eV$) and pyridinic ($398.6eV$) N atoms.

6.3.2.2 Triazine

The C1s line scan spectrum exhibits a peak located at $284.6eV$, corresponding to the graphite-like sp^2 hybridized carbon suggesting carbon atoms remain embedded within the honeycomb lattice. The quantitative analysis shows 2.6 at % of nitrogen content in the sample. FIGURE 6.8(b) shows N1s peak, corresponding to presence of only pyridinic N centered at 398.6eV. Very less amount of Pyrrolic and graphitic N found in the sample made from camphor and triazine. More optimization may be needed in order to get higher % of N. Controlling evaporation of

Triazine is very difficult which is the key problem in this case. Triazine may be not the best option to get higher amount of N in graphene.

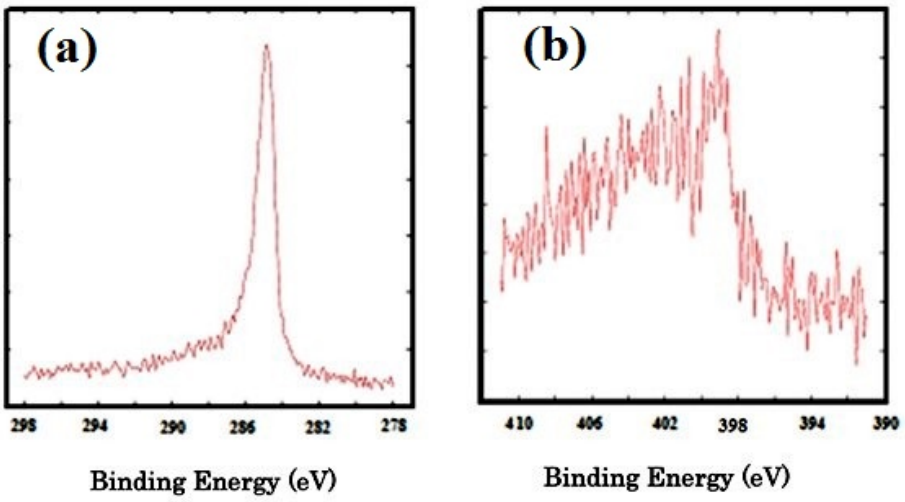

FIGURE 6.8: XPS (a) C1s (b) N1s peak showing the presence of Pyridinic ($398.6eV$) N atoms.

6.3.2.3 PAN

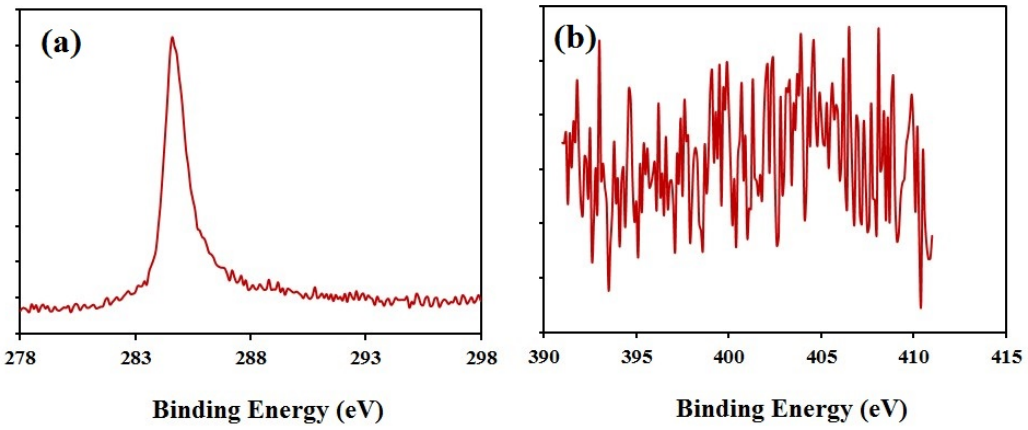

FIGURE 6.9: XPS (a) C1s (b) N1s spectra showing the presence of graphitic ($400.8eV$), pyrrolic ($400.5eV$) and pyridinic ($398.6eV$) N atoms.

In the case of graphene synthesized only from PAN, XPS study shows all characteristic peaks of N-doped graphene. Firstly, C1s spectra for sp^2 hybridized carbon can be seen in FIGURE 6.9(a). FIGURE 6.9(b) shows N1s peak, corresponding to presence of graphitic ($400.8eV$), pyrrolic ($400.5eV$) and pyridinic ($398.6eV$) nitrogen atoms. In this spectra also Pyrridinic N has higher intensity as seen in the case of graphene synthesized from Melamine and Camphor. Though intensities of all peaks are very small. In this n-doped graphene sample 0.7 at % of nitrogen content was estimated.

6.4 Conclusion

We have demonstrated the synthesis of N-doped graphene using different solid precursors by APCVD process. Raman and XPS analysis confirmed the incorporation of nitrogen in the synthesized graphene on the Cu foil. Our findings shows that graphitic nitrogen defects can be introduced in a large individual graphene grain by the developed solid source-based APCVD technique. N-doped graphene was synthesized using camphor and other N containing precursors. Melamine and Triazine was used with the combination of camphor whereas PAN was used alone. Ratio of camphor with this precursors was optimized to $1:3$. Different kinds of N substitutions were observed in these samples e.g. pyrridinic, pyrrolic and graphitic. Incorporation of graphitic N was difficult to achieve but in our experiments, we could observe sufficient amount of graphitic N. Which was confirmed by XPS analysis. The main purpose of this study was to find out material with highest N content. In above 3 materials, Melamine was the one with highest N content (5.2%) followed by Triazine (2.6%) and PAN (0.7%) respectively. By altering some experimental parameters more atomic % of N can be extracted from Melamine. This study can help to open a band gap in the graphene since band gap increases with the increase in the amount of N content.

References

[1] A.K Geim, K.S Novoselov, Nat Mater. 6 (2007) 183–191.

[2] A.K Geim, Science 324 (2009) 1530−1534.

[3] F.Schwierz, Nat Nanotechnol. 5 (2010) 487–496.

[4] F. Bonaccorso, Z. Sun, T. Hasan, A. C. Ferrari, Nat Photonics. 4 (2010) 611-622.

[5] Y .Shao, J. Wang, H .Wu, J .Liu, I.A Aksay, Y. Lin, Electroanalysis 22 (2010) 1027 1036.

[6] M.D Stoller, S .Park, Y. Zhu, J .An, R.S Ruoff, Nano Lett. 8 (2008) 3498–3502.

[7] K.S Novoselov, A.K Geim, S.V Morozov, D. Jiang, Y. Zhang, S.V Dubonos et al, Science 306 (2004) 666-669.

[8] Y. Zhang, Y.W Tan, H.L Stormer, P. Kim, Nature 438 (2005) 201-204.

[9] T .Lohmann, V. K Klitzing, J.H Smet, Nano Lett. 9 (2009) 1973-1979.

[10] L.S Panchakarla, et al, Adv Mater 21(2009) 4726-4730.

[11] A.V Krasheninnikov, P.O Lehtinen, AS Foster, P Pyykko, RM Nieminen, Phys Rev Lett. 102 (2009) 126807.

[12] J.M Carlsson, M .Scheffler, Phys Rev Lett. 96 (2006) 046806.

[13] H .Zeng, J .Zhao, J.W Wei, H.F Hu, Eur Phys J B 79 (2011) 335-340.

[14] Z. Hou, X. Wang, T .Ikeda, K. Terakura, M .Oshima, M. Kakimoto, Phys Rev B 87 (2013) 165401.

[15] T.V Vineesh, M.P Kumar, C. Takahashi, G .Kalita, S. Alwarappan, D.K Pattanayak, et al, Adv Energy Mater 5 (2015) 1500658.

[16] F. Lu, S.T Lo, J.C Lin, W. Zhang, J.Y Lu, F.H Liu et al. ACS Nano 7 (2013) 6522-6532.

[17] M.P Kumar, T. Kesavan, G. Kalita, P. Ragupathy, T.N Narayanana, D.K Pattanayak, RSC Adv. 4 (2014) 82014) 38689- 38697.

[18] Z. Luo, S .Lim, Z .Tian, J .Shang, L .Lai, B .MacDonald et al, J Mater Chem. 21 (2011) 8038-8044.

[19] H. Wang, T. Maiyalagan, X. Wang. ACS Catal. 2 (2012): 781-794.

[20] M .Rein, et al, ACS Nano 9 (2014) 1360-66.

[21] L .Qu, Y .Liu, J.B Baek, L .Dai, ACS Nano 4 (2010) 1321-26.

[22] K.S Kim, Y .Zhao, H. Jang, S.Y Lee, J.M Kim, K.S Kim et al., Nature 457 (2009) 706-710.

[23] X. Li, W .Cai, J .An, S. Kim, J. Nah, D .Yang et al, Science 324 (2009) 1312-1314.

[24] S. Bae, H. Kim, Y. Lee, X .Xu, J.S Park, Y. Zheng et al. Nat Nanotechnol. 5 (2010) 574–578.

[25] H .Wang, G .Wang, P .Bao, S. Yang, W. Zhu, X. Xie et al, J Am Chem Soc.134 (2012) 3627-3630.

[26] D .Wei, Y .Liu, Y. Wang, H. Zhang, L. Huang, G Yu, Nano Lett 9 (2009) 1752-1758.

[27] L .Zhao, R .He, K.T Rim, T Schiros, KS Kim, H Zhou et al, Science 333 (2011) 999-1003.

[28] Y. Xue, B. Wu, L. Jiang, Y. Guo, L. Huang, J Chen et al, J Am Chem Soc. 134 (2012) 11060-11063.

[29] R .Lv, Q .Li, A.R Botello-Méndez, T .Hayashi, B. Wang, A .Berkdemir et al, Sci Rep. 2 (2012) 586.

[30] L. Zhao, M .Levendorf, S. Goncher, T .Schiros, L .Pálová, A.Z Khosousi et al, Nano Letters 13 (2013) 4659-4665

[31] T. Wu, H. Shen, L .Sun, B .Cheng, B. Liu, J. Shen New J Chem 36 (2012) 1385-1391.

[32] F.M Hassan, V. Chabot, J .Li, B.K Kim, L.R Sandoval, A. Yu, J. Mater. Chem. A 1 (2013) 2904-2912.

[33] P .Rani, V.K Jindal, RSC Adv. 3 (2013) 802-812.

[34] Z .Sun, Z .Yan, J Y.ao, E Beitler, Y. Zhu, J .Tour. Nature 468 (2010) 549–552.

[35] Z .Wang, Li .P, Y Chen, J. Liu, H. Tian, J. Zhou et al, J Mater Chem C. 2 (2014) 7396–7401.

[36] C .Wang, Y. Zhou, L. He, T.W Ng, G .Hong, Q.H Wu et al, Nanoscale 5 (2013) 600-605.

[37] T. Mondal, A.K Bhowmick, R. Krishnamoorti, Chem Mater. 27 (2015) 716-725.

[38] J. Zhang, J. Li, Z. Wang, X .Wang, W. Feng, W. Zheng et al, Chem Mater. 26 (2014) 2460-2466.

[39] S .Sharma, G. Kalita, R. Hirano, S.M Shinde, R .Papon, H. Ohtani et al, Carbon 72 (2014) 66-73.

[40] Z. Zafar, Z.H Ni, X. Wu, H.N Shi, H.Y Nan, J .Bai et al, Carbon 61 (2013) 57-62.

[41] S.J Kang, T .Mori, S. Narizuka, W. Wilcke, H.C Kim, Nature Commun.5 (2014) 3937.

Chapter 7

Summary and Future Work

7.1 Summary

In the summary, synthesis processes of high quality graphene and MoS_2 layers are explored as well as their clean and damage free transfer onto arbitrary substrate for device fabrications is discussed. High quality graphene, CNT and MoS_2 have been synthesized in order to fabricate their heterostructures. High quality graphene was synthesized using camphor as a precursor and copper as a substrate by CVD technique. Similarly MoS_2 was synthesized using two-step process including thermal evaporation of MoO_3 followed by sulfurization by CVD method.

After synthesis, transfer was one of the most critical issue. To have application of these synthesized 2d materials, their clean and continuous transfer on arbitrary substrates is very important. In order to achieve this, different parameters had to optimize e.g. concentration of PMMA, baking time, Spin coating speed, etchant concentration, cleaning etc.

In this dissertation the transfer process of large-area graphene film onto flexible CA substrates by a hot press technique is discussed. The CA based substrate was not compatible with acetone and PMMA supporting layer in a conventional transfer process. The CA substrate was hot pressed onto the graphene synthesized Cu foil followed by etching of the base Copper to obtain the graphene coating directly on the CA substrate. A clean, continuous and damage-free graphene transferred onto the CA substrate was obtained. The graphene film on CA substrate is highly conducting as measured by electrical measurements, suggesting that it can be used as building block for paper based electronic devices.

Two kind of heterostructures have been discussed in the dissertation. Namely Graphene-CNT for interconnects and Graphene-MoS_2 for memory device application.

A 3D hybrid structure of Graphene and VAMWCNTs using a single solid carbon source (Camphor) has been fabricated. Optical and TEM study confirmed the out-of-the plane growth of the

CNTs on the transferred graphene film and structure of CNTs and graphene in the 3D system. I-V measurements were carried out to investigate electrical characteristics of the 3D system. This 3D system showed a contact resistance of 255Ω.

Graphene-MoS_2 heterostructure and its application in non-volatile memory device has been discussed. TEM and STEM-HAADF studies were carried out to observe the atomic level structure of the synthesized high quality MoS_2 crystals. An on/off ratio as high as 2:5E3 was obtained in the fabricated PMMA-MoS_2/graphene memory device which is attributed by charge trapping and de-trapping behaviour of MoS_2 in the presence of PMMA.

To introduce band gap in graphene, N-doped graphene synthesis using Melamine, PAN and Triazine as N-source and Camphor as C-source, respectively, by APCVD technique is explained. The at % of N was tuned by varying the amount of precursors. Raman and XPS analysis was carried out to confirm the presence and amount of N in given samples respectively. Melamine with camphor was turned out to be the best choice among above precursors since it provide 5.2 at % of N which is highest among them.

7.2 Future Work

Whether as a transducer in mediator-less glucose biosensors, photoactive material, electronic transfer aid, or charge collector platform, graphenes use has been gradually increasing and affecting modern day electronics. Hence, synthesis of high quality graphene and its transfer with least defect is the most important field we have to work. To achieve the best performance of the hybrid materials the graphene used must be of continuous and less defect. In order to do that treatment of copper substrate is the key factor and more work has to be done on that. The morphology of copper substrate is responsible for the quality of synthesized graphene. Hybridization of graphene with CNTs and semiconductors can be performed by innumerable methods. Despite its excellent properties, graphene still has a long way to go before it can replace silicon or tin oxide films, largely because its reproducibility and its large scale production with process control of layer number still remain a challenge. When designing graphene hybrid materials great attention must be paid towards optimizing the intrinsic properties of the components simultaneously with the interface structure and mechanisms of the electronic coupling, some of which are still unknown.

More research has to be done towards extracting the best performance out of these hybrid structures which will be my next objective. Amalgamation of these nanomaterials and their use in different application will be the key future goal. Absence of a band gap in graphene which is the only limitation it has, which can be eliminated by the doping of heteroatoms as discussed earlier. As a suggestion for the future work more research can be done on the doping study by

increasing atomic percentage of Nitrogen and hence increasing the band gap in the graphene using the several precursors.

Appendix A

List of Achievement

A.1 Publications in International Journals

- **Sachin M. Shinde**, Golap Kalita, Masaki Tanemura, (2014), "Fabrication of poly (methyl methacrylate)-MoS_2/graphene heterostructure for memory device application", *Journal of Applied Physics*, 116 (21), 214306.

- **Sachin M. Shinde**, Golap Kalita, Subash Sharma, Remi Papon, Mohd Zamri Yusop, Masaki Tanemura (2014), "Synthesis of a three dimensional structure of vertically aligned carbon nanotubes and graphene from a single solid carbon source", *RSC Advances*, 4 (26), 13355-13360

- **Sachin M. Shinde**, Golap Kalita, Subash Sharma, Zurita Zulkifli, Remi Papon, and Masaki Tanemura (2015), "Polymer-free graphene transfer on moldable flexible substrate by hot press technique", *Surface and Coatings Technology*, 275, 369-73

- Remi Papon, Golap Kalita, Subash Sharma, **Sachin M. Shinde**, Riteshkumar Vishwakarma, Masaki Tanemura (2014), "Controlling single and few-layer graphene crystals growth in a solid carbon source based chemical vapor deposition", *Applied Physics Letters*, 105 (13), 133103

- Golap Kalita, Muhammed E Ayhan, Subash Sharma, **Sachin M. Shinde**, Dilip Ghimire, Koichi Wakita, Masayoshi Umeno, Masaki Tanemura (2014), "Low temperature deposited graphene by surface wave plasma CVD as effective oxidation resistive barrier", *Corrosion Science*,78, 183-187

- Subash Sharma, Golap Kalita, Ryo Hirano, **Sachin M. Shinde**, Remi Papon, Hajime Ohtani, Masaki Tanemura (2014), "Synthesis of graphene crystals from solid waste plastic by chemical vapor deposition", *Carbon*, 72, 66-73

- Remi Papon, Subash Sharma, **Sachin M. Shinde**, Amutha Thangaraja, Golap Kalita, and Masaki Tanemura (2015), "Formation of graphene nanoribbons and Y-junctions by hydrogen induced anisotropic etching", *RSC Advances*, 5, 35297-35301

- A. Thangaraja, **Sachin M. Shinde**, G Kalita, M Tanemura (2015), "Effect of WO3 precursor and sulfurization process on WS2 crystals growth by atmospheric pressure CVD", *Materials Letters*, 156, 156-160

- Amutha Thangaraja, **Sachin M. Shinde**, Golap Kalita, Remi Papon, Subash Sharma, Riteshkumar Vishwakarma, Kamal P. Sharma and Masaki Tanemura (2015), "Structure dependent hydrogen induced etching features of graphene", Appl. *Phys. Lett.*, 106, 253106 (Equal Contribution)

- Zurita Zulkifli, **Sachin M. Shinde**, Subash Sharma, Takatoshi Suguira, Golap Kalita, and Masaki Tanemura (2015), "Fabrication of graphene and ZnO nanocones hybrid structure for transparent field emission device", *Applied Surface Science*, 356, 674-678

- Vishwakarma Riteshkumar, Sharma Subash, **Sachin M. Shinde**, Sharma Kamal, Thangaraja Amutha; Kalita Golap; Tanemura Masaki (2015), "Fabrication of particular structures of hexagonal boron nitride and boron-carbon-nitrogen layers by anisotropic etching", *Physica E*,79, 13-19

A.2 Publication in Press

- Amutha Thangaraja, **Sachin M. Shinde**, Golap Kalita, and Masaki Tanemura, "An effective approach to synthesize monolayer tungsten disulphide crystals using tungsten halide precursor", *Applied Physics Letters*.

- Kamal Sharma, **Sachin M. Shinde**, Mohamad Rosmi Subash Sharma Masaki Tanemura, "Effect of copper foil annealing process on large graphene domain growth by solid source based chemical vapor deposition", *Applied Surface Science*.

A.3 Conference Proceedings

- Zurita Zulkifli, Subash Sharma, **Sachin M. Shinde**, Golap Kalita, M Tanemura (2015), "Effect of annealing in hydrogen atmosphere on ZnO films for field emission display", *IOP Conference Series: Materials Science and Engineering*, Volume 99, conference 1.

A.4 Conference Presentation

- **Sachin M. Shinde**, Golap Kalita, Subash Sharma, Remi Pepon, Mohd Zamri Yusop, and Masaki Tanemura,"Synthesis of Three Dimensional Structure of Vertically Aligned CNTs and Graphene from Solid Carbon Source", *61st JSAP spring meeting*, Sagamihara campus, Aoyama Gakuin University, Japan, March 17-20, 2014.

- **Sachin M. Shinde**, Golap Kalita, Subash Sharma, Remi Papon and Masaki Tanemura, "Synthesis of MoS_2 crystals and fabrication of a heterostructure with graphene", *6th IEEE International Nano-electronics Conference*, IEEE INEC 2014, Hokkaido University, Sapporo, Japan, July 28 31, 2014.

- **Sachin M. Shinde**, Golap Kalita, Subash Sharma, Masaki Tanemura, "Synthesis of Elongated Hexagonal MoS_2 Crystals by Chemical Vapor Reaction Process", *IUMRS-ICA 2014*, Fukuoka University, Fukuoka, Japan. August 24-30, 2014.

- **Sachin M. Shinde**, Golap Kalita, Subash Sharma, Remi Papon and Masaki Tanemura, "Synthesis of Elongated Hexagonal MoS_2 Crystals by Chemical Vapor Reaction Process", *E-MRS 2014 Fall Meeting*, Warsaw University of Technology, Poland, September 15-18, 2014.

- **Sachin M. Shinde**, Golap Kalita, Subash Sharma, Remi Papon and Masaki Tanemura, "Synthesis of MoS_2 crystals and fabrication of heterostructure", International Conference on Chemical, Materials, and Biosciences for Sustainable Development *ICCMBSD- 2015*, Walchand College, Solapur, India, January 8-10, 2015

- **Sachin M. Shinde**, Golap Kalita and Masaki Tanemura, "Polymer-free clean graphene transfer on flexible cellulose acetate paper (CA) and nafion substrate", 4th *International Conference on Electronic Devices, Systems and Applications* (ICEDSA 2015), Kuala Lumpur, Malaysia, September 14 -15, 2015.

- **Sachin M. Shinde**, Golap Kalita and Masaki Tanemura, "Polymer-free clean graphene transfer on flexible cellulose acetate paper (CA) and nafion substrate", *The 76th JSAP Autumn Meeting*, Nagoya Congress Center, Nagoya, Japan, 13-16 September, 2015

- **Sachin M. Shinde**, E. Kano, G. Kalita, M. Takeguchi, A. Hashimoto and M. Tanemura, "Synthesis of nitrogen-doped graphene by solid source-based chemical vapor deposition", *JSAP SCTS*, Nagoya University, Nagoya, Japan, November 2015 (Poster)